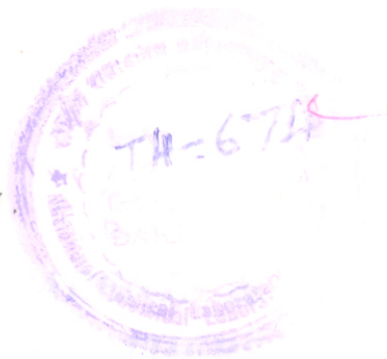# SYNTHESIS, CHARACTERIZATION AND CATALYTIC PROPERTIES OF A NEW HIGH SILICA MOLECULAR SIEVE

A THESIS

SUBMITTED TO THE

**UNIVERSITY OF POONA**

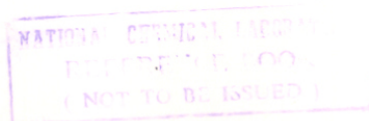FOR THE DEGREE OF

**DOCTOR OF PHILOSOPHY**

(IN CHEMISTRY)

BY

**K. RAMESH REDDY**

CATALYSIS DIVISION

NATIONAL CHEMICAL LABORATORY

PUNE - 411 008, INDIA

APRIL 1993

----- *TO MY BELOVED PARENTS &*

*BROTHERS*

# CERTIFICATE

Certified that the work incorporated in the thesis **"Synthesis, Characterization and Catalytic Properties of a new high silica molecular sieve"** submitted by Mr. K. Ramesh Reddy, for the degree of Doctor of Philosophy, was carried out by the candidate under my supervision in the National Chemical Laboratory, Pune, India. Such material as has been obtained from other sources has been duly acknowledged in the thesis.


**(P. RATNASAMY)**

**(Research Guide)**

# ACKNOWLEDGEMENTS

**K. RAMESH REDDY**

# Contents...

# GENERAL INTRODUCTION

# 1. PART A

## 1.1 ZEOLITES

### 1.1.1 Definition and Classification

Zeolites are crystalline microporous aluminosilicates with a framework based on an extensive three-dimensional network of oxygen ions, sharing the corners of tetrahedral sites formed by the oxygen can be either a $Si^{4+}$ or an $Al^{3+}$ ion. The $AlO_2^-$ tetrahedra in the structure determine the framework charge. This is balanced by a cation that occupies non-framework position. A representative empirical formula for a zeolite is written as:

$$M_{2/n}O. \ Al_2O_3. \ xSiO_2. \ yH_2O$$
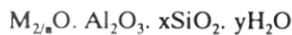
Where 'M' represents the exchangeable cation of valence 'n', generally from the group I or II ions, although other metal and organic cations may also be used to balance the framework charge. The value of 'x' is equal to or greater than 2 because $Al^{3+}$ does not occupy adjacent tetrahedral sites.

The primary building unit of a zeolite structure is the individual tetrahedral $TO_4$ unit, where T is either Si or Al. A secondary building unit (SBU) consists of selected geometric groupings of those tetrahedra. These secondary building units consist of 4, 6, and 8-member rings, 4-4, 6-6 and 8-8 member double rings, and 4-1, 5-1 and 4-4-1 branched rings which can be used to describe most of the known zeolite structures.

The Classification of zeolites can be made on the basis of their morphological characteristics[1-3], crystal structure[1,4], chemical composition[1,5a], effective pore diameter[1,5b] and natural occurrence. Classification of zeolites according to their chemical composition has been made on the basis of their silica-to-alumina[5a] ratio (SAR) into following groups: (a) low silica (SAR = 1-1.5), (b) medium silica (SAR = >1.5-5), (c) high silica (SAR = >5-several thousands) and (d) Al-free pure silica zeolites. The zeolites are also classified according to their pore

openings. Zeolites containing 8, 10 and 12 membered ring pore opening are referred to as small, medium and large pore zeolites, respectively. Some common zeolites are listed in Table 1.1 according to their pore opening. Table 1.1 includes both natural and synthetic zeolites.

### 1.1.2 Synthetic zeolites

The multivalent cation exchanged synthetic faujasites have been extensively used in petroleum and petrochemical processes for cracking, isomerization, alkylation, dealkylation, dehydrogenation, hydroisomerization, hydrocracking and related processes[6]. Type A zeolites have been used as molecular sieve adsorbents. These two types of zeolites (large and small pore zeolites) perhaps account for more than 90% of industrial application of all zeolites. The most important advance in zeolite catalysis has been achieved by altering and controlling the morphology and the size of the crystals, adjusting the concentration gradient of active sites and synthesizing zeolites with new framework structure. The controlling of all these characteristics is possible during the synthesis of zeolites. Zeolites have been synthesized in the earlier stages by reacting aluminosilicate gels with alkali cations under hydrothermal conditions. In the next generation of zeolite synthesis, the Si/Al ratio was increased in the reaction mixture which resulted in a number of zeolites with intermediate SAR viz. zeolite T and zeolite L[7]. Further advance in the synthesis of zeolites materials was the introduction of various amines and tetraalkylammonium cations during the hydrothermal synthesis. This resulted firstly in a number of zeolites having same structure but with higher SAR and secondly new zeolites particularly, high-silica medium pore zeolites (eg. ZSM-5 type) and their pure silica polymorphs[8-20]. The reasons for synthesizing higher SAR zeolites are to improve their hydrothermal stability, and modify their acidity and acid strength. High-silica zeolites, particularly medium and large pore ones are quite important in adsorption and catalysis.

## 1.2 ORGANIC ADDITIVES-ZEOLITE STRUCTURE RELATIONSHIP

### 1.2.1 The role of organic additives in zeolite synthesis

Lok et al. have reviewed the role of organic compounds in the synthesis of molecular sieves[21]. These organic molecules may be present in the zeolite void space as neutral species and/or as cations[22]. However, the exact role of organic guest molecules during zeolite formation

2

Table 1.1. Classification of zeolites according to the pore openings

| 8-membered ring (small pore) | 10-membered ring (medium pore) | 12-membered ring (large pore) |
|---|---|---|
| Linde A | dachiardite | cancrinite |
| bikitaite | epistilbite | Linde X, Y, L, EMT |
| brewsterite | ferrierite | gmelinite |
| chabazite | heulandite | mazzite |
| TMA-E | laumontite | mordenite |
| edingtonite | ZSM-5 | offretite |
| erionite | ZSM-11 | ZSM-12 |
| gismondine | EU-1 (ZSM-50) | Omega |
| ZK-5 | stilbite | Beta |
| Levynite | ZSM-23 | |
| merlinoite | ZSM-22 | |
| natrolite | ZSM-48 (EU-2) | |
| paulingite | ZSM-57 | |
| phillipsite | ZSM-25 | |
| Rho | ZSM-39 | |

is not yet clear. The fact that the same organic compound may lead to the formation of different zeolite structures and a particular zeolite structure can be synthesized using a variety of organic molecules having quite different shapes, sizes and structures is yet to be explained properly. Certain organic quaternary ammonium ions and amines have extensively been employed as "templating" additives in zeolite syntheses. A template theory was evolved to explain the structure-directing effect of these organic species[21]. The charge distribution, the size and the geometric shape of a template are believed to be the cause for their structure-directing effect[21].

Using TMA as template in zeolite synthesis, 17 different zeolite structures, listed in Table 1.2, are crystallized[8-20]. From the template theory point of view, the void volume of these zeolite cages should accommodate the TMA cation. The fit is better in some of the zeolites. It is proposed that the positively charged TMA ion has $SiO_2$ and $AlO_2^-$ tetrahedra around it with partially negatively charged oxygen atoms pointing towards the TMA ion[21]. Using such a picture, "templating" theory has been explained by electric-dipole interaction and stereo-specificity due to the size and shape of cation[21].

The other possibility of occupancy of organic cations is in the channel system. This is observed in the case of TEA, TPA and TBA organic templates. The TEA cation can crystallize different zeolite structures (Table 1.2). The fit of nearly spherical shape of the TEA ion in the channel system changes from a relatively loose fit in Beta or ZSM-20 to a near ideal in mordenite and finally to an over tight situation in ZSM-8. In order to resolve this too tight situation, a three dimensional 10-ring channel system appears to be required to accommodate the nitrogen moiety of TEA ion in the intersection of the channels with the arms stretching into channels[21]. A similar situation, most probably, occurs with tetrapropyl ammonium (TPA) in the ZSM-5 structure and tetrabutyl ammonium (TBA) in the case of ZSM-11[21].

The template theory was also supported by using organic diamines. By increasing the chain length of the diamine from $(-CH_2-)_2$ to $(-CH_2-)_{10}$, various zeolite structure types (Table 1.2), were formed[23-28]. The diamines with short chain ($C_2-C_4$) favour ferrierite, the one with medium chain ($C_5-C_6$), ZSM-5 and the long chain ($C_7-C_{10}$), ZSM-11, indicating a structure-directing effect.

Table 1.2. Organic template and zeolite-structure relationship.

| Organic template | Structure-type | References |
|---|---|---|
| Tetramethylammonium (TMA)⁺ | gismondine, sodalite, zeolite P, gmelinite, faujasite, zeolite E, zeolite A, ZSM-4, Nu-1, Fu-1, Holdstite zeolite O, offretite, ZSM-47, ZSM-6, ZSM-39, | 8-20 |
| Tetraethylammonium (TEA)⁺ | zeolite Beta, ZSM-8, ZSM-12, ZSM-20, mordenite, ZSM-25, ZSM-5 | 29,30b,32 |
| Tetrapropylammonium (TPA)⁺ | ZSM-5 | 30 |
| Tetrabutylammonium (TBA)⁺ | ZSM-11 | 31 |
| 1,2-Diaminoethane | ZSM-5, ZSM-21, ZSM-35 | 25,33b,23 |
| 1,3-Diaminopropane | ZSM-35, ZSM-5 | 25,26 |
| 1,4-Diaminobutane | ZSM-35, ZSM-5 | 25,26 |
| 1,5-Diaminopentane | ZSM-5 | 25,27 |
| 1,6-Diaminohexane | ZSM-5, ZSM-22 | 25,27 |
| 1,7-Diaminoheptane | ZSM-11 | 28 |
| 1,8-Diaminooctane | ZMS-11, ZSM-48 | 28,29 |
| 1,9-Diaminononane | ZSM-11 | 28 |
| 1,10-Diaminodecane | ZSM-11 | 28 |

## 1.2.2 Review of literature on organic additives for zeolite synthesis

The use of an organic cation, tetramethyl ammonium (TMA) in zeolite synthesis was first introduced by Barrer and Denny[8]. The presence of TMA affects the gel composition. This change in gel composition allows higher silica to alumina ratio materials[12] to be formed as compared to the same structure materials made without TMA.

The use of quaternary ammonium ions in zeolite synthesis clearly has had two major roles. The first is the extension of zeolites into the high SAR and the second is synthesis of zeolites with new framework structures. The synthesis of zeolite Beta by Wadlinger et al. marked the beginning of a new era in zeolite synthesis[29]. The synthesis of ZSM-5 using TPA cation was reported by Argauer and Landolt[30]. Then on, the syntheses of a number of other high-silica (Si/Al $\geq$ 20) such as ZSM-11[31], ZSM-12[32], ZSM-21[33], ZSM-22[34], ZSM-23[35], ZSM-25[36], ZSM-34[37], ZSM-48[38], ZSM-50[39] and ZSM-57[41a] etc. were reported by Mobil oil corporation. The syntheses of a series of other high silica zeolites viz. Nu-1[14a], Nu-2[14b], Nu-3[42], Nu-5[43], Nu-6[44], EU-1[40], EU-2[45], Fu-1[15a] and Fu-9[15b] were reported by ICI researchers.

The other organic templates such as alcohols, ketones, morpholine, glycerol and organic sulphur compounds have also been used in zeolite syntheses[43,46,47].

Like mono-quaternary ammonium cations, bis quaternary ammonium cations, when used as template in zeolite synthesis, result in different high-silica molecular sieves. Some commonly used bis quaternary cations may be represented by a general formula: $R_3$-$N^+$-$(CH_2)_x$-$N^+$-$R_3$ where R may be methyl, ethyl, propyl and butyl or mixture thereof and 'x' = 3-10. Depending upon the chain length of both terminal alkyl groups and the value of 'x', a number of zeolite structure can be synthesized. Table 1.3 lists bis quaternary salts and corresponding zeolites structure formed by these organic cations along with respective references. By systematically increasing the value of 'x' in bis quaternary salts and keeping their terminal alkyl groups as methyl, a number of zeolites viz. ZSM-39[41b] (x = 3), EU-4[41c] (x = 3), EU-1[41b,45] (x = 4,5,6), EU-2[38] (x = 6,9), ZSM-23[34,48] (x = 7,8), NU-87 (x = 10) are formed[41b]. High-silica medium pore zeolite ZSM-57 was also synthesized using a bis quaternary ammonium cation salt where R = ethyl and x = 5 (i.e. $(C_2H_5)_3$-$N^+$-$(CH_2)_5$-$N^+$-$(C_2H_5)_3$[41a]). ZSM-5 was obtained using bis quaternary salts

Table 1.3: Organic template and zeolite structure relationship

| Organic template | Structure | References |
|---|---|---|
| Trimethonium bromide | ZSM-39, EU-4 | 41b,41c |
| Tetramethonium bromide | EU-1 | 41b |
| Tetramethylene bis(ethyldimethylammonium bromide) | ZSM-12 | 49b |
| Pentamethonium bromide | EU-1 | 40 |
| Hexamethonium bromide | ZSM-48, EU-1 | 45,38 |
| Hexamethylene bis(ethyldimethylammonium bromide) | ZSM-12 | 49b |
| Hexamethylene bis(tripropyammonium bromide) | ZSM-5 | 49a |
| Hexamethylene bis(tributylammonium bromide) | ZSM-5 | 49a |
| Heptamethonium bromide | ZSM-23, MCM-10 | 34,48 |
| Octamethonium bromide | ZSM-23 | 34 |
| Nonoamethonium bromide | EU-2 | 38 |
| Decamethonium bromide | NU-87 | 41b |
| Pentamethylene bis (triethylammonium bromide) | ZSM-57 | 41a |
| Hexamethylene bis (triethylammonium bromide) | NCL-1 | 50 |

where R = propyl or butyl and x = 6 (i.e. $(C_3H_7)_3$-N$^+$-$(CH_2)_6$-N$^+$-$(C_3H_7)_3$ and $(C_4H_9)_3$-N$^+$-$(CH_2)_6$-N$^+$-$(C_4H_9)_3)^{49a}$. All these zeolites, synthesized by using bis quaternary ammonium cation, mentioned above are either clathrasil (ZSM-39, and EU-4) or high-silica medium pore zeolites. Recently, Szostak has claimed the synthesis of a high-silica large pore zeolite ZSM-12 using a mixed alkyl bis quaternary salt of the formula: $(C_2H_5)(CH_3)_2$-N$^+$-$(CH_2)_6$-N$^+$-$(CH_3)_2(C_2H_5)^{49b}$.

In the light of the above and aiming at the synthesis of high silica large pore zeolites, we have used a new bis quaternary ammonium salt viz. $(C_2H_5)_3$-N$^+$-$(CH_2)_6$-N$^+$-$(C_2H_5)_3$, which resulted a new high-silica zeolite, designated as NCL-1[50]. Zeolite NCL-1 can be synthesized in fairly large range of Si/Al ratios (between 20 and above). An Al-free, pure silica analog of NCL-1 was also synthesized and characterized.

## 1.3 STRUCTURAL CHARACTERIZATION THROUGH INSTRUMENTAL TECHNIQUES

### 1.3.1 X-ray Diffraction

Being a fingerprint of an individual crystalline structure, the X-ray powder diffraction indicates uniqueness in structure. The powder pattern can also provide information on the degree of crystallinity as well as phase purity. From X-ray diffraction data, unit cell parameters can be calculated.

One of the most important uses of the XRD technique is the structure determination, especially by single crystal methods[51]. Powder diffraction technique including ab initio structure determination and Rietveld refinements has also helped in structure determination of a number of zeolites[52].

### 1.3.2 Infrared spectroscopy

Infrared spectroscopy can yield information concerning structural details of the zeolites and it can be used to confirm acid characteristics and isomorphous substitution[53-55]. The lattice vibrations of the zeolites in the infrared spectrum is observed in the range of 300-1300 cm$^{-1}$.

These vibrations can be classified into two groups, (i) internal vibrations of the $TO_4$ units or structure insensitive vibrations and (ii) vibrations due to external linkages of the $TO_4$ units or structure sensitive vibrations[53]. The major infrared band assignments are as follows:

**Internal tetrahedra**

| | |
|---|---|
| Asymmetric stretching | 1250-950 $cm^{-1}$ |
| Symmetric stretching | 720-650 $cm^{-1}$ |
| T-O bend | 420-500 $cm^{-1}$ |

**External linkages**

| | |
|---|---|
| Double ring | 650-500 $cm^{-1}$ |
| Pore opening | 300-420 $cm^{-1}$ |
| Symmetric stretching | 750-820 $cm^{-1}$ |
| Asymmetric stretching | 1050-1150 $cm^{-1}$ |

Infrared spectroscopy is useful for quick identification of materials of the pentasil family[56]. The absorption bands near 550 $cm^{-1}$ have been assigned to the presence of 5-member rings in the structure[57,58]. There are three types of 5-member ring blocks: a 5-5 block, a 5-3 block and 5-3-1 block. The absorption band is observed at 550 $cm^{-1}$ in ZSM-5 and ZSM-11, which is a structure sensitive band and caused by the double 5-membered ring blocks of types 5-5 and 5-3. For mordenite family, the absorption are observed near 560 $cm^{-1}$, as reported for structures with the type 5-3 blocks[57,58].

### 1.3.3 Nuclear magnetic resonance spectroscopy

High resolution solid state MAS NMR spectroscopy has emerged as a powerful technique to characterize the framework/non-framework elements in zeolites[59-72]. In the zeolite systems, most of the Q-units are $Q^4$ type units (i.e. $Si(OT)_4$ where T atom is either Si or Al or mixture of them. From this, five different $Q^4$ units are possible such as Si(0Al)(4Si), Si(1Al)(3Si), Si(2Al)(2Si), Si(3Al)(1Si) and Si(4Al)(0Si). The $^{29}Si$ NMR spectrum of a zeolite may consist one to five peaks corresponding to the five possible Si(nAl)(4-nSi) environments in the zeolite framework. With increasing number of Al atoms (n) in the first coordination sphere of the

silicon atom in the $^{29}Si$ NMR spectrum, the peaks are systematically shifted to low field, where each Al substitution results in a shift contribution of about 5 ppm[61]. The ranges of $^{29}Si$ chemical shifts for various Si(nAl) environments in $Q^4$ aluminosilicates are about -80 to -125 ppm with respect to TMS.

The isotropic $^{27}Al$ chemical shifts of aluminosilicates are primarily determined by the coordination number of the aluminium atom. The shift ranges observed are about +50 to +80 ppm for $AlO_4$ ($T_d$) about -10 to +20 ppm for $AlO_6$ ($O_h$) and about +30 to +40 ppm for relatively rare $AlO_5$ (penta) unit[73]. Within the shift range of $AlO_4$ tetrahedra, characteristic low-field shifts are observed for layered aluminosilicates (shift range 70-80 ppm) in comparison with zeolite framework aluminosilicates (shift range 50-68 ppm).

Recently, Fyfe et al. have demonstrated three dimensional connectivities in zeolites ZSM-5, ZSM-11, ZSM-22 and ZSM-39[74-77]. High resolution liquid NMR ($^{29}Si$ and $^{27}Al$) has provided useful information on the silicate[78,79] and aluminosilicate[80-83] species present in the solution used in the zeolite synthesis.

### 1.3.4 Electron spin resonance spectroscopy

ESR spectroscopy is sensitive to environmental symmetry of paramagnetic metal ions. ESR spectroscopy is used to study the environment of the isomorphously substituted and exchanged cations and metal oxides within the pores or external zeolite matrix[84]. Various paramagnetic metals such as $V^{4+}$, $Fe^{3+}$, $Cr^{3+}$, have been studied extensively using ESR spectroscopy[85-87]. ESR technique[86] has been used to characterize solid-solid reaction between zeolite and metal oxide of elements such as Cu, Cr, Fe, V and Mo. The oxidation state, position, environment and redox property of V in vanadium silicate molecular sieves with MFI and MEL structures have recently been reported[87-89].

## 1.4 SHAPE SELECTIVITY: MEDIUM VERSUS LARGE PORE ZEOLITES

Shape selectivity plays a very important role in zeolite catalysis[90a]. Highly crystalline and regular channel structures are among the principal advantages of zeolites as catalysts over other materials. Shape selectivity in zeolites is classified into reactant shape selectivity, product shape

selectivity, or restricted transition state shape selectivity. Reactant shape selectivity results from the limited diffusivity of some of the reactants, which cannot effectively enter and diffuse inside the channel. Product shape selectivity occurs when smaller product molecules rapidly escape from the crystal leaving behind bulkier products which may undergo secondary reactions. Restricted transition state shape selectivity occurs when certain reactions are prevented because the corresponding transition state requires more space than is available in the cavities of a molecular sieve. In these cases the reaction will proceed through less bulky transition states without hinderance.

The shape and dimensions of the intracrystalline cavities in zeolites with ten- and twelve-membered rings are important factors which determine the product selectivity in many reactions such as $m$-xylene isomerization, 1-methyl-2-ethylbenzene, etc. For example, in $m$-xylene isomerization reaction, the $p/o$ ratio in twelve-member ring zeolites is also governed by transition state shape selectivity (RTSS), along with product shape selectivity (PSS), whereas in 10-membered ring zeolites, it is mainly governed by product shape-selectivity only[90b]. The preferential formation of $p$-xylene over $o$-xylene in 10-membered pore opening channels is explained by a faster diffusion of the $p$-xylene through the 10-membered ring channels, while $o$-xylene molecules spend more time in the channel and some of them are converted to the $p$-isomer before they can escape from the channel.

## 1.5 CHARACTERIZATION OF THE EFFECTIVE VOID SPACE OF ZEOLITES

### 1.5.1 Adsorption measurements

Adsorption measurements provide a wealth of information about void space of the zeolites or molecular sieves. The adsorption of oxygen, nitrogen, argon, water, or various hydrocarbon probe molecules provides information on the void volume of zeolites. The adsorption of these molecules within molecular sieves results in a type I adsorption isotherms[91,92]. An idea about the pore size of the molecular sieves is also obtained through adsorption measurements, by selecting adsorbates with different critical dimensions. This information on the size of the pores is important particularly if the crystal structure is unknown. This type of information is more

11

readily obtainable than a complete structure determination from powder XRD pattern, particularly for a new zeolitic material. This can also help in the identification of a given material for some specific catalytic application.

### 1.5.2 Catalytic test reactions

Various catalytic test reactions such as Mobil's constraint index, $m$-xylene isomerization, 1-methyl-2-ethylbenzene reaction, ethylbenzene disproportionation, n-decane test reaction and spaciousness index have been used to characterize the pore structure and shape of intracrystalline void space of zeolites and molecular sieves. Especially for the new zeolites with unknown crystallographic structures these fast screening methods provides quick and sometimes detailed information about the pore geometry of the microporous materials. An additional advantage of these catalytic test reactions is that they characterize the zeolitic void space under catalytic reaction conditions.

### 1.5.2.1 Mobil's Constraint index (CI)[93]

Mobil constraint index is the ratio of the first order rate constants of the n-hexane (n-hex.) and 3-methylpentane (3-M-Pn) in an equimolar mixture under same reaction conditions[93]. Constraint index, CI is defined as $\log(1-X_{n\text{-hex}})/\log(1-X_{3\text{-M-Pn}})$, where X is fractional conversion. This numerical (CI) value allows one to distinguish the zeolites with small (CI $\geq$ 12), medium (CI = 2-12) and large pore (CI $\leq$ 2) openings from one another. This reaction is normally carried out on the acid form of the zeolite. The main drawback of CI is that it depends on reaction temperature and conversion.

### 1.5.2.2 $m$-Xylene isomerization and disproportionation[94]

The $m$-xylene isomerization reaction has been used to determine the shape and dimensions of the intracrystalline void space of the zeolites[94-97]. The product selectivities of $m$-xylene conversion are sensitive to the pore shape and structure of the zeolite. For example, the value of initial $p$-xylene/$o$-xylene ($p/o$) ratio for medium pore zeolites is 1.5 and above, while large pore zeolites exhibit around 1.0 (equilibrium value). Hence, from $p/o$ ratio, it is possible to distinguish medium pore zeolites from the large pore zeolites and vice-versa. The enhanced

12

para selectivity in medium pore zeolites has been explained on the basis of product shape selectivity[94]. Other important criteria are the ratio of isomerization to disproportionation (i/d) and the distribution of the trimethylbenzenes (disproportionated products) which are used to determine the pore shape and structure of zeolites[94]. Jacobs et al. have correlated the pore architecture of the zeolites with the distribution of trimethylbenzenes in $m$-xylene disproportionation by considering the space required to accommodate the possible bimolecular (diphenyl methane-type) transition state intermediate in the void space of the zeolite[94,96].

### 1.5.2.3 1-Methyl-2-ethylbenzene conversion[98]

The 1-methyl-2-ethylbenzene (1M2EB) reaction, developed by Csicsery, can reveal some important information about the zeolites[98,99] such as minimum pore opening (reactant/product shape selectivity) and void space around active sites (restricted transition state shape selectivity). A rough idea about acid strength of active sites (transalkylation/isomerization selectivity) may also be obtained. At equal conversion levels, the ratio of primary-to-secondary reaction products depends on the ratio of the corresponding rate constants and on the extent of diffusion constraint. The reactant and product shape selectivity are caused by diffusional constraint and therefore they are affected by crystallite size. If the shape selectivity is unaffected by the size of the catalyst crystals, the presence of restricted transition state shape selectivity is suggested[58,59]. However, the probe molecule (1M2EB) is rather costly and the product analysis quite complicated.

### 1.5.2.4 Ethylbenzene disproportionation[100,101]

The disproportionation of ethylbenzene reaction has been proposed as a test reaction for the rapid discrimination between large and medium pore zeolites[100,101]. From this reaction, various criteria have been proposed[100] such as the presence or absence of an induction period, the rate of deactivation, the ratio of yield of diethylbenzene ($Y_{DE-Bz}$) and benzene ($Y_{Bz}$) and the distribution of the diethylbenzene isomers. In general, in large pore zeolites, an induction period and slow deactivation rate were observed whereas in medium pore zeolites, no induction period and faster deactivation were observed[101]. From the ratio of yield of diethylbenzene ($Y_{DE-Bz}$) to benzene ($Y_{Bz}$) a criterion has been proposed to discriminate between medium pore zeolites and

13

large pore zeolites[101]. For example, the ratio of $Y_{DE-Bz}/Y_{Bz}$ is nearer to unity in the large pore zeolites (for zeolite Y the ratio is 0.9) whereas in medium pore zeolite the ratio is less than unity (for zeolite ZSM-5 the ratio is 0.75).

### 1.5.2.5 n-Decane test reaction (modified constraint index)[102]

The bifunctional conversion of long-chain paraffins is an attractive reaction for the characterization of void space in zeolites[102-105] particularly medium pore ones. From the distribution of isomerized and hydrocracked products, a method have been developed for the determination of the zeolite void space[103-105]. The modified constraint index is the ratio of 2-methylnonane and 5-methylnonane in isomerization of n-decane (at around 5% conversion) over bifunctional zeolite catalysts (noble metal loaded acidic zeolite). The modified constraint index ($CI^*$) decreases with increasing intracrystalline void space. This reaction is very useful for characterization of medium pore zeolites. Even the structurally related zeolites ZSM-5/ZSM-11 and ZSM-22/ZSM-23 can be distinguished from each other whereas for large pore zeolites, it has limited applications because the range is rather narrow (from 1.0 to 2.3).

### 1.5.2.6 Spaciousness index (SI)[95]

The spaciousness index (SI) is the ratio of i-butane and n-butane in the hydrocracked products of butylcyclohexane reaction over bifunctional catalyst. This spaciousness index is quite useful for characterizing the effective pore width of molecular sieve catalysts[95,104,105] particularly for large pore zeolites. The spaciousness index increases with the increasing intracrystalline void space. Weitkamp et al. observed that the SI does not depend on the yield of the hydrocracked products, as well as on the conversion level of butylcyclohexane[95]. They also suggested that the $C_{10}$-napthenes are suitable for the determination of SI. However, to minimize the risk of diffusional limitations, butylcyclohexane is suitable for the determination of SI.

**PART B**

## 1.6 MOLECULAR SIEVES AS OXIDATION CATALYSTS

### 1.6.1 Titanium silicate molecular sieves

Most of the catalytic application of zeolites are in acid/base catalysis. Isomorphous substitution of $Si^{4+}$ or $Al^{3+}$ by $Ga^{3+}$, $Fe^{3+}$, $B^{3+}$ etc. modify the acidic properties of these molecular sieves. The discovery of titanium silicates, where Ti is isomorphously substituted for $Si^{4+}$ has opened a new era in oxidation catalysis. Taramasso et al. synthesized titanium silicalite molecular sieve with MFI framework topology (TS-1)[106]. Later, Reddy et al. have reported another titanium silicalite molecular sieve with MEL framework topology (TS-2)[107]. The first commercial process using titanium silicates (TS-1) as a catalyst is the hydroxylation of phenol to catechol and hydroquinone by Enichem, Italy[108]. TS-1 and TS-2 are active in many oxidation reactions[109-120] in the presence of hydrogen peroxide. The uniformly distributed and tetrahedrally coordinated Ti is reported to be responsible for the catalytic activity of TS-1 and TS-2 in the oxidation reactions.

### 1.6.2 Vanadium silicate molecular sieves

The introduction of vanadium into the MFI lattice was reported in 1978 by Marosi et al.[121] followed by Inui et al.[122] and Miyamoto et al.[123]. These materials either contained aluminium or were thermally unstable, being transformed into α-crystobolite upon calcination. Recently, Kornatowski et al.[88] and Rigutto et al.[89] synthesized vanadium silicate molecular sieve with MFI topology (VS-1), which are thermally stable and free from aluminium impurities. Rigutto et al.[105] concluded that the vanadium ions are not in the tetrahedral framework positions and that the vanadium species are probably connected to the framework at defect sites. Centi et al.[124] suggest that the vanadium species are present either in the real tetrahedral sites of the zeolite framework or as species anchored to the surface defect sites.

Rao et al.[125] reported a thermally stable vanadium silicate molecular sieve (VS-2) with MEL topology and their application in oxidation reactions[125-127]. Recently we have synthesized and characterized a vanadium silicate analog of NCL-1 (V-NCL-1) which is a large pore molecular sieve[128,129]. The V-NCL-1 is also active in oxidation of bulky hydrocarbons[128,129].

## 1.7 SCOPE OF THE THESIS

High-silica zeolites are of great significance in the area of adsorption and catalysis. Though, most of the medium pore high-silica zeolites (ZSM-5, -11, -22, -48) can be synthesized in Al-free, silica polymorphic form, ZSM-12 is the only high-silica large pore zeolite which can be synthesized in a wide Si/Al ratio including the Al-free silica polymorph. In general, the diquaternary salts favour the formation of high-silica zeolites. From this point of view a new diquaternary salt (hexamethylene bis(triethylammonium bromide)) was used as the organic template, which crystallized a new high-silica zeolite designated as NCL-1. The adsorption and catalytic properties of this new zeolite are characteristic of large pore molecular sieves. Further, this zeolite can be synthesized in a wide range of Si/Al ratios including the Al-free silica polymorph.

The vanadium containing molecular sieves are quite interesting catalysts in many oxidation reactions. The vanadium ions in the vanadium silicate zeolites may be present either at tetrahedral sites or anchored at defect sites. We were able to incorporate vanadium in the NCL-1 structure. V-NCL-1 is the first large pore vanadium silicate oxidation catalyst and the other two reported (VS-1 and VS-2) vanadium silicates are medium pore catalysts. The advent of the large pore oxidation catalyst may be used to explore the oxidation reactions involving bulky molecules.

**THE MAJOR OBJECTIVE OF THE PRESENT THESIS IS TO STUDY THE SYNTHESIS, CHARACTERIZATION AND CATALYTIC PROPERTIES OF THE NEW HIGH-SILICA LARGE PORE MOLECULAR SIEVE, NCL-1 AND ITS VANADIUM SILICATE ANALOG (V-NCL-1)**

**Chapter II** describes the synthesis and physico-chemical characterization of the aluminosilicate and the silica polymorph of NCL-1 by using XRD, SEM, IR, MAS NMR, TG-DTA, ion-exchange capacities and sorption techniques. From the sorption measurements, a rough estimation of the pore openings of the NCL-1 was obtained.

**Chapter III** describes the studies carried out on the crystallization kinetics of this new high-silica large pore molecular sieve. The influence of various synthesis parameters (Si/Al, OH⁻/Si, R⁺/Si, Na⁺/Si molar ratios, temperature, etc.) on the kinetics of crystallization is studied.

66.097.3 (043)

**Chapter IV** describes the catalytic activity of NCL-1 samples in several model reactions such as (1) *m*-xylene isomerization, (2) ethylbenzene disproportionation, (3) constraint index (CI) and (4) spaciousness index (SI). By comparing the product distribution in the above reactions with that of other zeolites with known structure, the classification of NCL-1 will be made according to the pore dimensions.

**Chapter V** is divided into two parts, Part A describes the synthesis and characterization of vanadium silicate analogs of NCL-1 through XRD, ESR, IR, TG-DTA and sorption studies. Part B describes the catalytic properties of vanadium silicate analogs of NCL-1 in the oxidation reactions such as oxyfunctionalization of n-octane and cyclohexane, oxidation of toluene, xylenes, trimethylbenzenes and naphthalene.

**Chapter VI** summarizes the salient features of synthesis, characterization and catalytic properties of NCL-1 and its vanadium silicate analog.

## 1.8 REFERENCES

1.  a) D.W. Breck, "Zeolite Molecular Sieves: Structure, Chemistry and Use", London, Wiley (1974).

    b) R.M. Barrer, "Hydrothermal Chemistry of Zeolites", London, Academic Press (1982).

2.  W.M. Meier, D.H. Olson, "Atlas of zeolite structure types", London, Butterworths, (1987).

3.  W.L. Bragg, "The Atomic Structure of Minerals", Cornell University press, Ithaca, New York, (1937).

4.  W.M. Meier, "Molecular sieves, Soc. of Chem. Ind., London., p.10 (1968).

5.  a) E.M. Flanigen, "in Proceedings of the 5th International Conference on Zeolites", (L.V.C. Rees, Eds.), Naples, Italy, June 2-6, p.760 (1980).

    b) L.B. Sand, Econ. Geol., p.191 (1967).

6.  a) V.J. Frilette, P.B. Weisz and R.G. Golden, J. Catal., 1, 301 (1962).

    b) N.Y. Chen and J.F. Degnan, Chem. Eng. Progr., 84, 32 (1988).

    c) T. Inui and F. Okazumi, J. Catal., 90, 366 (1984).

7.  E.M. Flanigen, Proc. of 5th Int. Conference on Zeolites, (Ed. L.V.C. Rees), (1980).

8.  R.M. Barrer and P.J. Denny, J. Chem. Soc., 971 (1961).

9.  (a) C. Baerlocher and W.M. Meier, Helv. Chem. Acta, 52, 1853 (1969);

    (b) ibid 53, 1285 (1970).

10. R. Allello and R.M. Barrer, J. Chem. Soc. A, 1470 (1972).

11. R.M. Barrer and D.E. Mainwaring, J. Chem. Soc. A, 254 (1972).

12. N.A. Acara US Pat. 3 414 602 (1968).

13. E.M. Flanigen and E.B. Kellberg US Pat. 4 241 036 (1968).

14. (a) T.V. Whittam US Pat. 4 060 590 (1977);

    (b) T.V. Whittam EP Pat. Appl. 55 046 (1982).

15. (a) T.V. Whittam US Pat. 4 209 498 (1980);

    (b) D. Seddon and T.V. Whittam, EP Appl. 55 529 (1982).

16. M. K. Rubin Ger. Offen. 1 806 154 (1969).

17. Union Carbide Corporation, B. P. Pat. 909 624 (1962).

18. G.T. Kokotailo and S. Sawruk, US Pat. 4 187 283 (1980).

19. (a) F.G. Dwyer and E.E. Jenkins, US Pat. 4 287 166 (1981);

    (b) B.G. Pelrine US Pat. 4 259 306 (1981).

20. (a) P. Chu, Eur. Pat. Appl. 0 023 089 (1981);
    (b) Chu, Chinu-chiun US Pat. 4 206 843 (1981).

21. B.M. Lok, T.R. Cannan and C.A. Messina, Zeolites, **3**, 282 (1983).

22. G. Engelhardt and D. Michel, "High Resolution Solid State NMR of Silicates and zeolites" (John Wiley, New York) 348 (1987).

23. C.J. Plank, E.J. Rosinski and M.K. Rubin, US Pat. 4 016 245 (1977).

24. M.K. Rubin C.J. Plank and E.J. Rosinski, US Pat. 4 104 151 (1978).

25. (a) D.A. Hichkson BE Pat. 8 886 833 (1981);
    (b) L.D. Rollmann, US Pat. 4 296 083 (1981).

26. L. Marosi, M. Schwarzmann and J. Stabenow, Eur. Pat. Appl. 49 386 (1982).

27. L.D. Rollmann and E.W. Valyocsik, US Pat. 4 139 600.

28. L.D. Rollmann and E.W. Valyocsik, US Pat. 4 108881.

29. R.L. Wadlinger, G.T. Kerr and E.J. Rosinski, US Pat. 3 308 069 (1967).

30. (a)R.J. Argauer and G.R. Landolt, US Pat. 3 702 886 (1972);
    (b) Mobil Oil Corp. Neth. Pat. 7 014 807 (1971).

31. P. Chu, US Pat. 3 709 979 (1973).

32. (a) E.J. Rosinski and M.K. Rubin, US Pat. 3 832 449 (1974);
    (c) J. Ciric, US Pat. 3 972 983 (1976);
    (c) P. Chu, US Pat. 3 766 093 (1973);
    (d) G.G. Doherty, C. Plank and E.J. Rosinski, US Pat. 4 247 416 (1981).

33. (a) C.J. Plank, M.K. Rubin and E.J. Rosinski, US Pat. 4 105 541 (1978); (b) C.J. Plank, E.J. Rosinski, and M.K. Rubin, US Pat. 4 046 859 (1977).

34. E.W. Valyocsik, US Pat. 4 481 177 (1984).

35. C.J. Plank, E.J. Rosinski and M.K. Rubin, US Pat. 4 076 842 (1978).

36. H.G. Dohety, E.J. Rosinski and C.J. Plank, EP Appl. 15 702 (1980).

37. M.K. Rubin, E.J. Rosinski and C.J. Plank, US Pat. 4 086 186 (1978).

38. L.D. Rollmann and E.W. Valyocsik, EP Appl. 15 132 (1980).

39. P. Chu, J.C. Vartuti and A.J. Herbst, EP Appl. 1 27 399 (1984).

40. J.L. Casci, B.M. Lowe and T.V. Whittam, EP Appl. 42 226 (1981).

41. a) EP 174 121 (1986).
    b) J.L. Casci, Stud. Surf. Sci. Catal., **28**, 215 (1986).
    c) E.W. Valyocsik, US Pat. 4 585 786 (1986).

42. G.D. Short and T.V. Whittam, EP Appl. 0 040 016 (1981).

43. T.V. Whittam, EP Appl. 0 054 386 (1982).

44. T.V. Whittam, EP Appl. 54 363 (1982).

45. J.L. Casci, B. Lowe and T.V. Whittam, UK Pat. Appl. 2 077 709 (1982).

46. (a) C.J. Plank, E.J. Rosinski and M.K. Rubin, US Pat. 4 175 114 (1978).

47. (a) J.A. Kaduk, US Pat. 4 323 481 (1982).
    (b) Idemistsu Kosan Co., Ltd. Jpn Kokal Tokkyo Kono JP 82 07 816 (1982).

48. US Pat. 4 623 527.

49. (a) US Pat. 4 585 638 (1986).
    (b) R. Szostak, US Pat. 4 585 639 (1986).

50. (a) R. Kumar, K.R. Reddy, A. Raj and P. Ratnasamy, 9th Intern. Zeolite Conf., Montreal, Canada, 1992, Paper A6.
    (b) R. Kumar, K.R. Reddy and P. Ratnasamy, Ind. Pat. Appl. No. 766/DEL/91 (1991).
    (c) R. Kumar, K.R. Reddy and P. Ratnasamy, EP Appl. No 92300166.3 (1991).
    (d) R. Kumar, K.R. Reddy and P. Ratnasamy, US Appl. No. 07/816, 211 (1991)

51. J.J. Pluth, J.V. Smith and J.M. Bennett, Acta. Crystallogr., **C 42**, 283 (1986).

52. P.R. Rudolf, C. Saldarriaga-Molina and A. Clearfield, J. Phy. Chem., **90**, 6122 (1986).

53. E.M. Flanigen, H. Khatami and H.A. Szymanski, Molecular Sieve Zeolite-1, Adv. in Chem. Series, **101**, 210 (1971).

54. E.M. Flanigen, Zeolite Chemistry and Catalysis, (Ed. J.A. Rabo) ACS Monograph, **171**, 80 (1976).

55. J.W. Ward, Zeolite Chemistry and Catalysis, (Ed. J.A. Rabo) ACS Monograph, **171**, 118 (1976).

56. J.C. Jansen, F.J. Van der Gaag and H. Van Bekkum, Zeolites, **4**, 369 (1984).

57. P.A. Jacobs, H.K. Beyer and J. Valyan, Zeolites, **1**, 161 (1981).

58. G. Coudurier, C. Naccache and J.C. Vedrine, J. Chem. Soc. Chem. Commun., 1413 (1982).

59. G. Engelhardt, D. Kunath, M. Magi, A. Samoson, M. Tarmak and E. Lippmaa, in Workshop on Adsorption of Hydrocarbons in Zeolites, (Berlin Adlershof 1979).

60. E. Lippmaa, M. Magi, A. Samoson, G. Engelhardt and A.R. Grimmer, J. Amer. Chem. Soc., **102**, 4889 (1980).

61. G. Engelhardt, U. Lohse, E. Lippmaa, M. Tarmak and M. Magi, Z. Anorg. Allg. Chem., **482**, 49 (1981).

62. M. Magi, A. Samoson, M. Tarmak, G. Engelhardt and E. Lippmaa, Dok. Akad. Nauk USSR, **261**, 1169 (1981).

63. G. Engelhardt, E. Lippmaa and M. Magi, J. Chem. Soc., Chem. Commun., 712 (1981)

64. S. Ramdas, J.M. Thomas, J. Klinowski, C. A. Fyfe and J.S. Hartman, Nature, **292**, 228 (1981).

65. J.M. Thomas and J. Klinowski, Adv. Catal., **33**, 199 (1985).

66. J.M. Thomas, J. Klinowski, C.A. Fyfe, J.S. Hartman and L.A. Bursill, J. Chem. Soc., Chem. Commun., 678 (1981).

67. J. Klinowski, J.M. Thomas, M. Audier, S. Vasudevan, C.A. Fyfe and J.S. Hartman, J. Chem. Soc., Chem. Commun., 570 (1981).

68. J.B. Nagy, J.P. Gilson and E.G. Derouane, J. Chem. Soc., Chem. Commun., 1129 (1981).

69. D. Greude and H.J. Behrens, Cryst. Res. Technol., **16**, 1236 (1981).

70. C.A. Fyfe, J.M. Thomas, J. Klinowski and G.C. Gobbi, Angew. Chem., Int. Ed. Engl., **22**, 259 (1983).

71. J. Klinowski, Prog. Nucl. Magn. Reson. Spectrosc., **16**, 237 (1984).

72. J.B. Nagy, G. Engelhardt and D. Michel, Adv. Colloid Interface Sci., **23**, 67 (1985).

73. Ref. no. 22 p.144 (1987).

74. C.A. Fyfe, H. Grondey, Y. Feng, and G.T. Kokotailo,; Chem. Phys. Lett., **173**, 211 (1990).

75. C.A. Fyfe, Y. Feng, H. Grondey, G.T. Kokotailo and A. Mar., J. Phys. Chem., **95**, 3747 (1991).

76. C.A. Fyfe, Y. Feng, H. Gies, H. Grondey, and G.T. Kokotailo., J. Am. Chem. Soc., **112**, 3264 (1990).

77. C.A. Fyfe, H. Gies, and Y. Feng., J. Am. Chem. Soc., **111**, 7702 (1989).

78. S.D. Kinrade, and T.W. Swaddle., J. Am. Chem. Soc., **108**, 7159 (1986).

79. A.V. McCormick, A.T. Bell, and C.J. Radke., Zeolites, **7**, 183 (1987).

80. A.V. McCormick, A.T. Bell, and C.J. Radke., Stud. Surf. Sci. Catal., **28**, 247 (1988).

81. J.P. Van den Berg, C.P. de Jong-Versloot, J. Keijsper, and M.F.M. Post., Stud. Surf. Sci, Catal., **37**, 85 (1988).

82. A. Thangaraj, and R.Kumar., Zeolites, **10**, 117 (1990).

83. A. Thangaraj, R. Kumar and P. Ratnasamy, Zeolites, **11**, 573 (1991).

84. B.I. Whittington and J.R. Anderson, J. Phys. Chem., **95**, 3306 (1991).

85. P. Ratnasamy and R. Kumar, Catal. Today, **9**, 329 (1991).

86. (a) A.V. Kucherov and A.A. Slinkin, Zeolites, **7**, 43 (1987).
    (b) ibid: **8**, 110 (1988).

87. P. Fejes, I. Marsi, I. Kirisci, J. Halasz, I. Hannus, A. Rockenbauer, Gy. Tasi, L. Korecz and Gy. Schobel, Stud. Surf. Sci. Catal., **69**, 173 (1991).

88. J. Kornatowski, M. Sychev, V. Goncharuk and W.H. Baur, Stud. Surf. Sci. Catal., **65**, 581 (1990).

89. M.S. Rigutto and H. Van Bekkum, Appl. Catal., **68**, L1 (1991).

90. a) S.M. Csicsery, Zeolites, **4**, 202 (1984).
    b) A. Corma, "Guidelines for Mastering the Properties of Molecular Sieves", NATO ASI Series, **221**, 299 (1990).

91. S. Brunauer, The Adsorption of Gases and Vapors, Princeton University Press, Princeton, N.J. 68-82 (1945).

92. L. Gurvitsch, J. Phys. Chem. Soc. Russ., **47**, 805 (1915).

93. V.J. Frilette, W.O. Haag and R.M. Lago, J. Catal., **67**, 218 (1981).

94. J.A. Martens, J. Perez-Pariente, E. Sastre, A. Corma and P.A. Jacobs, Appl. Catal., **45**, 85 (1988).

95. P.A. Jacobs and J.A. Martens, Stud. Surf. Sci. Catal., **28**, 23 (1986).

96. J. Perez-pariente, E. Sastre, V. Fornes, J.A. Martens, P.A. Jacobs and A. Corma, Appl. Catal., **69**, 125 (1991).

97. J. Dewing, J. Mol. Catal., **27**, 25 (1984).

98. S.M. Csicsery, J. Catal., **23**, 124 (1971).

99. S.M. Csicsery, J. Catal., **108**, 433 (1987).

100. J. Weitkamp, S. Ernst, P.A. Jacobs and H.G. Karge, Erdol Kohle-Erdgas-Petrochem., **39**, 13 (1986).

101. H.G. Karge, J. Ladebeck, Z. Sarbak, K. Hatada, Zeolites, **2**, 94 (1982).
     c) H.G. Karge, K. Hatada, Y. Zhang and R. Fiedorow, Zeolites, **3**, 13 (1983).

102. J.A. Martens, M. Tielen, P.A. Jacobs and J. Weitkamp, Zeolites, 4, 98 (1984).

103. J.A. Martens and P.A. Jacobs, Zeolites, **6**, 334 (1986).

104. J. Weitkamp and S. Ernst, Stud. Surf. Sci. Catal., **38**, 367 (1988).

105. R. Kumar, S. Ernst, G.T. Kokotailo and J. Weitkamp, Stud. Surf. Sci. Catal., **37**, 451 (1987).

106. M. Taramasso, G. Perego and B. Notari, US Pat. 4 578 521 (1983).

107. J.S. Reddy, R. Kumar and P. Ratnasamy, Appl. Gatal., **58**, L1 (1990).

108. B. Notari, Stud. Surf. Sci. Catal., **37**, 413 (1987).

109. T. Tatsumi, M. Nakamura, S. Negishi and H. Tominaga, J. Chem. Soc., Chem. Commun., 476 (1990).

110. D.C. Huybrechts, L.D. Bruyeker and P.A. Jacobs, Nature, **345**, 240 (1990).

111. G. Perego, G. Bellussi, C. Corno, M. Taramasso, F. Buonomo and A. Esposito, Stud. Surf. Sci. Catal., **28**, 129 (1986).

112. U. Romano, A. Esposito, F. Maspero, C. Neri and M.G. Clerici, Stud. Surf. Sci. Catal., **55**, 33 (1990).

113. J.S. Reddy, S. Sivasanker and P. Ratnasamy, J. Mol. Catal., **69**, 383 (1991).

114. J.S. Reddy, S. Sivasanker and P. Ratnasamy, J. Mol. Catal., **70**, 335 (1991).

115. J.S. Reddy, S. Sivasanker and P. Ratnasamy, J. Mol. Catal., **71**, 373 (1991).

116. J.S. Reddy and S. Sivasanker, Ind. J. Technol., **30**, 64 (1992).

117. A. Thangaraj, R. Kumar and P. Ratnasamy, J. Catal., **131**, 294 (1991).

118. T. Tatsumi, M. Nakumara, K. Yuasa and H. Tominaga, Chem. Lett., 297 (1990).

119. M.G. Clerici, G. Bellussi and U. Romano, J. Catal., **129**, 159 (1991).

120. R.S. Reddy, J.S. Reddy, R. Kumar and P. Kumar, J. Chem. Soc., Chem. Commun., 84 (1991).

121. L. Marosi, J. Stabenow and M. Schwarzmann, Ge. Pat. 2831631 (1978).

122. T. Inui, D. Medhanavyn, P. Praserthdam, K. Fukuda, T. Ukawa, A. Sakamoto and A. Miyamoto, Appl. Catal., **18**, 311 (1985).

123. A. Miyamoto, D. Medhanavyan and T. Inui, Appl. Catal., **28**, 89 (1986).

124. G. Centi, S. Perathoner, F. Trifiro, A. Aboukais, C.F. Aissi and M. Guelton, J. Phys. Chem., **96**, 2617 (1992).

125. P.R. Hari Prasad Rao, A.V. Ramaswamy and P. Ratnasamy, J. Catal., **137**, 225 (1992).

126. P.R. Hari Prasad Rao and A.V. Ramaswamy, J. Chem. Soc. Chem. Commun., 1245 (1992).

127. P.R. Hari Prasad Rao and A.V. Ramaswamy, Appl. Catal. A, **93**, 123 (1993).

128. K. Ramesh Reddy, A.V. Ramaswamy and P. Ratnasamy, J. Chem. Soc. Chem. Commun., 1613 (1992).

129. K. Ramesh Reddy, A.V. Ramaswamy and P. Ratnasamy, J. Catal. (in press).

# SYNTHESIS AND CHARACTERIZATION

## 2.1 INTRODUCTION

The use of bis-quaternary ammonium cations, as templates in zeolite synthesis, has been reviewed in chapter 1 (Table 1.3). Hence, aiming at the synthesis of high-silica large pore zeolites, we undertook detailed studies on zeolites synthesis using bis-quaternary ammonium salts, where the nature of the terminal alkyl group (methyl, ethyl and propyl) or the number of the methylene groups ($C_5$, $C_6$ or $C_7$) was systematically varied. Bis-quaternary ammonium salts used in the zeolite synthesis were $(C_2H_5)_3$-$N^+$-$(CH_2)_n$-$N^+$-$(C_2H_5)_3$ (n = 5, 6 or 7) and $R_3$-$N^+$-$(CH_2)_6$-$N^+$-$R_3$ R = methyl, ethyl or propyl). The results are presented in Table 2.1. The use of hexamethylene bis(triethylammonium bromide) resulted in a new, high-silica, large pore, zeolite, designated as NCl-1[1]. Zeolite NCL-1 can be synthesized in a fairly large range of Si/Al ratios (20 and above) including the Al-free, pure silica analog of NCL-1.

This chapter describes the synthesis and characterization of NCL-1 molecular sieve using techniques such as X-ray diffraction (XRD), framework IR, scanning electron microscopy (SEM), $^{29}Si$ and $^{27}Al$ MAS NMR, thermal analysis (TG-DTA) and adsorption ($N_2$ and other probe molecules like n-hexane, cyclohexane, mesitylene, etc.). It is shown that NCL-1 is a new, single phase, high-silica, large pore (12-membered ring) zeolite. Additional support is obtained from catalytic test reactions (chapter 4).

## 2.2. SYNTHESIS AND CHARACTERIZATION OF THE ORGANIC ADDITIVE: HEXAMETHYLENE BIS(TRIETHYLAMMONIUM BROMIDE)

The organic additive, hexamethylene bis(triethylammonium bromide) has been synthesized by quaternizing the triethylamine with 1,6-dibromohexane in the presence of acetone as solvent. The molar ratio of reactants, triethylamine to 1,6-dibromohexane was 2 according to the following reaction:

$$2\,(C_2H_5)_3N \;+\; \overset{Br}{\underset{|}{C}}H_2(CH_2)_4\overset{Br}{\underset{|}{C}}H_2 \xrightarrow[\text{refluxing}]{\text{acetone}} \left[(C_2H_5)_3N(CH_2)_6N(C_2H_5)_3\right]^{2+} 2\,Br^-$$

(highly hygroscopic white solid)
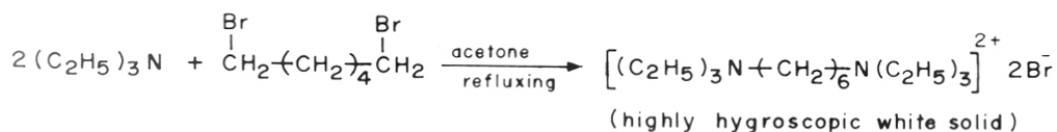
Table 2.1 Bis-quaternary organic templates and zeolite structure relationship.

| Organic template | Zeolite structure |
|---|---|
| $(C_2H_5)_3$-$N^+$-$(CH_2)_5$-$N^+$-$(C_2H_5)_3$ | ZSM-57 |
| $(C_2H_5)_3$-$N^+$-$(CH_2)_6$-$N^+$-$(C_2H_5)_3$ | NCL-1 |
| $(C_2H_5)_3$-$N^+$-$(CH_2)_7$-$N^+$-$(C_2H_5)_3$ | ZSM-23 |
| $(CH_3)_3$-$N^+$-$(CH_2)_6$-$N^+$-$(CH_3)_3$ | ZSM-48, ZSM-50 |
| $(C_3H_7)_3$-$N^+$-$(CH_2)_6$-$N^+$-$(C_3H_7)_3$ | ZSM-5 |

**Synthesis procedure:** 25 g of triethylamine (AR grade) and 20 g of acetone (AR grade) were taken in a 250 ml RB flask. To this mixture, 30 g of 1,6-dibromohexane (aldrich >99%) was added. Finally, 50 g of acetone was added. The homogeneous reaction mixture was refluxed for 10 h. After the completion of the reaction, a white salt (diquaternary salt) was formed in >90% yield m.p 220° C, (highly hygroscopic). This was separated from the reaction mixture and dried in vacuum.

The white solid was characterized by $^{1}$H and $^{13}$C NMR spectroscopy (200 MHZ in $D_2O$) and mass spectrometry (Finnigan-Mat-1020 instrument using direct inlet system at 70 ev).

The $^{1}$H NMR spectrum of the sample is shown in Fig. 2.1. The chemical shifts δ 1.01-1.37 (t, 6-C$\underline{H}_3$ 18H), 1.38-1.55 (m, 2-N-$CH_2$-$CH_2$-C$\underline{H}_2$- 4H), 1.58-1.80 (m, 2-N-$CH_2$-C$\underline{H}_2$- 4H) and 3.05-3.44 (m, 8-N-C$\underline{H}_2$ 16H). The observed chemical shift positions and integration values (from the $^{1}$H NMR spectrum) match calculated values. Thus $^{1}$H NMR data clearly suggest that the resulting sample (white solid) is hexamethylene bis(triethylammonium bromide).

$^{13}$C NMR ($D_2O$): The $^{13}$C NMR spectrum of the sample is shown in Fig.2.2. The chemical shift (δ) values and corresponding assignments are: 7.9 (6-$\underline{C}H_3$), 22.0 (2 -N-$CH_2$-$CH_2$-$\underline{C}H_2$-), 26.3 (2-N-$CH_2$-$\underline{C}H_2$-), 53.7 (6-N-$\underline{C}H_2$-$CH_3$) and 57.6 (2-N-$\underline{C}H_2$-$CH_2$-), respectively.

The Mass spectrum of the sample is shown in Fig.2.3. The lines are assinged to: m/e 228 (4%, M$^+$-2$C_2H_5Br$), 199 (7%, 228-$C_2H_5$), 154 (7%), 142(12%), 126(8%), 108(55%, $C_2H_5Br$), 101(14%, N($C_2H_5$)$_3$), 86(100%, ($C_2H_5$)$_2$N$CH_2$$^+$<--->($C_2H_5$)$_2$N$^+$=$CH_2$)), 81(11%), 72(9%, 86-$CH_2$) and 58(19%, 86-$C_2H_5$).

The IR spectrum of the sample in chloroform is shown in Fig.2.4. The absorption bands at 2926 cm$^{-1}$ (strong), 1484 cm$^{-1}$ (medium) and 1200-1240 cm$^{-1}$ are due to C-H stretching, C-H bending and C-N stretching vibrations, respectively. Absorption band due to C-Br vibration in the range of 500-600 cm$^{-1}$ has not been observed. This confirms the absence of reactant (1,6-dibromohexane) in the product.
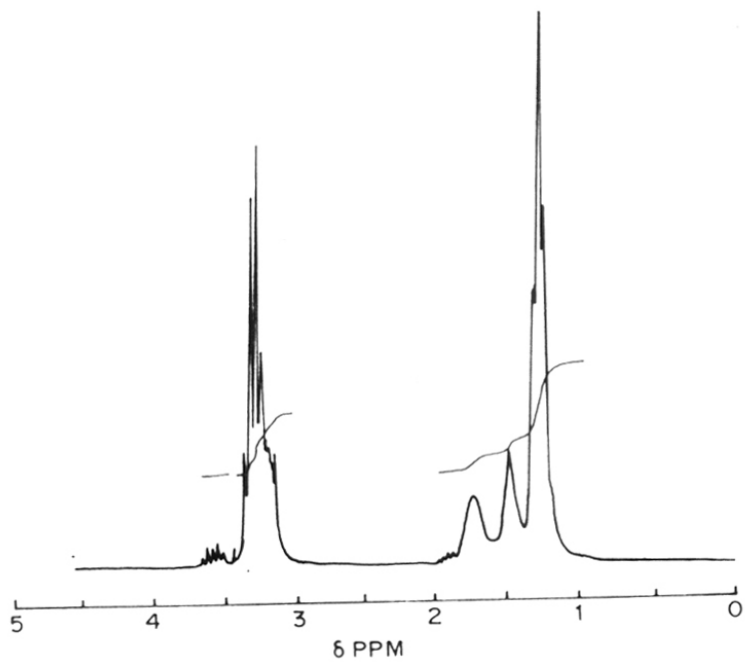
Fig.2.1　　　$^1$H NMR spectrum of hexamethylene bis(triethylammonium bromide)
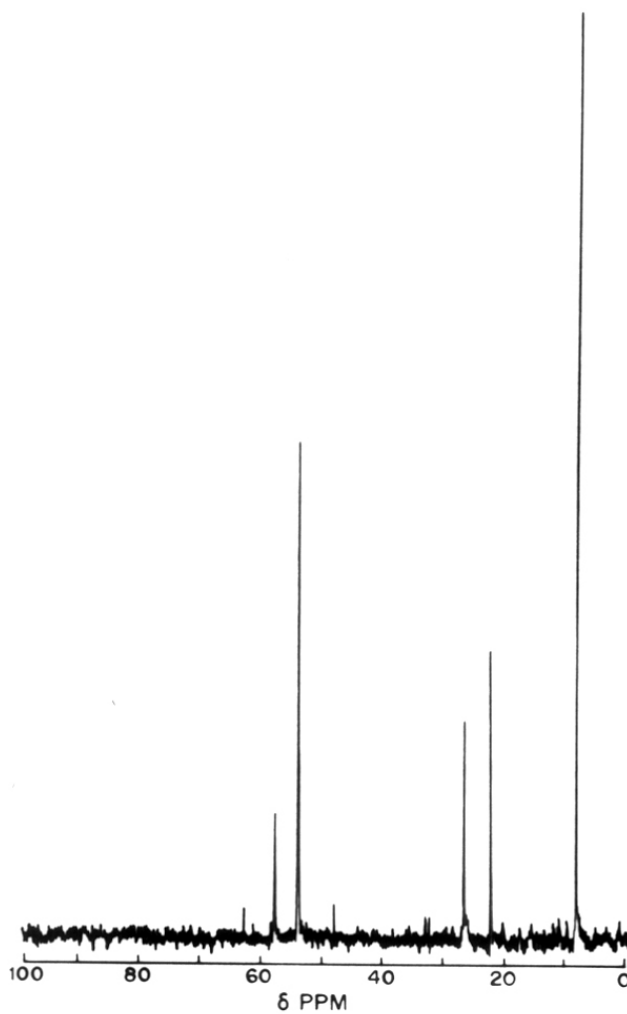
Fig.2.2        $^{13}$C NMR spectrum of hexamethylene bis(triethylammonium bromide)
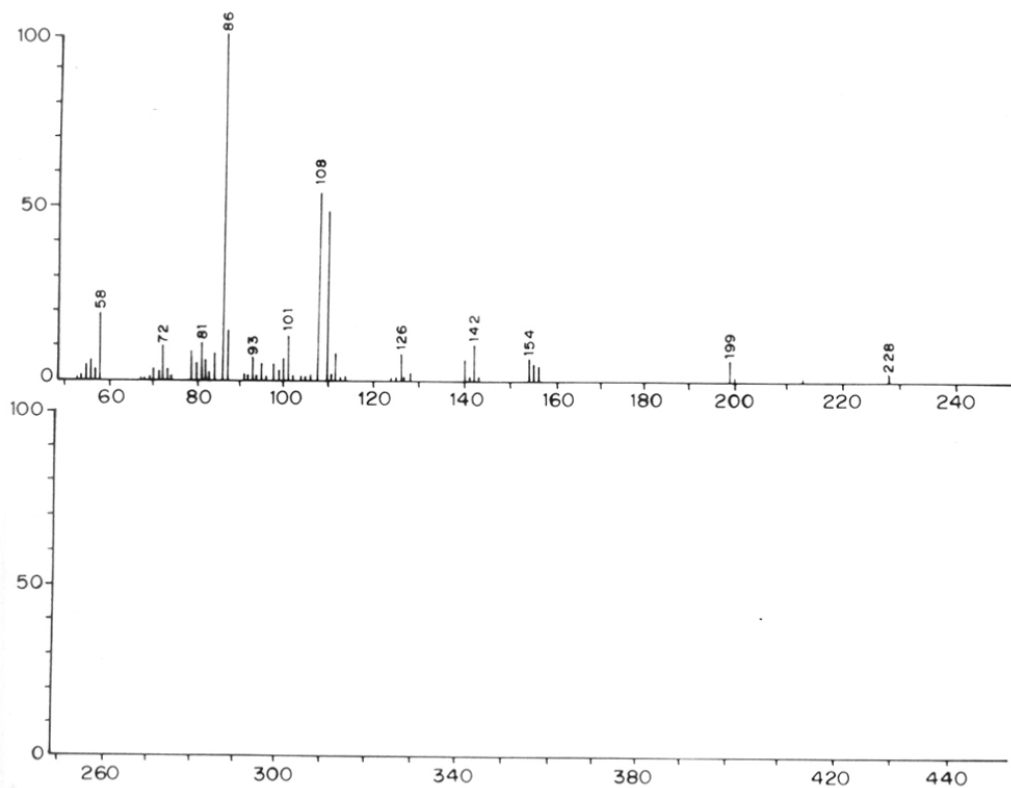
Fig.2.3    Mass spectroscopy of hexamethylene bis(triethylammonium bromide)
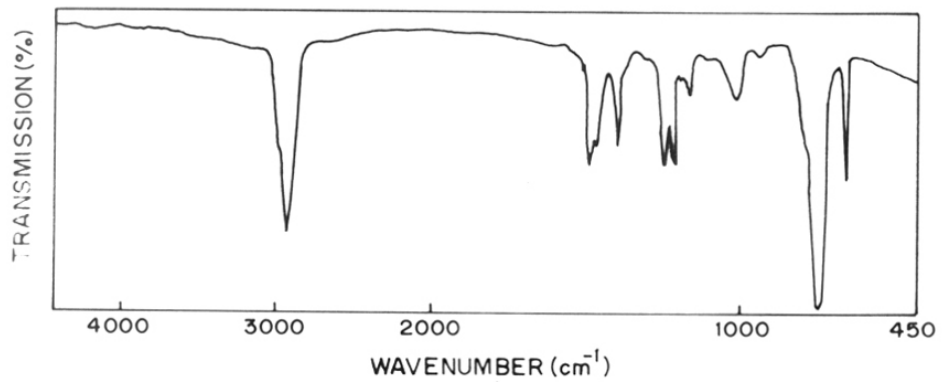
Fig.2.4        IR spectrum of hexamethylene bis(triethylammonium bromide)

Chemical analysis:

| Calculated $C_{18}H_{42}N_2Br_2$ wt.% | Found wt.% |
|---|---|
| C, 48.4 | C, 48.7 |
| H, 9.4 | H, 9.5 |
| N, 6.3 | N, 6.2 |
| Br, 35.9 | Br, 35.6 |

The above data confirm the resulting salt to be hexamethylene bis(triethylammonium bromide).

## 2.3 EXPERIMENTAL

### 2.3.1 X-ray diffraction

Rigaku (model D/MAX III VC, Japan) X-ray diffractometer, with Ni filtered Cu-Kα radiation ($\lambda$ = 1.5404 Å) was used to record powder diffraction patterns. The samples were scanned from 5 to 50 2θ° at a scan rate of 0.25° min$^{-1}$. Based on the preliminary experiments, a sample with the highest crystallinity was taken as the reference sample to compare the phase purity and crystallinity of other samples. Peak areas were calculated from the collected data, using a semi-quantitative software programme provided with the instrument. Silicon was used as the internal standard for calibrating the 2θ° values.

### 2.3.2 Infrared spectroscopy

The infrared spectra of the samples were recorded in PYE UNICAM SP3 300 spectrometer in the wavenumber range of 200-1300 cm$^{-1}$ using the Nujol mull technique. KCN was used as the internal standard.

### 2.3.3 Adsorption studies

The sorption measurements for water, n-hexane, cyclohexane, benzene, $o$-xylene and mesitylene were carried out gravimetrically using a Cahn electromicrobalance (Model: Cahn-2000 G). The calcined sample of about 60 mg was pressed into a pellet and weighed into an

aluminium bucket which was attached to the balance. The system was evacuated to a pressure of $1.33 \times 10^{-4}$ Pa at 673 K. After four hours, the temperature was lowered to the 298 K. The sorbate was admitted into the sample at a constant pressure and the weight gain was recorded as a function of time. After an adsorption measurement, the catalyst was heated to 673 K under vacuum and used for the next experiment.

### 2.3.4 Surface area measurements

Omnisorb 100 CX unit (supplied by COULTER Corporation, USA) was used for the measurement of nitrogen adsorption. The samples were activated at 673 K for 4 h in high vacuum ($1.33 \times 10^{-4}$ Pa). After the treatment, the anhydrous weight of the sample was taken. Adsorption of $N_2$ was carried out at liquid $N_2$ temperature (77 K). From the adsorption isotherm, the BET surface area was calculated[2].

### 2.3.5 Solid state MAS NMR spectroscopy

The high resolution MAS NMR (magic angle spinning) spectra for $^{29}$Si were obtained at room temperature on a Bruker MSL-300 spectrometer, operating in Fourier transform mode[3]. A 90° pulse with 3 seconds delay-time was used for $^{29}$Si nuclei and chemical shifts ($\delta$) in ppm were measured with respect to tetramethylsilane (TMS) as an external reference. The rotor (sample holder) was spun at a rate of 4.0 KHz.

$^{27}$Al MAS NMR spectra were obtained using a 45° pulse with 1 second delay-time. Chemical shifts in ppm were measured with respect to aqueous (0.1N) $Al(NO_3)_3$ solution $(Al(H_2O)_6^{3+})$ as an external standard.

### 2.3.6 Thermal analysis

Simultaneous TG-DTA analyses of as-synthesized samples were carried out in a computer controlled thermal analyzer instrument (Setaram, France, model TG-DTA-92). A linear rate of heating of 10° min$^{-1}$ in the range from room temperature to 1173 K in air flow (30 ml min$^{-1}$) was employed to find out the temperature of decomposition of the organic additive and weight loss. 30 mg of sample was taken with inert $\alpha$-alumina as a reference.

### 2.3.7 Ion-exchange capacities

The calcined samples were treated with saturated NaCl solution for 10 h at 298 K to get the Na-form of the zeolites. This was then washed thoroughly with distilled water and exchanged with 1 N KCl for 8 h at 353 K. The solid was filtered, washed thoroughly with distilled water and dried at 373 K for 10 h. The resultant material (Na-form and K-form) were analyzed for sodium, potassium and aluminium.

### 2.3.8 Scanning electron microscopy

The morphology of the samples was investigated using a scanning electron microscope (model JSM 5200, JEOL, Japan). The sample was dusted on alumina and coated with a thin film of gold to prevent surface charging and to protect zeolite material from thermal damage by the electron beam. In all the analyses a uniform thickness of about 0.1 mm was maintained.

### 2.3.9 Chemical analysis

An known amount of sample ($W_1$) was taken in a platinum crucible with a lid and ignited. The sample was then cooled in desiccator and weighed ($W_2$). The difference in weights ($W_1$-$W_2$) gave the weight loss on ignition. The anhydrous weight of the sample was noted, and the sample was then treated with hydrofluoric acid (40 wt.% electronic grade) and evaporated on a hot plate to remove silicon in the form of $H_2SiF_6$. This treatment was repeated three times and the sample was again ignited, cooled in desiccator and weighed. The loss in the weight of the sample indicated the content of silica. The residue was fused with potassium pyrosulfate and dissolved in distilled water. The solution was then analyzed for Al and Na by atomic absorption spectroscopy.

## 2.4 RESULTS AND DISCUSSION

### 2.4.1 Hydrothermal synthesis of NCL-1

The hydrothermal syntheses were carried out using 100 ml capacity stainless steel autoclaves (Fig.2.5) under agitation (60 rpm). Before use, the autoclaves were thoroughly cleaned with 40% HF to minimize the possible seeding effect of residual crystalline products. The raw materials used in the syntheses were fumed silica (Sigma, USA, S-5005, 99.9%),

TEFLON GASKET
80 × 65 × 3

BOLT & NUT
Ø 10 × 30 mm Long

7 mm

150 mm

Ø 55 mm

Ø 65 mm
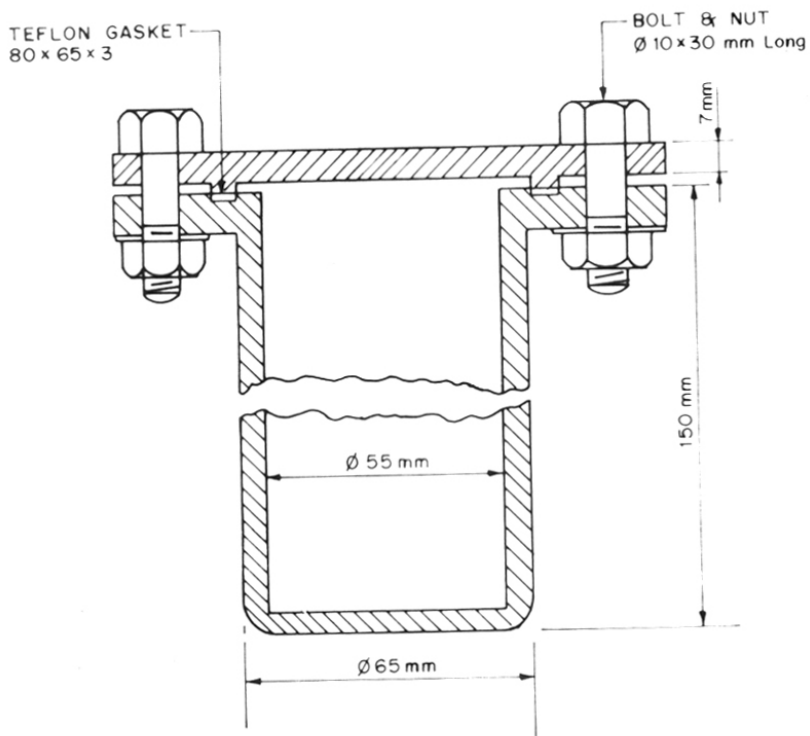
Fig.2.5    Stainless steel (316) autoclave with teflon gasket was used in the hydrothermal synthesis.

$Al_2(SO_4)_3.16H_2O$ (98%), sodium hydroxide (99% AR), sulfuric acid (96%) and hexamethylene bis(triethylammonium bromide) as an organic additive. The following molar gel composition of the reaction mixture was used for the synthesis of NCL-1 samples with Si/Al ratios (in the gel) 20, 80, 150, 250 and Al-free silica polymorph.

$R^{2+}/Si = 0.05$; $OH^-/Si = 0.12$; $Na^+/Si = 0.25$; $H_2O/Si = 52$.

(where $OH^- = [Na^+] - 2\,[SO_4^{2-}]$)

The $OH^-/Si$ ratio was adjusted at 0.12 by adding appropriate amount of sulfuric acid. In a typical preparation, the following procedure was used: A solution containing 0.75 g NaOH in 10 g $H_2O$ was added to a slurry of 4.5 g fumed silica in 30 g $H_2O$. This mixture was stirred for 45 min at 298 K. To the above mixture, the required amount of aluminium sulphate solution (1.18, 0.29, 0.16 and 0.09 g of $Al_2(SO_4)_3.16H_2O$ in 10 g of water, to yield Si/Al ratios 20, 80, 150 and 250, respectively) was added. The mixture was stirred for 20 min before adding to it a solution of 1.71 g hexamethylene bis(triethylammonium bromide) in 15 g $H_2O$. Finally, 0.36, 0.42, 0.45 and 0.5 g $H_2SO_4$ in 10 g water was added (for Si/Al ratios 80, 150, 250 and $\infty$, respectively). No $H_2SO_4$ was added for the sample having Si/Al ratio of 20. The resultant reaction mixture was stirred for 1 h and then autoclaved. The crystallization was conducted at $443 \pm 2$ K in a rotating (60 rpm) container placed in an oven. The crystallization times were 3, 4, 7, 10 and 13 days for samples having Si/Al = $\infty$, 250, 150, 80 and 20, respectively. After crystallization, the solid was filtered, washed with water and dried at 393 K and finally calcined in flowing dry air at 723 K. The yield of crystalline solid ranged between 85 and 90 for all the samples.

### 2.4.2 Chemical analysis

The chemical compositions of all Al-NCL-1 as determined from chemical analysis, are given in Table 2.2. Si/Al ratios in the gel and in the products were almost similar. The Si/Al molar ratio of the calcined (product) samples are 23, 84, 156, 257 and >3000, these samples were prepared from the gel containing Si/Al ratio 20, 80, 150, 250 and >3000, respectively.

Table 2.2: Physico-chemical properties of NCL-1 molecular sieves

| Sample | Si/Al in gel | Si/Al in product | $K^+$/Al | Surface area, $m^2/g$[a] | Unit cell volume,[b] $\text{Å}^3$ | Sorption capacity, (wt.%)[c] | | | | | |
|---|---|---|---|---|---|---|---|---|---|---|---|
| | | | | | | n-hexane | benzene | cyclohexane | o-xylene | mesitylene | water |
| NCL-1 | 20 | 23 | 0.86 | 315 | 2874 | 6.7 | 7.74 | 6.36 | 7.24 | 4.68 | 8.76 |
| NCL-1 | 80 | 84 | 0.89 | 318 | 2871 | 6.84 | 7.78 | 6.45 | 7.32 | 4.72 | 5.20 |
| NCL-1 | 150 | 156 | 0.91 | 323 | 2869 | 6.91 | 7.85 | 6.43 | 7.22 | 4.80 | 4.62 |
| NCL-1 | 250 | 257 | 0.90 | 329 | 2867 | 6.89 | 7.81 | 6.49 | 7.25 | 4.69 | 4.12 |
| Si-NCL-1 | >3000 | >3000 | -- | 339 | 2867 | 6.96 | 7.84 | 6.50 | 7.4 | 4.77 | 3.77 |

[a] From $N_2$ adsorption ($p/p_o$ = 0.005-0.01).

[b] Considering orthorhombic symmetry with a = 1.195±0.003, b = 0.836±0.003, c = 2.870±0.004 nm.

[c] Gravimetric adsorption at 298 K and at $p/p_o$ = 0.5.

### 2.4.3 Characterization

### 2.4.3.1 X-ray diffraction

The X-ray powder diffraction pattern of NCL-1 samples with different Si/Al ratios are shown in Fig.2.6. The profiles 'a' to 'e' refer to the calcined samples having Si/Al mole ratio of (in product) 23, 84, 156, 257, >3000 (i.e. silica polymorph of NCL-1 (Si-NCL-1)), respectively and profile 'f' represents the as-synthesized form of Si-NCL-1. The Fig.2.6 shows that after calcination (compare profile 'e' and 'f'), the intensities of the peaks at lower $2\theta°$ range (5-10 $2\theta°$) increased substantially. The increase in intensity is due to the removal of organic cations, present in the crystalline voids. Similar results have been reported for EU-1 and pentasil zeo-lites[4,5].

During crystallization of NCL-1 samples, all the major lines grow simultaneously and the relative intensity of all the major peaks remain unchanged even when the crystallization period is further extended (after the complete crystallization). The fully crystalline samples of NCL-1 obtained during detailed crystallization kinetic study (Chapter 3), exhibited essentially the same XRD pattern with similar relative intensities. Further, scanning electron microscopy (Fig.2.13) also shows that the morphology of NCL-1 is like either needles or probably bundle of needles (oblong shaped). These observations suggest that NCL-1 is a single crystalline phase.

Recently, during our survey of the available literature to compare the XRD pattern of NCL-1 with that of reported materials, we found that NCL-1 and SSZ-31 (synthesized using N,N,N-trimethyl-8-ammonium tricyclo[5.2.1.0$^{2.6}$]decane as organic additive and filed for US patent by Chevron researchers[6]), have some common major XRD lines (Fig.2.7). The XRD pattern (line diagrams simulated from $2\theta°$/d Å and $I/I_o$ values) of NCL-1, SSZ-31[6], ZSM-12[7] and ZSM-48[8] are depicted in Fig.2.7. To check the possibility of the presence of one of these zeolites (SSZ-31, ZSM-12 or ZSM-48) either individually or along with some other crystalline phase, we have analysed the data carefully. Considering the possibility of minor shift in $2\theta°$ due to different experimental and instrumental conditions for XRD data available in the literature (Table 2.3), we have followed two criteria for comparing the XRD patterns: Criterion I: the difference between the $2\theta°$ values of two most strong lines ($\Delta 2\theta(I)$) in the $2\theta$ region: 7 to 9°,
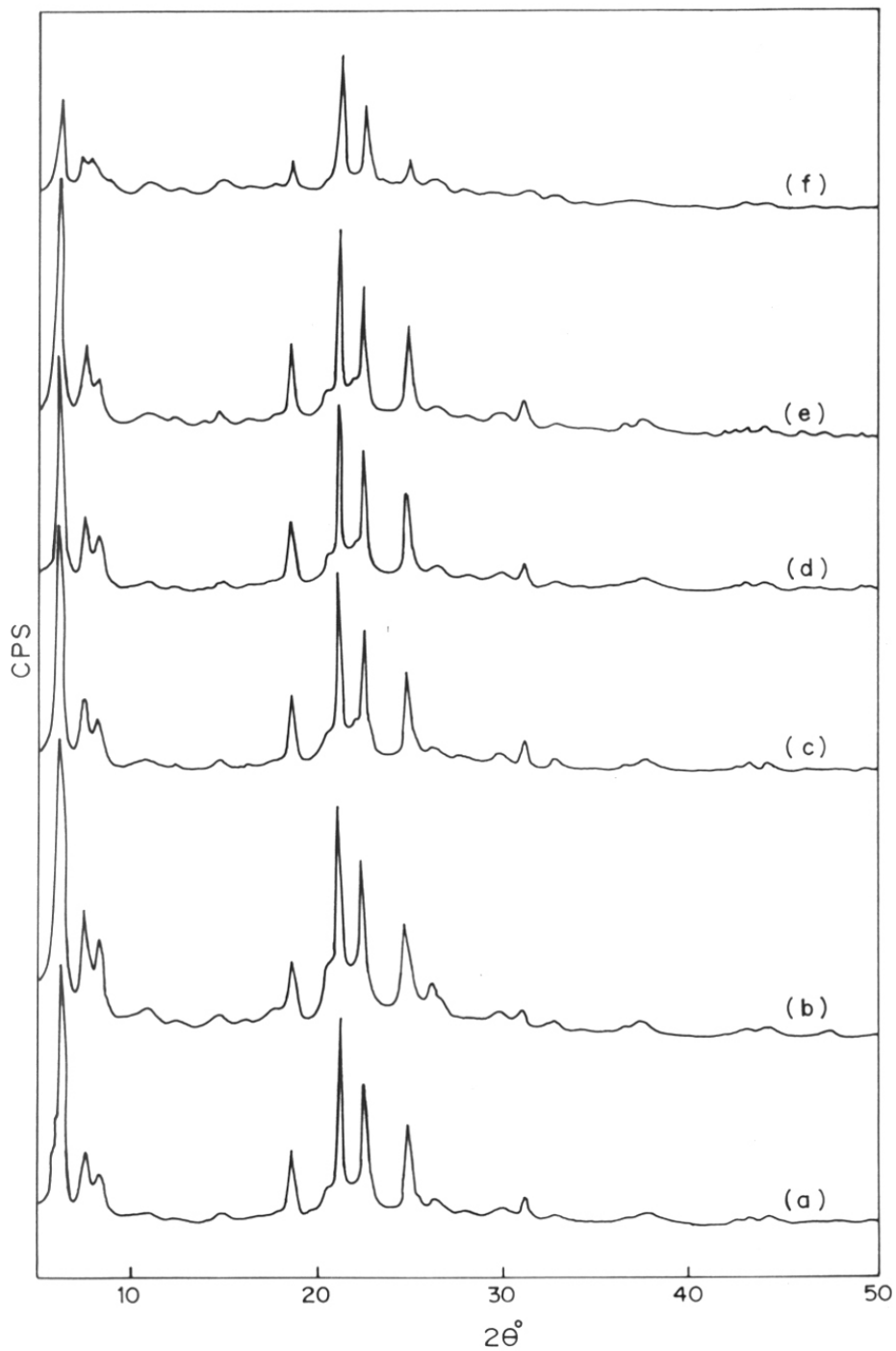
Fig.2.6    X-ray diffraction patterns of calcined NCL-1 samples, curves 'a' to 'f' refer to
samples with Si/Al (molar ratio) of 23, 84, 156, 257, >3000 and >3000 (as-
synthesized form), respectively.
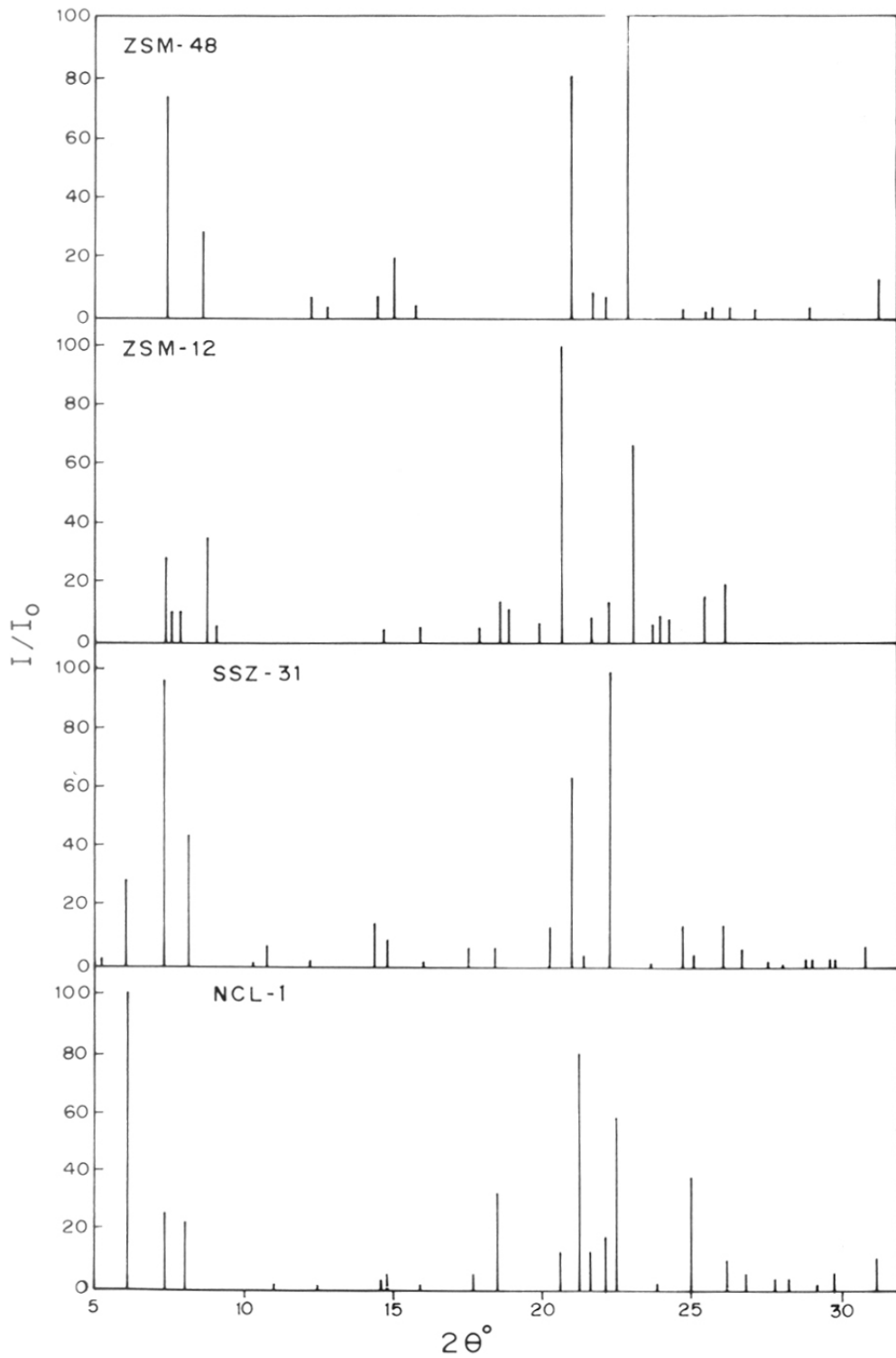
Fig.2.7       XRD pattern of NCL-1, SSZ-31, ZSM-12 and ZSM-48. The line diagrams simulated from $2\theta°$ or 'd' Å and $I/I_o$.

Table 2.3 X-ray diffraction data of different zeolites

| NCL-1 | | SSZ-31 | | ZSM-12 | | ZSM-48 | |
|---|---|---|---|---|---|---|---|
| 2θ° | I/Io | 2θ° | I/Io | 2θ° | I/Io | 2θ° | I/Io |
| -- | -- | 5.045 | 2 | -- | -- | -- | -- |
| 6.154 | 100 | 6.094 | 27 | -- | -- | -- | -- |
| 7.392 | 25 | 7.385 | 96 | 7.423 | 27 | 7.479 | 74 |
| -- | -- | -- | -- | 7.615 | 10 | -- | -- |
| 8.046 | 22 | 8.18 | 43 | 7.923 | 10 | -- | -- |
| -- | -- | -- | -- | 8.818 | 35 | 8.67 | 29 |
| -- | -- | -- | -- | 9.091 | 5 | -- | -- |
| -- | -- | 10.338 | 1 | -- | -- | -- | -- |
| -- | -- | 10.807 | 6 | -- | -- | -- | -- |
| 11.023 | 2 | -- | -- | -- | -- | -- | -- |
| 12.44 | 1 | 12.198 | 2 | -- | -- | 12.3 | 7 |
| -- | -- | -- | -- | -- | -- | 12.838 | 3 |
| -- | -- | 14.37 | 14 | -- | -- | -- | -- |
| 14.58 | 2 | -- | -- | -- | -- | 14.509 | 7 |
| 14.777 | 5 | 14.827 | 9 | 14.703 | 5 | 15.106 | 20 |
| 15.91 | 1 | 15.985 | 1 | 15.898 | 5 | 15.784 | 4 |
| 17.66 | 4 | 17.512 | 5 | 17.868 | 5 | -- | -- |
| 18.508 | 32 | 18.446 | 6 | 18.665 | 14 | -- | -- |
| -- | -- | -- | -- | 18.865 | 11 | -- | -- |
| -- | -- | 20.352 | 13 | 19.936 | 6 | -- | |
| 20.639 | 12 | -- | -- | 20.736 | 100 | -- | -- |
| 21.238 | 81 | 21.085 | 64 | -- | -- | 21.085 | 82 |
| 21.6 | 13 | 21.514 | 4 | 21.657 | 8 | 21.765 | 9 |
| 22.13 | 17 | -- | -- | -- | -- | -- | -- |
| 22.433 | 59 | 22.381 | 100 | 22.319 | 14 | 22.262 | 8 |
| -- | -- | -- | -- | 23.082 | 67 | 22.842 | 100 |
| 23.86 | 2 | 23.758 | 1 | 23.707 | 5 | 23.771 | 3 |
| -- | -- | -- | -- | 23.966 | 9 | -- | -- |
| -- | -- | -- | -- | 24.366 | 7 | 24.571 | 3 |
| 24.992 | 38 | 24.829 | 14 | -- | -- | 24.780 | 4 |
| -- | -- | 25.179 | 4 | 25.502 | 16 | -- | -- |
| 26.188 | 10 | 26.181 | 14 | 26.267 | 20 | -- | -- |
| 26.83 | 6 | 26.782 | 6 | -- | 20 | 26.426 | 4 |
| 27.84 | 4 | 27.681 | 2 | -- | -- | 27.249 | 4 |
| 28.26 | 4 | 28.181 | 1 | -- | -- | -- | -- |
| -- | -- | 28.927 | 3 | -- | -- | -- | -- |
| 29.22 | 4 | 29.159 | 3 | -- | -- | 29.062 | 4 |
| 29.82 | 6 | 29.807 | 3 | -- | -- | -- | -- |
| -- | -- | 29.970 | 3 | -- | -- | -- | -- |
| -- | -- | 30.971 | 7 | -- | -- | -- | -- |
| 31.137 | 11 | -- | -- | -- | -- | 31.361 | 14 |
| -- | -- | 32.291 | 3 | -- | -- | -- | -- |
| -- | -- | 32.827 | 3 | -- | -- | -- | -- |

and criteria II: the difference between the $2\theta°$ values of two most intense lines ($\Delta\ 2\theta$ (II))in the $2\theta$ region: 20.5 to 23.5°, because all the four zeolites exhibit very strong lines in this region. If, the position as well as the $\Delta2\theta$ (I) and $\Delta2\theta$ (II) values of these strong peaks are similar, then there is a possibility that the materials are similar. The values for both the criteria are listed in Table 2.4. The value (in $2\theta°$) of $\Delta2\theta$(I) increases in the order: 0.654 (NCL-1) ≤ 0.795 (SSZ-31) < 1.191 (ZSM-48) < 1.391 (ZSM-12). The criterion II i.e. the value (in $2\theta°$) of $\Delta2\theta$(II) also follows the similar trend: 1.195 (NCL-1) ≤ 1.296 (SSZ-31) < 1.757 (ZSM-48) < 2.346 (ZSM-12). Further, the relative intensities of the major peaks follow different trend in all the samples. Hence, on the basis of above discussion it may be argued that : (i) the presence of ZSM-12 and ZSM-48 in NCL-1 can safely be ruled out, (ii) NCL-1 and SSZ-31 are perhaps related structures. Although, the XRD patterns of NCL-1 and SSZ-31 show quite similarity, there are some lines which are not common, (Fig. 2.7 and Table 2.3). For example, the XRD peaks at $2\theta = 20.639°$, 22.13° and 31.137° with $I/I_o$ 12, 17 and 11, respectively of NCL-1 are absent in that of SSZ-31. Similarly, the peaks at $2\theta = 14.37°$, 20.352° and 30.971° with $I/I_o = 14$, 13 and 7, respectively exhibited by SSZ-31 are absent in the pattern of NCL-1. Apart from these differences, the relative $I/I_o$ values of most of the lines (both strong and weak) of NCL-1 and SSZ-31 are quite different. Since the information available about SSZ-31 is very much limited (only 'd' and $I/I_o$ values), we, therefore, tentatively conclude, on the basis of similarities and dissimilarities between XRD pattern of NCL-1 and SSZ-31, that these two materials are not the same. However, it is quite likely that they may be the members of same family, like ZSM-5 and ZSM-11 or FAU, EMT, ZSM-20 etc. It may be recalled here that NCL-1 (hexamethylene bis(triethylammonium bromide) and SSZ-31 (N,N,N-trimethyl-8-ammonium tricyclo[$5.2.1.0^{2.6}$]decane) are synthesized with different organic additives.

The main peaks of the calcined Si-NCL-1 sample are listed in Table 2.5. The interplanar 'd' spacings were calibrated using silicon as a internal standard and given in nm. The relative intensities ($I/I_o$) of the lines were obtained by smoothing, background correction and $K\alpha_2$ stripping. The indexing was performed by trial and error method using PDP11 software. After indexing the lines, the unit cell parameters and crystal symmetry were examined critically and was found to fit into orthorhombic symmetry. From this it was found that NCL-1 possesses

Table 2.4 The criteria I and II of different zeolites.

| Zeolite | Criterion I $\Delta 2\theta = 7\text{-}9°$ | Criterion II $\Delta 2\theta = 20.5\text{-}23.5°$ |
|---------|------------|------------|
| NCL-1 | 8.046 - 7.392 = 0.654 | 22.433 - 21.238 = 1.195 |
| SSZ-31 | 8.180 - 7.385 = 0.795 | 22.381 - 21.085 = 1.296 |
| ZSM-48 | 8.670 - 7.479 = 1.191 | 22.842 - 21.085 = 1.757 |
| ZSM-12 | 8.818 - 7.423 = 1.391 | 23.082 - 20.736 = 2.346 |

Table 2.5. XRD pattern of calcined Si-NCL-1[a].

| d(expt.) nm | I/I$_o$ | hkl | d(calc.) nm |
| --- | --- | --- | --- |
| 1.435 | 100 | 002 | 1.435 |
| 1.195 | 25 | 100 | 1.195 |
| 1.098 | 22 | 101 | 1.102 |
| 0.802 | 2 | 110 | 0.808 |
| 0.711 | 1 | 004 | 0.712 |
| 0.607 | 2 | -- | -- |
| 0.599 | 5 | 014 | 0.599 |
| 0.556 | 1 | 113 | 0.556 |
| 0.502 | 4 | 203 | 0.501 |
| 0.479 | 32 | 006 | 0.478 |
| 0.430 | 12 (sh) | 213 | 0.431 |
| 0.418 | 81 | 020 | 0.418 |
| 0.411 | 13 (sh) | 205 | 0.411 |
| 0.401 | 17 (sh) | 214 | 0.401 |
| 0.396 | 59 | 300 | 0.398 |
| 0.373 | 2 | -- | -- |
| 0.356 | 38 | 008 | 0.358 |
| 0.340 | 10 | --- | --- |
| 0.332 | 6 | 222 | 0.331 |
| 0.320 | 4 | 314 | 0.320 |
| 0.316 | 4 | 026 | 0.315 |
| 0.305 | 4 | 208 | 0.305 |
| 0.299 | 6 | -- | -- |
| 0.287 | 11 | 0010 | 0.287 |

[a] Orthorhombic symmetry with a = 1.195±0.003, b = 0.836±0.003 and c = 2.870±0.004 nm.

orthorhombic symmetry with a = 1.195 ± 0.03, b = 0.836 ± 0.003 and c = 2.870 ± 0.004 nm. The 'd' values calculated on the basis of the above unit cell dimensions compare reasonably well with those observed experimentally (Table 2.5).

### 2.4.3.2 Infrared spectroscopy

The framework IR spectra (1300-200 cm$^{-1}$ region) of the calcined samples of NCL-1 with Si/Al ratios 23, 84, 156, 257 and >3000 are shown in Fig. 2.8 and the values are presented in Table 2.6. The Figure 2.8 exhibits distinct absorption bands at 1230, 1098, 793, 548, 468, 395 and 610 cm$^{-1}$. Based on literature values[9] for crystalline aluminosilicate molecular sieves, these absorption bands are tentatively assigned to internal asymmetric stretch (1230 cm$^{-1}$), external asymmetric stretch (1098 cm$^{-1}$), external symmetric stretch (793 cm$^{-1}$), double rings (548 cm$^{-1}$) and TO bending vibrations of TO$_4$ tetrahedra (468 cm$^{-1}$) (T = Si or Al). The presence of the band around 610 cm$^{-1}$ probably due to external links of 5-membered rings. The bands around 590-620 cm$^{-1}$ are observed in ZSM-5 type zeolites and are usually assigned to external links of complex 5-membered rings[10].

Infrared spectroscopy is useful technique for quick identification of subunits present in a zeolite[11]. The absorption around 550 cm$^{-1}$ is attributed to a structure-sensitive band caused by 5-5 and 5-3 type double 5-member ring blocks that are present in pentasil zeolites (ZSM-5 and ZSM-11) structures[12,13]. For the mordenite family, the absorptions bands are observed near 560 cm$^{-1}$, as reported for structures with the type 5-3 block[12,13]. The structure sensitive absorption band at 550 cm-1, observed in NCL-1, is perhaps, due to the presence of 5-5 and 5-3 type double 5-member ring blocks.

### 2.4.3.3 Adsorption studies

One of the distinguishing properties of molecular sieves is their ability to discriminate amongst molecules of different sizes. Those molecules whose critical diameter is smaller than the dimensions of the pore openings are easily adsorbed while those that are larger are either excluded or adsorbed with difficulty. Thus, the rates and extent of adsorption of molecules with different critical diameter provide insight into the size of the pore openings in the zeolite.
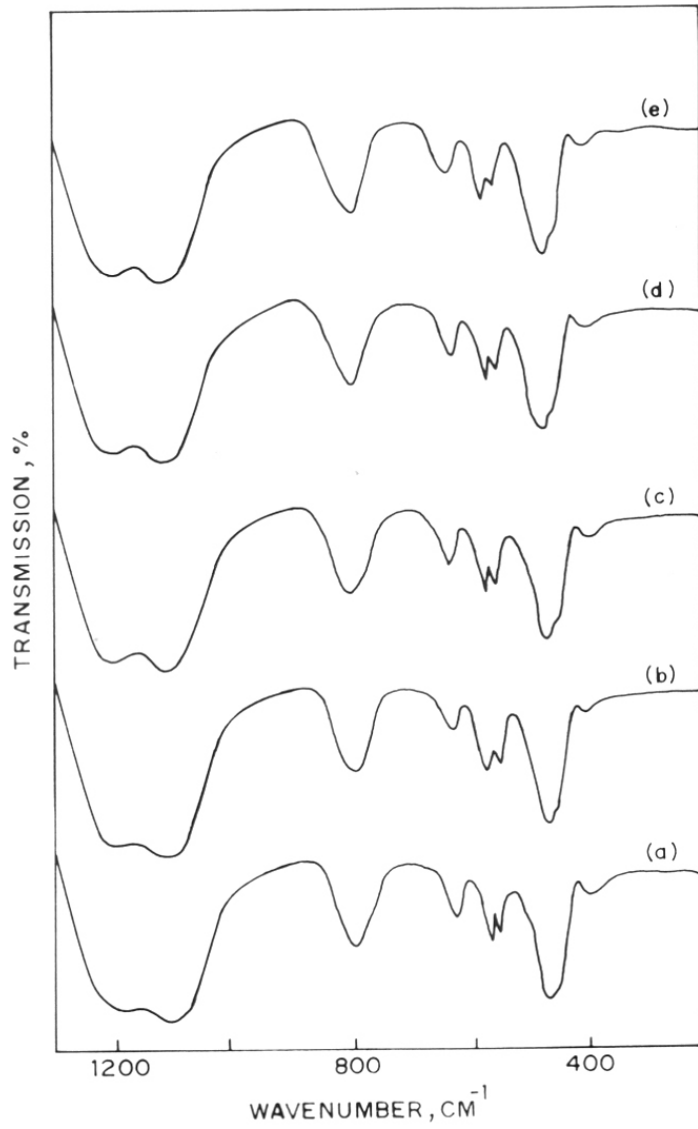
Fig.2.8    Framework IR spectra of NCL-1 calcined samples. Curves 'a' to 'e' refer to samples with Si/Al (molar ratio) of 23, 84, 156, 257 and >3000, respectively.

Table 2.6 Tentative assignment of infrared bands of Si-NCL-1

Internal Tetrahedra

| | |
|---|---|
| Asymmetric stretching | 1230 cm$^{-1}$ |
| T-O bend | 468 cm$^{-1}$ |

External linkages

| | |
|---|---|
| Double ring | 548 cm$^{-1}$ |
| Pore opening | 395 cm$^{-1}$ |
| Symmetric stretching | 793 cm$^{-1}$ |
| Asymmetric stretching | 1098 cm$^{-1}$ |

The adsorption isotherms of $N_2$, benzene and $p$-xylene on Si-NCL-1 are shown in Fig. 2.9. These adsorption isotherms are type I and reversible, and are characteristic of molecular sieves. The adsorption of six sorbate molecules of varying critical diameters on NCL-1 samples with different Si/Al ratio is listed in Table 2.2. The amount of uptake of $H_2O$ increases with a decrease in Si/Al ratio. Uptake of water is indicative of the relative hydrophobicity/hydro-philicity of the zeolite and increases with Al content.

Table 2.7 shows the amount of adsorption of three sorbate molecules of varying critical diameters in the pores of the silica polymorph of NCL-1, along with the adsorption values in other zeolites belonging to the small, medium and large pore categories whose openings are constituted by 8, 10 and 12 $TO_4$ (T = Si or Al) tetrahedra, respectively. From the adsorption volume of mesitylene (critical diameter = 0.78 nm) on NCL-1, it can be inferred that NCL-1 belongs to the large-pore category with pore openings made up of 12-membered ring tetrahedra.

The sorption data also provide information about the secondary cage structure. The measured sorption capacities of Si-NCL-1 (Table 2.2) are 7.4 wt.% for $o$-xylene and 6.96 wt.% for n-hexane, respectively. The agreement between these values demonstrates that all of the pore volume accessible to n-hexane is also accessible to $o$-xylene. This rules out the possible occurrence of accessible secondary cages with 8-ring apertures, which would admit n-hexane while excluding $o$-xylene.

Fig. 2.10 illustrates the rates of adsorption of n-hexane, cyclohexane, mesitylene, and water on Si-NCL-1 sample at $p/p_o = 0.5$. The equilibrium value of adsorption of n-hexane and cyclohexane are reached in around 3 min. The equilibrium value for mesitylene (0.78 nm critical diameter) is also reached in about the same time. Hence, NCL-1 probably belongs to the category of large pore zeolites. The diffusion coefficients of NCL-1 for n-hexane, cyclohexane and 1,3,5-trimethylbenzene (mesitylene) were measured from the corresponding rates of adsorption (Fig.2.10). From the initial, linear portion of the plots of $(Q_t/Q_x)$ versus $\sqrt{t}$ ($Q_t$ and $Q_x$ are the amount adsorbed at time t and equilibrium value, respectively) and using values of the average particle size, obtained from scanning electron microscopy[14], the diffusivity values for n-hexane, cyclohexane and mesitylene were found to be 8.5, 3.4 and 0.6 X $10^{-11}$ $cm^2$ $sec^{-1}$, respectively.
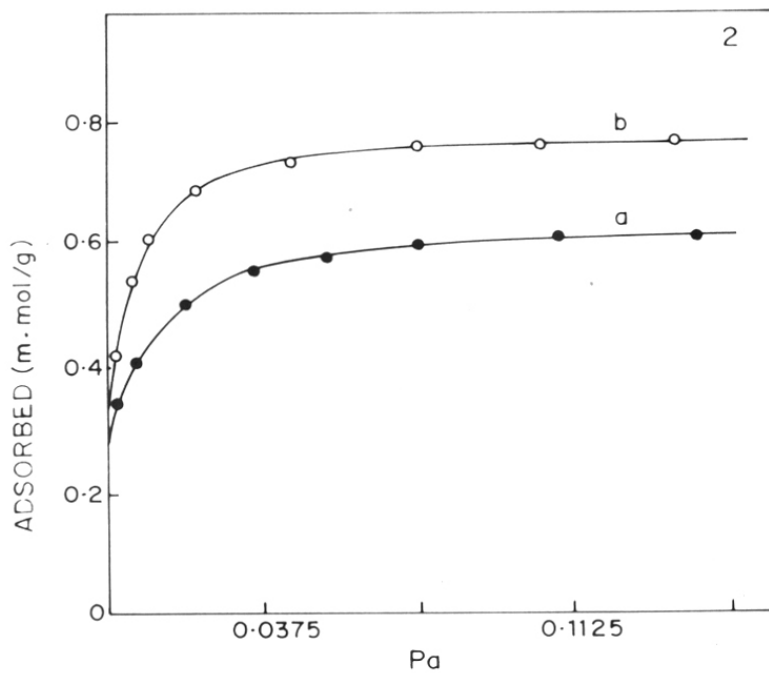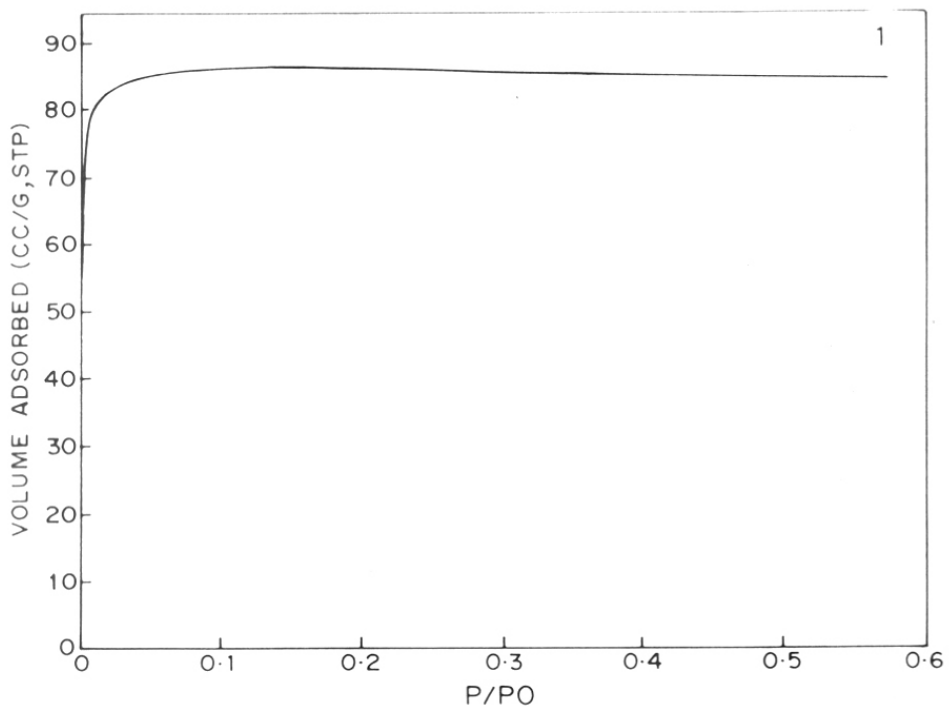
Fig.2.9    Adsorption isotherms of N₂ at 77 K (curve 1), p-xylene (curve 2'a') and benzene (curve 2'b') at 298 K, respectively.

Table 2.7: Adsorption (wt.%) in zeolites 298 K, p/p$_o$ =0.5.

| Sorbate | n-hexane | Cyclohexane | Mesitylene |
|---|---|---|---|
| Critical dia., (nm) | 0.49 | 0.61 | 0.78 |
| **Small pore** | | | |
| Linde 5A | 14.90 | 0.80 | 0.40 |
| **Medium pore** | | | |
| ZSM-5 | 13.50 | 6.80 | 0.50 |
| ZSM-23 | 8.50 | 4.30 | 1.00 |
| ZSM-48 | 5.80 | 3.20 | <0.10 |
| **Large pore** | | | |
| Zeolite Y | 20.90 | 21.80 | 24.00 |
| Mordenite | 11.40 | 11.70 | 7.20 |
| ZSM-12 | 8.30 | 10.30 | 2.60 |
| Beta | 15.90 | 18.30 | 17.00 |
| NCL-1 | 6.96 | 6.50 | 4.80 |
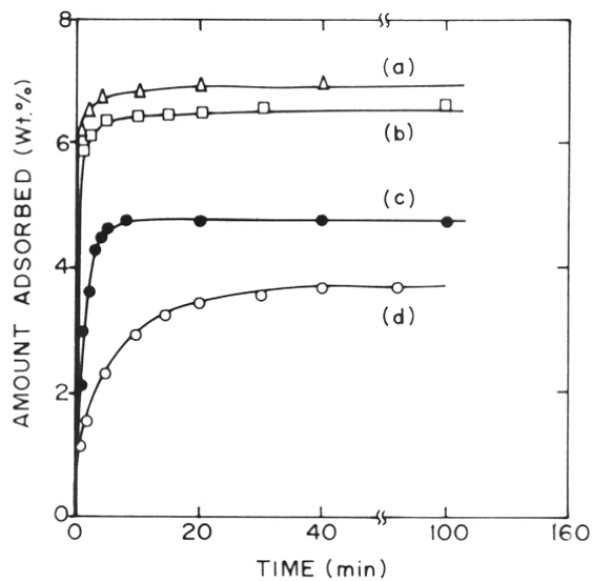
Fig.2.10 The amount adsorbed in Si-NCL-1 sample (conditions: Temp. 298 K and $p/p_o$ = 0.5). Curves 'a' to 'd' refer to sorbates n-hexane, cyclohexane, mesitylene and water, respectively.

### 2.4.3.4 Surface area measurements

The low pressure ($p/p_o$ = 0.005-0.01) nitrogen adsorption isotherm at liquid nitrogen temperature is typical of microporous material. The apparent surface area of the NCL-1 sample with different Si/Al ratios are given in Table 2.2. From the adsorption isotherms of $N_2$, BET surface area was calculated[2a]. The mesopore area was calculated from the t-plots[2b]. The surface area of the sample are in the range of 315 to 340 $m^2/g$ and t area (due to mesoporous impurities) of only 5-20 $m^2/g$, indicate the absence of any appreciable amount of amorphous phase in the samples.

### 2.4.3.5 Solid state MAS NMR spectroscopy

The solid state MAS NMR spectra of $^{29}$Si and $^{27}$Al in calcined samples of NCL-1 of varying Si/Al ratios are illustrated in Fig.2.11. The $^{29}$Si spectrum exhibited only one major signal at -112 ppm (with respect to TMS attributable to Si(OAl) tetrahedra). A very weak shoulder at -101 ppm is observed in samples containing aluminium which is attributable to Si(1Al). The position of $^{29}$Si NMR signal at -112 ppm of NCL-1 sample is similar to that in silica-rich aluminosilicates[15]. The samples containing aluminium exhibited only one signal at 52 ppm in the $^{27}$Al spectrum (Fig.2.11('a' and 'b')) characteristic of tetrahedral Al[15]. The intensities of the signal increased with aluminium content and no signal due to octahedral $Al^{3+}$ was observed. As expected, the $^{27}$Al spectrum of Si-NCL-1 (Fig. 2.11(c)) did not show any signal suggesting the absence of aluminium in the silica polymorph, Si-NCL-1, sample.

### 2.4.3.6 Ion-exchange capacities

After saturating the calcined NCL-1 samples (Si/Al ratio = 23, 84, 156 and 257) with $Na^+$ ions, the molar ratios of Na/Al in the solid were found to be 0.86, 0.88, 0.91 and 0.90, respectively. After ion-exchanging the $Na^+$-form of the samples with $K^+$ the K/Al molar ratios were 0.84, 0.85, 0.87 and 0.88, respectively (Table 2.2). The ion-exchange properties of zeolites are due to the tetrahedral $AlO_2^-$ groups in the framework positions. Recently, Szostak and Thomas[16,17] have demonstrated that the ion exchange capacities of the zeolites can be taken as convincing
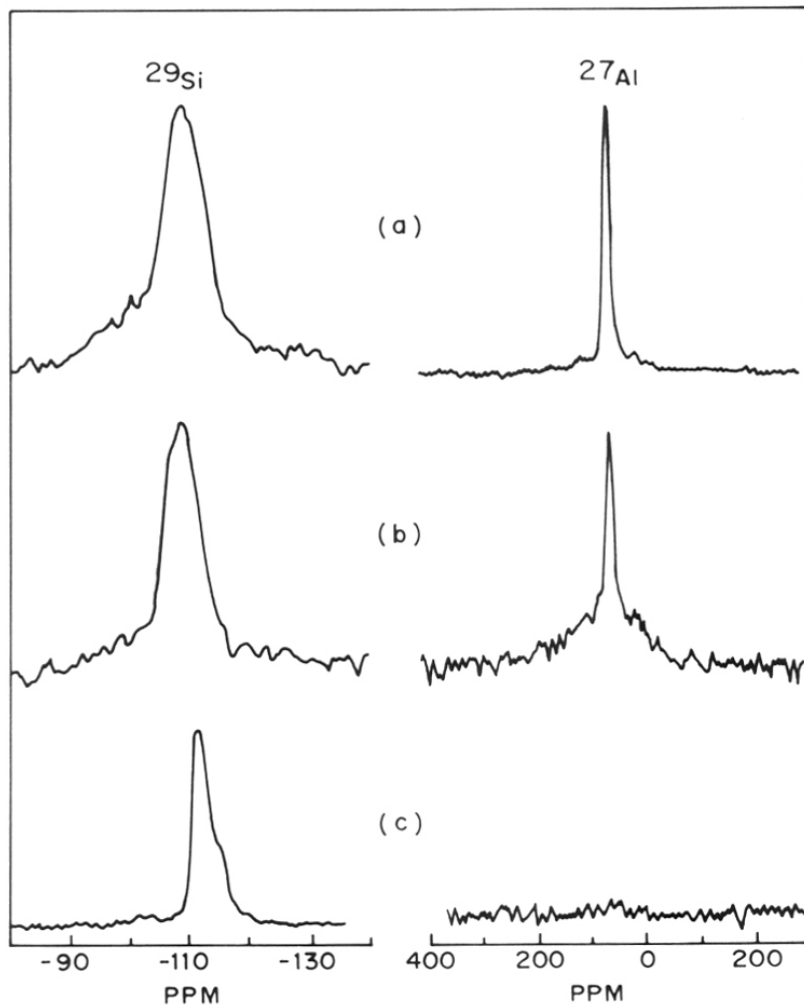
Fig.2.11 $^{29}$Si and $^{27}$Al MAS NMR spectra of NCL-1 samples. Spectra 'a' to 'c' refer to Si/Al molar ratio of 23, 84 and >3000, respectively.

evidence for the presence of $M^{3+}$ ions in the framework positions in the zeolite lattice. Hence, the substantial ion exchange capacity of the calcined Al-NCL-1 samples is a strong evidence for the presence of $Al^{3+}$ ions in NCL-1 framework.

### 2.4.3.7 Thermal analysis

Simultaneous TG-DTA analyses show that the calcination of the as-synthesized samples in air occurs exothermally (Fig. 2.12). During the thermal decomposition of organics in Si-NCL-1, two distinct weight losses are observed at 345-480 K and around 550-650 K, respectively. The former is due to the loss of water and the latter is due to the oxidative decomposition of the organic material in the pore system of the zeolite. The amount of weight loss due to oxidative decomposition of the organic material is found to be 7.5 wt.% (550-650 K).

### 2.4.3.8 Scanning electron microscopy

The scanning electron micrographs of NCL-1 samples are shown in Fig. 2.13 (micrographs 'a' to 'c' refer to samples with Si/Al molar ratio of 84, 257 and >3000, respectively) indicating the absence of amorphous material in the samples. These micrographs show that when the amount of aluminium increases in the sample, the morphology of the crystals changes [from oblonged shape (probably close packed bundles of needles) to needle shape]. Almost no oblong-shaped (probably close packed bundles of needles) crystals are present in the samples with Si/Al molar ratio of 83 and 257 (Fig. 2.13 'a' and 'b', respectively). In the silica polymorph of NCL-1 (Si-NCL-1), most of the crystals are oblong-shaped (close packed bundles of needles) (Fig. 2.13(c)).
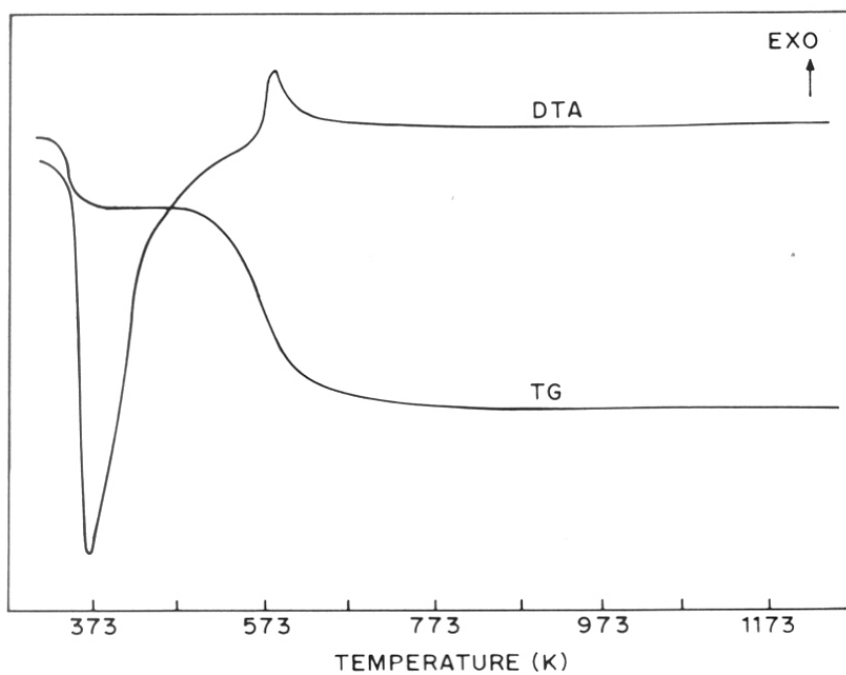
Fig.2.12    Simultaneous TG-DTA of as-synthesized sample of Si-NCL-1.

Fig.2.13    Scanning electron micrographs of samples with Si/Al molar ratio of 83 (micrograph 'a'), 257 (b) and >3000 (c).

## 2.5 CONCLUSIONS

1.  The X-ray powder diffraction pattern of zeolite NCL-1 is new. The crystals of NCL-1 have an orthorhombic symmetry with a = 1.195 ± 0.003, b = 0.836 ± 0.003 and c = 2.87 ± 0.004 nm. Samples with different Si/Al ratio are fully crystalline and free from impurities.

2.  The presence of a structure sensitive absorption band in the IR spectra of NCL-1 sample at 550 cm$^{-1}$ is indicative of the double 5-rings in the structure of NCL-1.

3.  From the adsorption volumes of mesitylene, it can be deduced that NCL-1 belongs to the large pore category with 12-membered ring pore openings.

4.  The diffusion coefficients for n-hexane, cyclohexane and mesitylene were 8.5, 3.4 and 0.6 X 10$^{-11}$ cm$^2$/sec., respectively.

7.  The $^{29}$Si and $^{27}$Al MAS NMR spectra of NCL-1 are similar to high silica molecular sieves and the position of the peak suggests that Al$^{3+}$ ions are in tetrahedral positions of NCL-1 framework.

## 2.6 REFERENCES

1.  (a) R. Kumar, K.R. Reddy, A. Raj and P. Ratnasamy, 9th Intern. Zeolite Conf., Montreal, Canada, 1992, Paper A6.
    (b) R. Kumar, K.R. Reddy and P. Ratnasamy, Ind. Pat. Appl. No. 766/DEL/91 (1991).
    (c) R. Kumar, K.R. Reddy and P. Ratnasamy, EP Appl. No. 92300166.3 (1991).
    (d) R. Kumar, K.R. Reddy and P. Ratnasamy, US Pat. Appl. No. 07/816,211 (1991).

2.  (a) S. Lowell and J.E. Sheilds, "Powder Surface Area and Porosity" 2nd Edition, Powder Technology Series, Chapman and Hall London p.14 (1984).
    (b) S. Lowell and J.E. Sheilds, ibid p.80 (1984).

3.  G. Engelhardt and D. Michel, High-resolution solid-state NMR of silicates and zeolites, Wiley, London, p.111 (1987).

4.  J.L. Casci, V.T. Whittam and B.M. Lowe, Proc. 6th Int. Conf. on Zeolites, Reno, p. 894 (1983).

5.  S.B. Kulkarni, V.P. Shiralkar, A.N. Kotasthane, R.B. Borade and P. Ratnasamy, Zolites, **2**, 313 (1982).

6.  R. Szostak, "Hand Book of Molecular Sieves" Van Nostrand Reinhold, p. 454 (1992).

7.  P.A. Jacobs and J.A. Martens, "Synthesis of high-silica aluminosilicate zeolites", Stud. Surf. Sci. Catal., **33**, 317 (1987).

8.  P.A. Jacobs and J.A. Martens, "Synthesis of high-silica aluminosilicate zeolites", Stud. Surf. Sci. Catal., **33**, 39 (1987).

9..  E.M. Flanigen, H. Khatami and H.A. Szymanski, Advances in Chemistry Series, **101**, 201 (1971).

10. S.B. Kulkarni, V.P. Shiralkar, A.N. Kotasthane, R.B. Borade and P. Ratnasamy, Zeolites, **2**, 313 (1982).

11. J.C. Jansen, F.J. Van der Gaag and H. Van Bekkum, Zeolites, **4**, 369 (1984).

12. P.A. Jacobs, H.K. Beyer and J. Valyan, Zeolites, **1**, 161 (1981).

13. G. Coudurier, C. Nacceache and J.C. Vedrine, J. Chem. Soc., Chem. Commun., 1413 (1982).

14. D.M. Ruthven, M. Eic and E. Richard, Zeolites, **11**, 647 (1991).

15. C.A. Fyfe, G.T. Kokotailo, G.J. Kennedy and C. de Schutter, J. Chem. Soc., Chem. Commun., 306 (1985).

16. R. Szostak and T.L. Thomas J. Catal., **100**, 555 (1986).

17. R. Szostak and T.L. Thomas, J. Chem. Soc., Chem. Commun., 113 (1986).

# CRYSTALLIZATION KINETICS

## 3.1 INTRODUCTION

This chapter describes the kinetics of crystallization of NCL-1[1]. The influence of various synthesis parameters, such as Si/Al, OH$^-$/Si, R$^{2+}$/Si (R$^{2+}$ = hexamethylene bis(triethylammonium bromide) as an organic additive), Si/Na$^+$, H$_2$O/Si (molar ratios) and temperature on crystallization kinetics and phase purity of NCL-1 molecular sieves is studied.

The experimental procedures for hydrothermal synthesis, X-ray diffraction, infrared spectroscopy, scanning electron microscopy and chemical analysis were described in sections 2.4.1, 2.3.1, 2.3.2, 2.3.8 and 2.3.9, respectively.

## 3.2 RESULTS AND DISCUSSION

### 3.2.1 Characterization

#### 3.2.1.1 Chemical analysis

The chemical compositions of Al-NCL-1 obtained from chemical analysis, are given in Table 3.1. The Si/Al ratio of the calcined samples (in the product) are 23, 84, 156, 257 and >3000 these samples were prepared from the gels containing Si/Al ratio 20, 80, 150, 250 and $\infty$, respectively. The aluminium content of the samples in the gel and in the product is similar for all the samples (Table 3.1).

#### 3.2.1.2 X-ray diffraction

Fig.3.1 depicts the x-ray powder diffraction profiles of the products crystallized at different intervals of time (curves 'a' to 'd', refer to crystallization times of 20, 31, 36 and 48 h, respectively) and demonstrate the evolution of the crystalline material from the gel mixture of the following molar composition:-

100 SiO$_2$ : 5 R$^{2+}$ : 25 NaOH : 5200 H$_2$O

The fully crystalline material, free from any other phases (impurities) was obtained after 48 h at the crystallization temperature of 443 K (Fig.3.1, curve 'd'). The crystallinity of the samples collected at different intervals of time (Fig.3.1, curves a-c) were 7, 28 and 73%

59

Table 3.1. Si/Al molar ratios of NCL-1 samples in gel and product

| Samples | Si/Al ratio in the gel[a] | Si/Al in the product[b] |
|---------|---------------------------|--------------------------|
| NCL-1 | 20 | 23 |
| NCL-1 | 80 | 84 |
| NCL-1 | 150 | 156 |
| NCL-1 | 250 | 257 |
| Si-NCL-1 | $\infty$ | >3000 |

[a] Initial gel composition.

[b] Obtanied from chemical analysis.

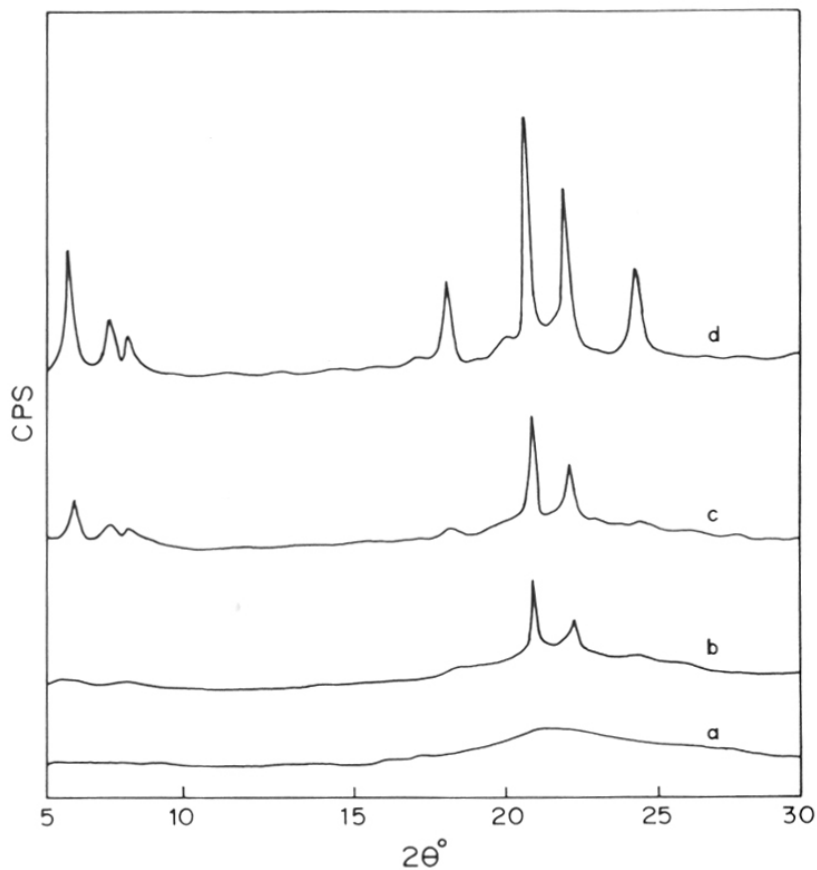Fig.3.1    The evolution of NCL-1 phase as seen from X-ray powder diffraction profiles of samples withdrawn at different intervals of time. Curves 'a' to 'd' refer to samples withdrawn at 19, 31, 36 and 48 h, corresponding to 8, 28, 73 and 100% crystalline material, respectively.

Synthesis conditions: Si/Al = ∞, $R^{2+}$/Si = 0.05, OH⁻/Si = 0.25, Na⁺/Si = 0.25, $H_2O$/Si = 52 and temperature = 443 K under agitation (60 rpm).

respectively, with reference to the fully crystalline (100%) sample (curve d). The crystallinity was calculated from the integrated intensities of 2θ lines between 17 and 25.5°. During crystallization, all the major lines grow simultaneously and the relative intensity of all the major peaks remain unchanged even when the crystallization period is further extended after the complete crystallization. This suggest that NCL-1 is free from any crystalline impurities.

### 3.2.1.3 Infrared spectroscopy

The framework IR spectra of NCL-1 samples are shown in Fig. 3.2.Curves 'a' to 'd' refer to the same set of samples as described in Fig.3.1. Based on the literature values[2], the observed absorption bands are tentatively assigned to internal asymmetric stretching ($1230$ cm$^{-1}$), external asymmetric stretching ($1098$ cm$^{-1}$), external symmetric stretching ($793$ cm$^{-1}$), double ring ($548$ cm$^{-1}$) and T-O bending vibrations of TO$_4$ tetrahedra ($468$ cm$^{-1}$) (T= Si or Al), respectively (Chapter 2 Table 2.6). Though the origin of the band around $610$ cm$^{-1}$ is not clear, the intensity of this band as well as the intensity of the band at $548$ cm$^{-1}$ (assigned to double ring) increases with increasing crystallinity of the samples. The intensity of the band at $468$ cm$^{-1}$ (assigned to T-O bending vibrations of TO$_4$ tetrahedra) remains constant with the crystallinity. The IR crystallinity was calculated by comparing the ratios of the intensities of IR bands of different crystalline samples at wave numbers $548$ (intensity of this band increases with crystallinity) to $468$ cm$^{-1}$ (intensity of this band remains constant with the crystallinity) with that of the 100% crystalline sample. Fig.3.3 depicts the IR crystallinity vs. XRD crystallinity of the same samples. Although, a direct correlation was observed between XRD and IR crystallinity, the IR crystallinity is found to be always higher (except for 100% crystalline sample) than the XRD crystallinity. This is due to the fact that the XRD technique requires larger particles (>5 nm) than what is required for IR technique.

### 3.2.1.4 Scanning electron microscopy

The scanning electron micrographs of samples with 7, 28 and 100% crystallinity are shown in Fig.3.4. The results indicate that at a crystallization period of 19 h, the product is found to be amorphous. However, at the longer crystallization time (31 h), the formation of oblong-shaped
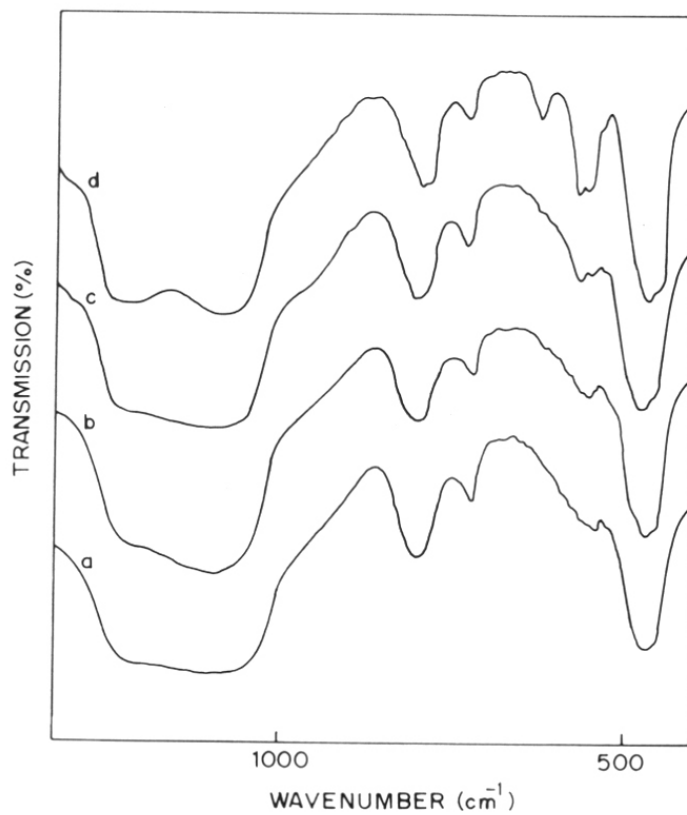
Fig.3.2    Framework IR spectra of samples withdrawn at various intervals of time during the crystallization of Si-NCL-1. Legend for curves 'a' to 'd' as given in the Figure 3.1.

Synthesis conditions: as given in Fig.3.1.
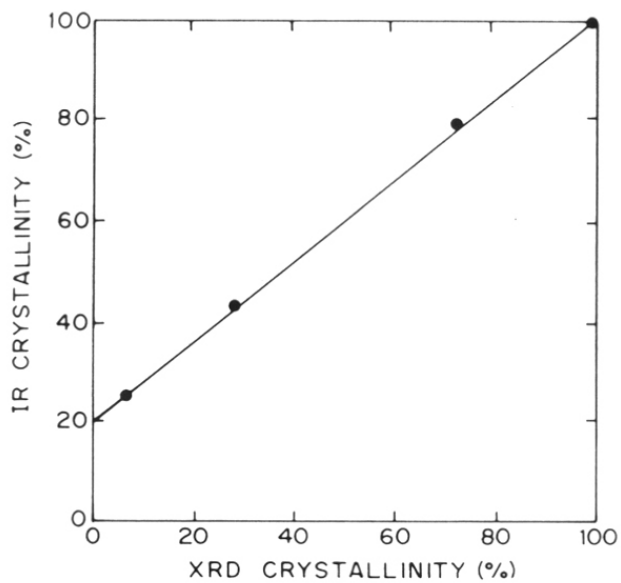
Fig.3.3     XRD crystallinity (integrated intensities of all peaks) vs. IR (the ratio of intensity of 548 to 468 cm$^{-1}$ bands) crystallinity of Si-NCL-1 samples.
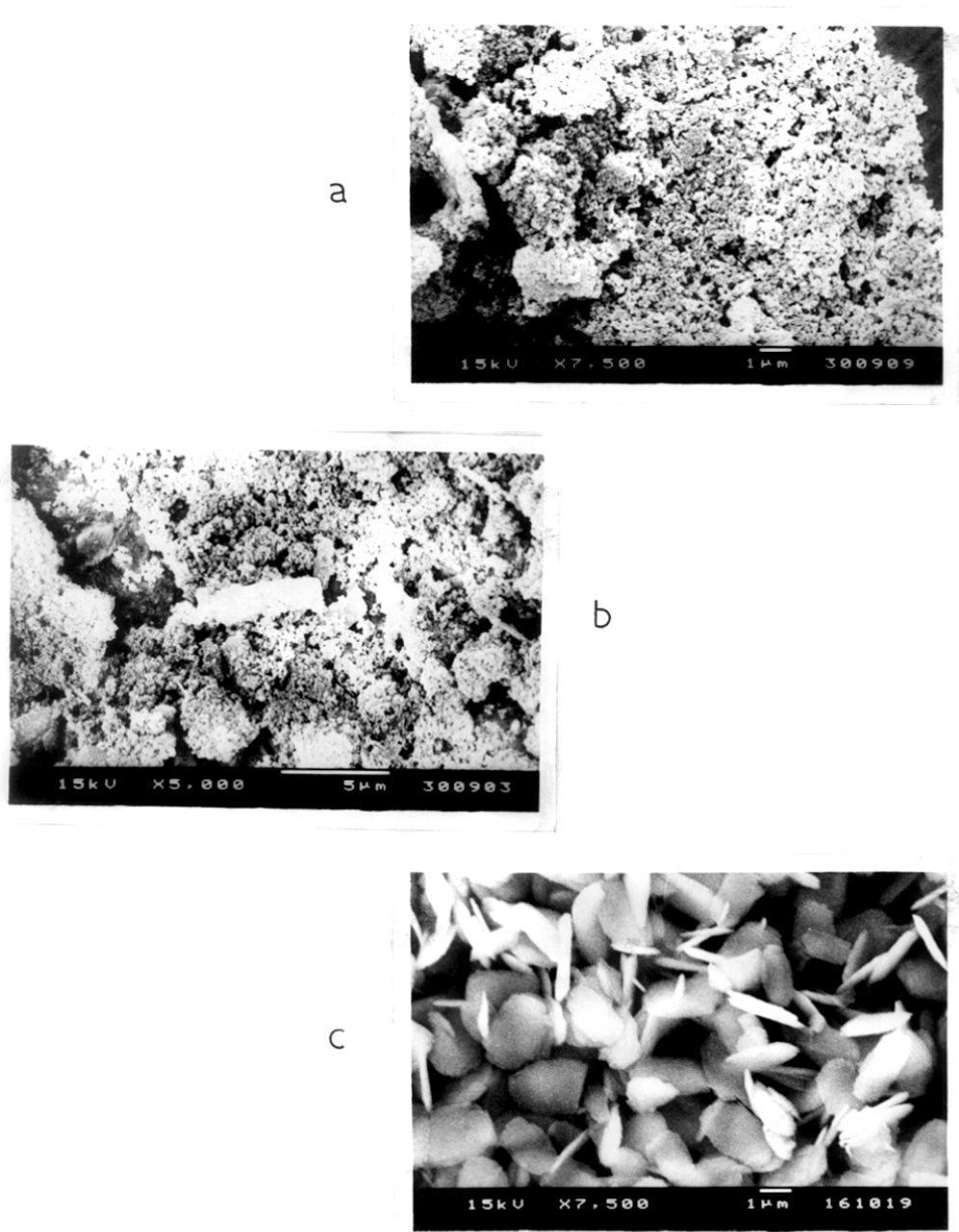
Fig.3.4    Scanning electron micrographs 'a' to 'c' refer to sample with 8%, 28% and 100% crystallinity, respectively.

Synthesis conditions: Si/Al = ∞, $R^{2+}$/Si = 0.05, $OH^-$/Si = 0.25, $Na^+$/Si = 0.25, $H_2O$/Si = 52 and temperature = 443 K under agitation (60 rpm).

crystals occurs and their concentration increases with time. Finally, at a crystallization time of 48 h, nearly 100% crystalline material is obtained and the crystals (most of which) are oblong in shape.

### 3.2.2 Kinetics of crystallization

#### 3.2.2.1 Influence of Si/Al ratio

The following gel composition was used for the synthesis of NCL-1 samples with Si/Al ratios (in the gel) 20, 80, 150, 250 and Al-free silica polymorph. The $OH^-/SiO_2$ ratio was adjusted to 0.12 by adding appropriate amount of the $H_2SO_4$.

$OH^-/SiO_2 = 0.12$,

$Si/Na^+ = 4$

$Si/R^{2+} = 20$

$H_2O/SiO_2 = 52$

The effect of Si/Al ratio on the rate of crystallization of NCL-1 is shown in Fig.3.5. Curves 'a' to 'e' in the Fig.3.5 refer to the crystallization from reaction mixtures of Si/Al = 20, 80, 150, 250 and Al-free silica polymorph, respectively. With an increase in Al content in the reaction mixture, the rate of crystallization decreases. This is a common observation in the synthesis of high silica molecular sieves[3-5]. The incorporation of aluminium (vis-a-vis Si) in a growing silica network is a difficult process[3-5]. As growth occurs and $Al^{3+}$ ions get incorporated, the charge compensating cations ($Na^+$ or organic cation) must be included in the zeolite. Such a requirement can also slow down the crystallization process compared to the crystallization of Al-free silicate species. However, NCL-1 can be crystallized in a fairly large range of Si/Al ratio of 20 and above. Attempts to prepare zeolite NCL-1 with still higher Al concentration (Si/Al < 20) were not successful.

### 3.2.2.2 Influence of OH⁻/Si ratio

The alkalinity of the reaction mixture is one of the major factors which govern the nucleation as well as the crystallization processes during zeolite synthesis. Hence, the OH⁻ ion concentration (OH⁻/Si molar ratio) was adjusted by adding an appropriate amount of sulphuric
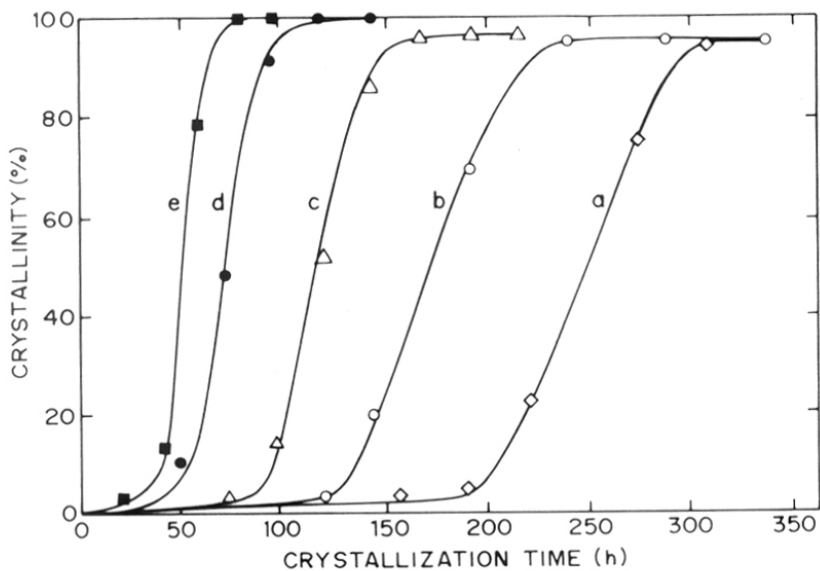
Fig.3.5    The influence of the Si/Al ratio on the crystallization of NCL-1. Curves 'a' to
'e' refer to Si/Al molar ratio 20, 80, 150, 250 and $\infty$, respectively.
Synthesis conditions: $R^{2+}/Si = 0.05$, $OH^-/Si = 0.12$, $Na^+/Si = 0.25$, $H_2O/Si = 52$
and temperature = 443 K under agitation (60 rpm).

acid and keeping the $Na^+$ ion concentration same ($Si/Na^+ = 4$). Fig. 3.6 shows the effect of $OH^-/Si$ on the nucleation and crystallization of the silica polymorph of NCL-1. At lower $OH^-$ concentration, ($OH^-/Si = 0.12$), both the nucleation and the subsequent crystallization were very slow (curve a), though fully crystalline material was obtained after 76 h. An increase in the $OH^-/Si$ ratio from 0.12 to 0.2 enhanced the rate of crystallization considerably, leading to fully crystalline material after 60 h (curve b). At $OH^-/Si = 0.25$, nucleation and crystallization rates were further accelerated (curve c) and fully crystalline material was obtained after 48 h. This is in accordance with the general observation that the rate of crystallization increases with the concentration of the free base ($OH^-$), a mineralizing agent, in the synthesis of high silica zeolites[3-7]. An increase in $OH^-/Si$ ratio results in the increased solubility of the reactants at higher alkalinity. This leads to enhanced supersaturation of the mother liquor and hence, a decrease in nucleation and crystallization time. In the synthesis of aluminosilicates ($Si/Al = 20, 80$ and 150), however, an increase in the alkali concentration i.e., $OH^-/Si$ ratio of 0.12 to 0.20 or more resulted in a mixture of NCL-1 and other crystalline impurities (like ZSM-5). This observation suggest that there exists an optimum range of $OH^-/SiO_2$ (~0.12) molar ratio for successful synthesis of aluminosilicate of NCL-1, like other high silica zeolites[7].

The change in the pH of the mother liquor during the course of crystallization is shown in Fig. 3.7 (curves 'a' to 'c'). During the synthesis of high-silica aluminosilicate, EU-1 (ZSM-50), Casci and Lowe[8] showed that a large increase in the pH of the mother liquor during the crystallization suggested the formation of stable and highly crystalline material. An insignificant change or decrease in the value of pH indicates either the redissolution of the less metastable phase formed initially or the presence of amorphous material or both. Depending on the $OH^-/Si$ ratio, the initial pH of the reaction mixture varies. At higher ratios, the initial pH is higher. However, the change in pH, i.e., $\Delta pH$, after the completion of crystallization ranged between 0.5 and 0.62 for all the three preparations (curves a-c, Fig. 3.7).

Fig.3.6    The influence of concentration of alkali on the crystallization of Si- NCL-1.
Curves 'a' to 'c' refer to OH'/Si = 0.12, 0.2 and 0.25, respectively.
Synthesis conditions: Si/Al = $\infty$, $R^{2+}/Si$ = 0.05, $Na^+/Si$ = 0.25, $H_2O/Si$ = 52 and
temperature = 443 K under agitation (60 rpm).
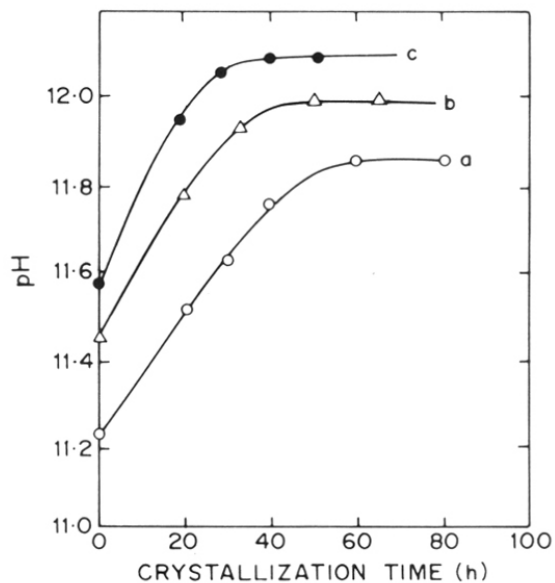
Fig.3.7    The change in pH during the crystallization of NCL-1. Legend for curves 'a' to 'c', as given in Figure 3.6.

Synthesis conditions: as given in Fig.3.6.

### 3.2.2.3 Influence of Na⁺/Si ratio

In order to study the role of alkali metal ion ($Na^+$) during the synthesis of NCL-1, further experiments were carried out by adding a calculated amount of NaCl to the gel system while keeping the $OH^-$/Si ratio constant at 0.25. Fig. 3.8 depicts the influence of $Na^+$ concentration on the nucleation and crystallization of the silica polymorph of NCL-1. At high $Na^+$ concentration ($Na^+$/Si ratios of 0.33 and 0.5), it is observed that much before the complete crystallization of NCL-1, dense phases like $\alpha$-quartz or crystobalite start to crystallize in the system at the expense of NCL-1. At $Na^+$/Si =0.5, the formation of the dense phases starts only after 10 h with a maximum of about 20% crystallinity of NCL-1 (curve a). At $Na^+$/Si = 0.33, the formation of dense phases starts after about 40 h with 80% maximum crystallinity of NCL-1 (curve b). For the preparation of silica polymorph of NCL-1, the optimum value of $Na^+$ ion concentration in the gel corresponds to a $Na^+$/Si ratio of $\leq$ 0.25, when the $OH^-$/Si ratio is also optimally at 0.25 (curve c).

### 3.2.2.4 Influence of R²⁺/Si ratio

Fig. 3.9 depicts the effect of the concentration of organic additive ($R^{2+}$/Si molar ratios) on the nucleation and crystallization of the silica polymorph (curves 'a' to 'e' refer to $R^{2+}$/Si molar ratios of 0.1, 0.05, 0.033, 0.02 and 0.00, respectively). An optimal amount of the organic additive seems to be necessary for obtaining a 100% crystalline material ($R^{2+}$/Si = 0.05, curve b, Fig.3.9). In the absence of organic additive the reaction mixture (curve e) was amorphous even after 25 days, indicating that the organic additive is essential for the crystallization of NCL-1.

### 3.2.2.5 Influence of H₂O/Si ratio

The effect of changing $H_2O$/Si molar ratio in the initial reaction mixture on the crystallization of silica polymorph of NCL-1 is depicted in Fig.3.10. The rate of crystallization decreases marginally with dilution. A faster rate of crystallization and nucleation, obtained in the concentrated system can be rationalized if it is considered that with decreasing amount of water in the reaction mixture, the concentration of reactants and, therefore, pH increases leading to higher supersaturation of the mother liquor[7]. This has the same effect as an increase in the $OH^-$/Si ratio discussed above.
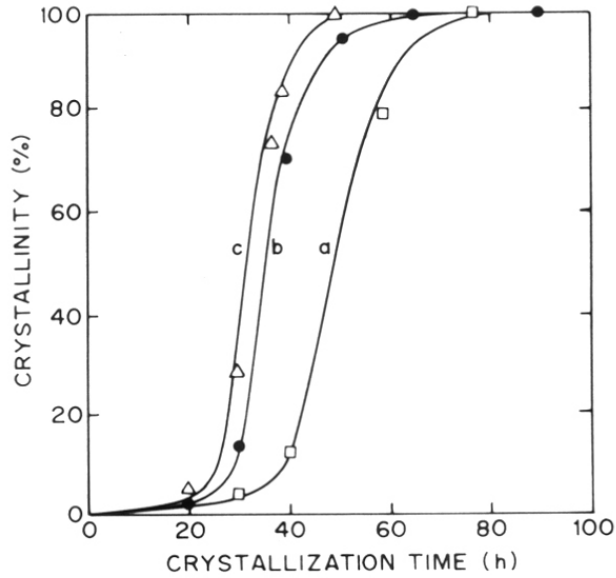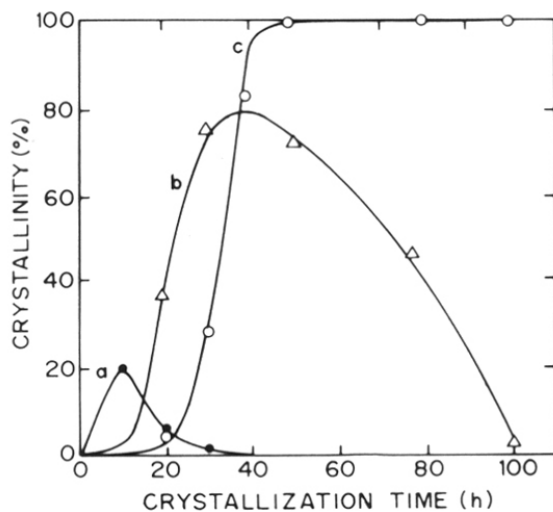
Fig.3.8    The influence of Na$^+$ concentration on the crystallization of NCL-1. Curve 'a' to 'c' refer to Na$^+$/Si = O.5, 0.33 and 0.25, respectively.
Synthesis conditions: Si/Al = ∞, R$^{2+}$/Si = 0.05, OH$^-$/Si = 0.25, H$_2$O/Si = 52 and temperature = 443 K under agitation (60 rpm).
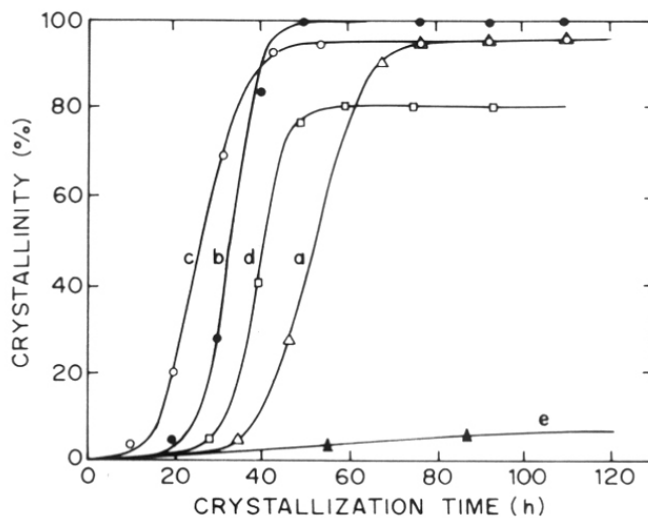
Fig.3.9    The influence of template concentration on the crystallization. Curves 'a' to 'e' refer to $R^{2+}/Si$ ratios of 0.1, 0.05, 0.033, 0.02 and 0.00, respectively. Synthesis conditions: $Si/Al = \infty$, $OH^-/Si = 0.25$, $Na^+/Si = 0.25$, $H_2O/Si = 52$ and temperature = 443 K under agitation (60 rpm).
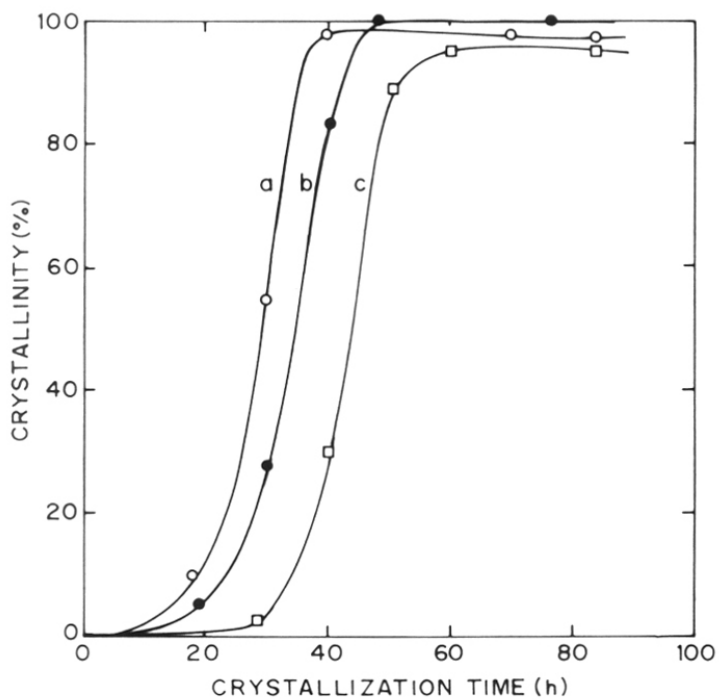
Fig.3.10    The influence of dilution on the crystallization.  Curve 'a' to 'c' refer to $H_2O/Si$
ratios of 33, 52 and 70, respectively.
Synthesis conditions: $Si/Al = \infty$, $R^{2+}/Si = 0.05$, $OH^-/Si = 0.25$, $Na^+/Si = 0.25$ and
temperature 443 K under agitation (60 rpm).

### 3.2.2.6 Influence of crystallization temperature

In all the above-mentioned studies, the crystallization was done at 443 K. Fig.3.11 depicts the influence of temperature on nucleation and crystallization of silica polymorph of NCL-1. Curves a, b and c represent the crystallization process at 423, 443 and 473 K, respectively. Higher temperatures enhance the rates of both the nucleation and the crystallization of NCL-1. At all temperatures, almost fully crystalline material was obtained.
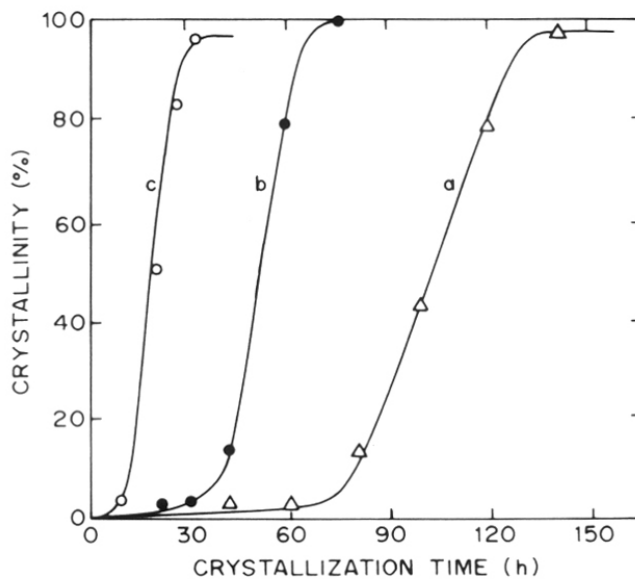
Fig.3.11    The influence of temperature on the crystallization of NCL-1. Curves 'a' to 'c' refer to crystallization at 423, 443 and 473 K, respectively.
Synthesis conditions: Si/Al = ∞, $R^{2+}$/Si = 0.05, OH⁻/Si = 0.12, Na⁺/Si = 0.25 and $H_2O$/Si = 52 under agitation (60 rpm).

## 3.3 CONCLUSIONS

The following conclusions are drawn from studies of the kinetics of crystallization of NCL-1 zeolite

1.  NCL-1 can be synthesized using hexamethylene bis(triethylammonium bromide) as the organic additive.

2.  An increase in Si/Al ratio in the reaction mixture or the crystallization temperature enhances the rate of crystallization.

3.  The optimum range of OH⁻/Si ratio is 0.12-0.25; at higher ratios, NCL-1 co-crystallizes with ZSM-5 or MOR and at lower values, the nucleation and the crystallization are very slow.

4.  Above $Na^+$/Si ratio of 0.25, dense phases like $\alpha$-quartz or crystobalite start to crystallize in the system.

## 3.4 REFERENCES

1.  (a) R. Kumar, K.R. Reddy, A. Raj and P. Ratnasamy, 9th Intern. Zeolite Conf., Montreal, Canada, 1992, Paper A6;
    (b) R. Kumar, K.R. Reddy and P. Ratnasamy, Ind. Pat. Appl. No. 766/DEL/91 (1991).
    (c) R. Kumar, K.R. Reddy and P. Ratnasamy, EP Appl. No. 92300166.3 (1991).
    (d) R. Kumar, K.R. Reddy and P. Ratnasamy, US Pat. Appl. No. 07/816,211 (1991).

2.  E.M. Flanigen, H. Khatami and H.A. Szymanski, Advances in Chemistry Series, **101**, 201 (1971).

3.  (a) L. Ghamami and L.B. Sand, Zeolites, **3**, 155 (1983).
    (b) R.M. Barrer, Zeolites, **1**, 130 (1981).

4.  S. Ernst, P.A. Jacobs, J.A. Martens and J. Weitkamp, Zeolites, **7**, 458 (1987).

5.  P.A. Jacobs and J.A. Martens, Stud. Surf. Sci. Catal., **33**, 58 (1987).

6.  R.N. Bhat and R. Kumar, J. Chem. Tech. Biotech., **48**, 458 (1990).

7.  S. Ernst, R. Kumar and J. Weitkamp, ACS Monograph, **398**, 560 (1989).

8.  J.L. Casci and and B.M. Lowe, Zeolites, **3**, 186 (1983).

# CATALYTIC TEST REACTIONS

## 4.1 INTRODUCTION

The use of catalytic test reactions is a widely accepted method for characterizing the effective pore widths of zeolites and related molecular sieve materials[1-3]. Its main advantages are that (i) the characterization can be carried out under catalytically relevant conditions, and (ii) the possibility to detect both mass transfer effects (shape selectivity) and intrinsic chemical effects[4-6]. The latter are not detectable by sorption experiments where no chemical transformations take place.

The main experimental approach is to measure the selectivities of a catalytic reaction over a number of zeolites with known pore structure. Once the method is standardized in this way, the selectivities of the same reaction measured over a zeolite with unknown structure give valuable information on its effective pore width and architecture. A detailed introduction of various catalytic test reactions has already been given in Chapter 1 (Section 1.5).

This chapter describes the characterization of the pore structure of the NCL-1 molecular sieve through catalytic test reactions such as *m*-xylene conversion, ethylbenzene disproportionation, Mobil's constraint index and spaciousness index.

## 4.2 EXPERIMENTAL

### 4.2.1 Catalytic reactions

The catalytic reactions were carried out in a fixed bed down flow tubular silica reactor, at atmospheric pressure. The reactor consists of a fused silica tube, 1.5 cm in inner diameter and 35 cm length provided with a thermowell. The reactor was inserted in a furnace. The catalyst powder was pressed, pelleted, crushed and sieved to obtain 20-30 mesh particles and 1 g of catalyst (on dry basis) was charged in the middle of the reactor in such a way that the catalyst bed was sandwiched by inert porcelain beads. The top portion of the reactor, serving as a vapourizer-cum-preheater, was packed with inert porcelain beads. The catalytic reactor assembly shown in Figure 4.1 was attached to a heated sampling valve which was attached to GC. The products were analyzed by using on line high resolution capillary GC (HP 5890). The

Air / H$_2$ / N$_2$

A - DRIER, 4A
B - FLOW METER
C - PREHEATER
D - FEED PUMP
E - FURNACE
F - CATALYST
G - RECEIVER
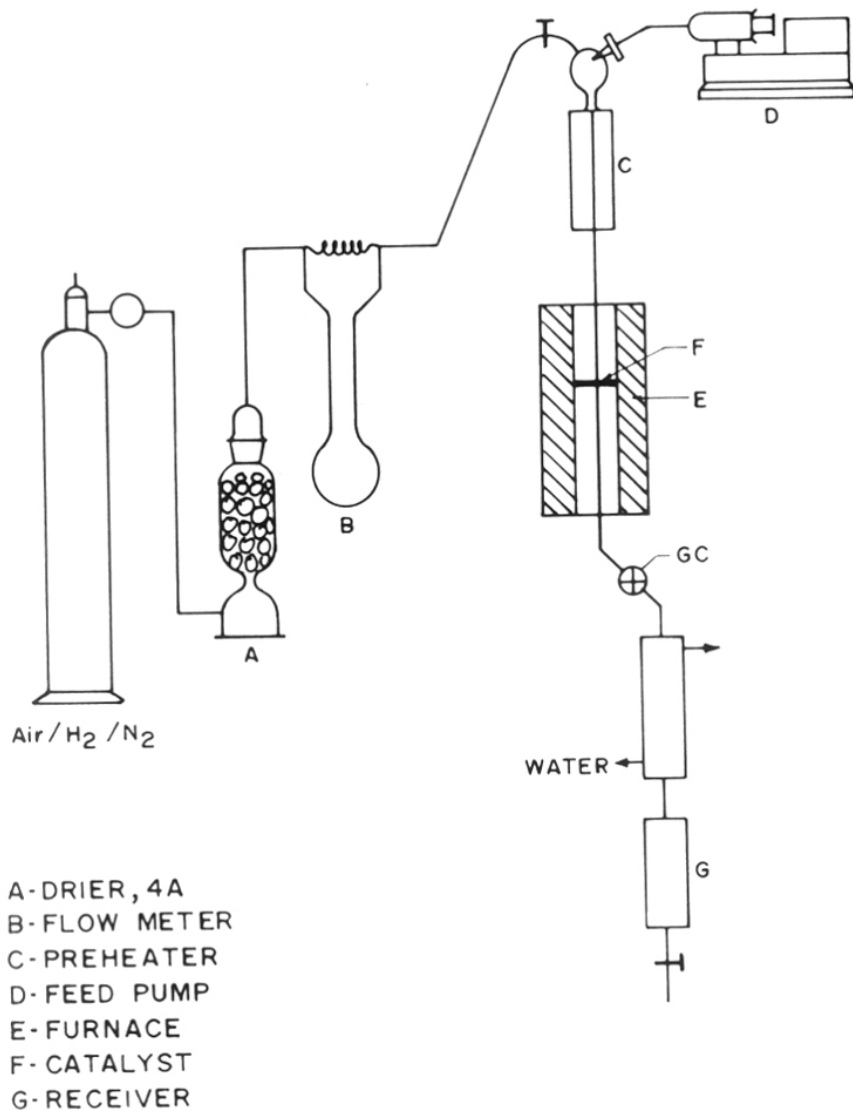
Fig.4.1 Fixed bed down-flow reactor.

product stream from sampling valve was collected after passing through a condenser cooled with chilled water. In the case of *m*-xylene conversion, the products were analysed using Shimadzu GC(R1A) equipped with 5% bentone + 5% diisodecylphthalate column (2 m long).

Prior to reaction, the catalyst was activated in a flow of air at 813 K for 10 h. The catalyst was then flushed with nitrogen and cooled to reaction temperature. The reactants were passed into the reactor by a syringe pump (Sage Instruments, Model 352) at a constant feed rate.

### 4.2.2 Preparation and characterization of catalysts.

All the zeolites (other than NCL-1) in this study were prepared according to the published procedures. The details are given in Table 4.1. All the samples are fully crystalline and free from impurity. The crystal size and shape of the zeolites are also presented in Table 4.1. H-form of the zeolites was prepared by calcining the as-synthesized sample for 16 h at 823 K (in air flow to remove the organic matter). Then subjected to ion-exchanges with 0.1 M ammonium nitrate solution at 353 K for 6 h. This exchange was repeated three times. The $NH_4^+$ form of the zeolite was calcined at 723 K to get the H-form.

The noble metal (Pd) were introduced from an aqueous solution containing the appropriate amount of the $(NH_4)_2PdCl_6$ to get 0.27 wt.% Pd in the zeolite samples.

The H-form of the zeolite (NCL-1 or other zeolites) were used for *m*-xylene conversion, ethylbenzene disproportionation and constraint index (CI) reactions. The noble metal loaded zeolites (0.27 wt.% Pd loaded on H-form zeolites) were used for spaciousness index determination.

### 4.3. m-XYLENE CONVERSION

### 4.3.1 m-Xylene isomerization

The *p*-xylene/*o*-xylene (p/o) ratio is plotted against *m*-xylene conversion (Fig.4.2). The *m*-xylene conversion was varied by changing the temperature, (643-683 K for ZSM-5 and ZSM-12, 473-558 K for mordenite and Beta, and 523-623 K for NCL-1, respectively). The WHSV and time-on-stream were 3.47 and 30 min, respectively. The p/o ratio of ZSM-5 (1.7) (a medium pore zeolite) is well above the equilibrium value. The enhanced para selectivity in

Table 4.1 Physico-chemical properties of zeolites

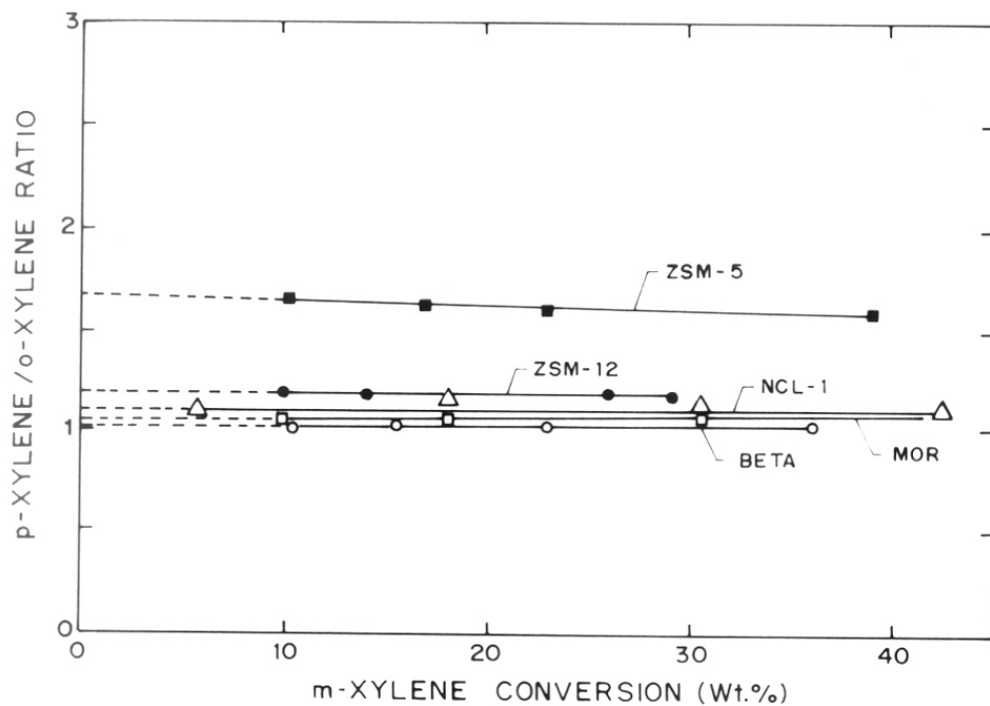| Zeolite | Si/Al molar ratio | Crystal morphology | | Ref. for synthesis |
|---------|-------------------|---------|------------------|--------------------|
|         |                   | Shape   | Average size, μm |                    |
| ZSM-5   | 43                | Cuboid  | 0.5              | 7                  |
| MOR     | 4.5               | Cuboid  | 1.5              | Supplied by Norton, Zeolon-900 |
| ZSM-12  | 80                | Needle  | 4 X 0.3          | 8                  |
| Beta    | 22                | Cuboid  | 0.5              | 9                  |
| NCL-1   | 23                | Needle  | 3-10 X 0.2-1.2   | chapter 2          |
| NCL-1   | 84                | Needle  | 3-8 X 0.2-1.8    | -do-               |
| NCL-1   | 156               | Needle  | 3-8 X 0.3-2.2    | -do-               |
| NCL-1   | 257               | Needle  | 3-9 X 0.4-2.5    | -do-               |

Fig.4.2    *p*-Xylene/*o*-xylene ratio against *m*-xylene conversion on medium and large pore

zeolites.

medium pore zeolites is due to the diffusion controlled product shape selectivity[10-13]. In the case of large pore zeolites, the *p/o* ratio is around 1±0.2 (i.e. near equilibrium value) (Fig.4.2) indicating the absence of diffusionally controlled product shape selectivity. NCL-1 with a *p/o* ratio of around 1.1 behaves like large pore zeolites (Fig.4.2).

### 4.3.2 Disproportionation of m-xylene

The ratio of isomerization to disproportionation (molar ratio of (*p*-xylene+*o*-xylene) to trimethylbenzenes)) is given as log(I/D). This log(I/D) is plotted as a function of *m*-xylene conversion (Fig.4.3). Unlike the *m*-xylene isomerization, its disproportionation is controlled by the restricted transition state shape selectivity (RTSS) exerted by the void space available around the active sites. The value of log (I/D), at lower or extrapolated to zero conversion can be used to rank zeolites according to their void space. The log(I/D) depends upon *m*-xylene conversion (Fig.4.3). The log(I/D) value exhibited by NCL-1 (1.02) is between that shown by mordenite and Beta zeolites (these two are large pore zeolites). This suggests that NCL-1 is probably a large pore zeolite.

The disproportionation of *m*-xylene to toluene and trimethylbenzenes, is a bimolecular reaction involving diphenylmethane type intermediates which are bulkier than both reactants and products[14,15]. From the product distribution in the reaction of xylenes over ZSM-5, ZSM-4, MOR and FAU zeolites, Olson and Haag[12] concluded that the reaction probes the largest cavity in the pores, not the window size and that the observed selectivities are a result of steric inhibitions of the large diphenylmethane-type intermediate. The selectivity for TMB's in the products in *m*-xylene conversion may thus form a basis to discriminate the zeolites according to the void space contained in their pore system. Fig 4.3 shows that the log(I/D) values at zero conversion reflect the effective void space of both 10-membered ring and 12-membered ring zeolites. Weisz[12] and Mavrodinova[16,17] also concluded that the I/D selectivity in zeolites depends mainly on their intracrystalline void space.

Fig.4.4 illustrates the influence of *m*-xylene conversion on the 1,3,5/1,2,4-trimethylbenzene ratio. For the medium pore zeolite (ZSM-5) this ratio, when extrapolated to zero conversion is zero. For all the large pore zeolites this value is positive (Fig.4.4). Further, its value (at zero
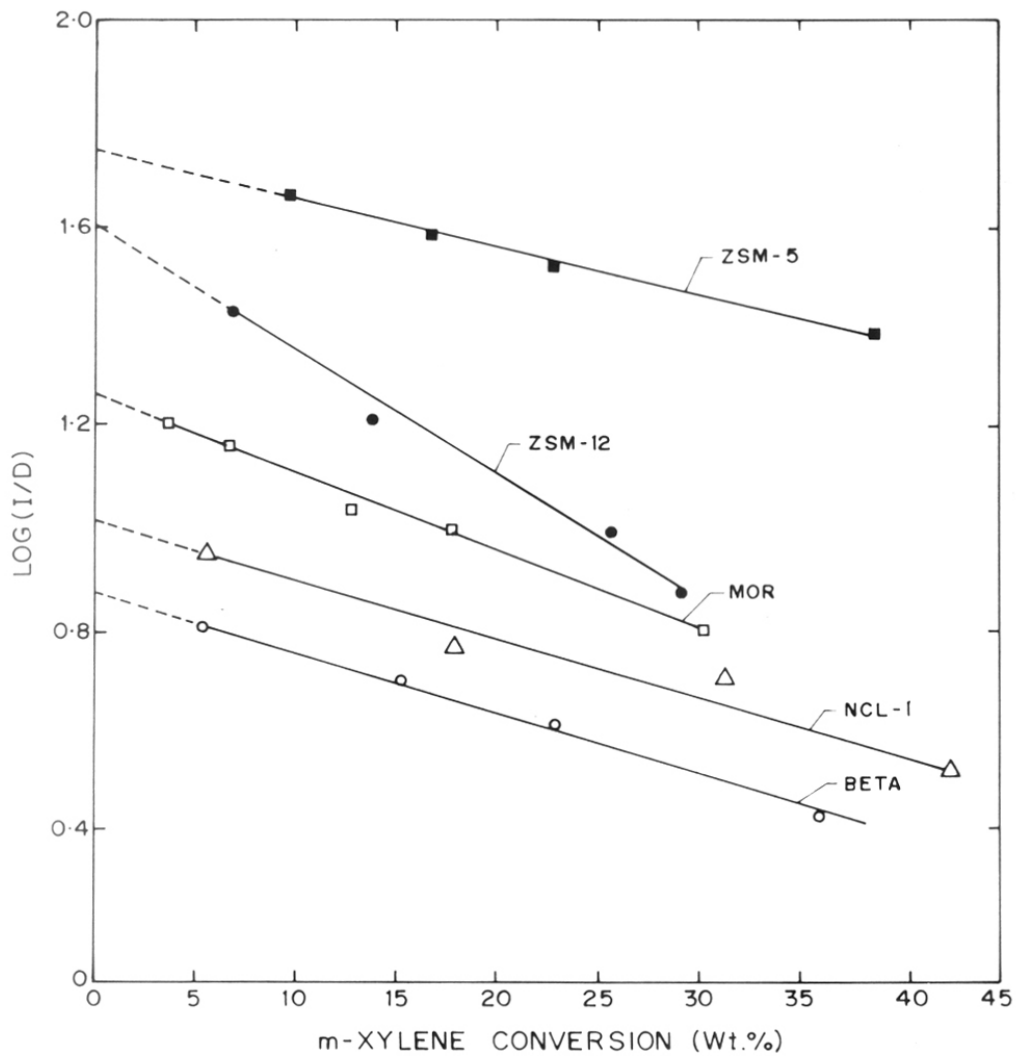
Fig.4.3Log (I/D) against *m*-xylene conversion.
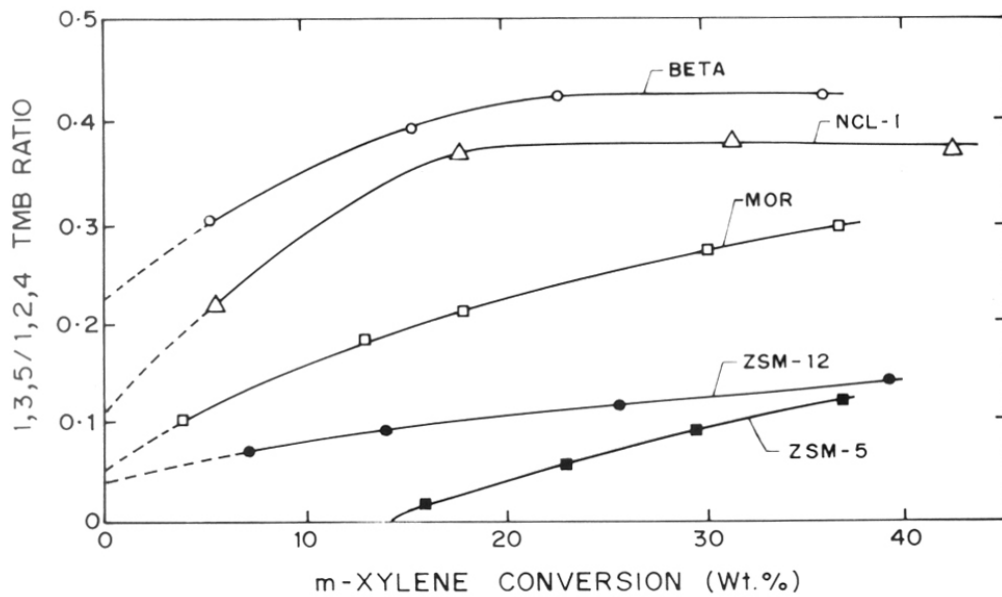
Fig.4.4    The ratio of 1,3,5-trimethylbenze to 1,2,4-trimethylbenzene against *m*-xylene conversion.

conversion), increases with the void space of zeolites. The value of this ratio for NCL-1 (0.11) lies again between that of mordenite (0.05) and Beta (0.22), clearly characterizing NCL-1 as a large pore zeolite. Martens et al[14]. have extensively discussed the accommodation of possible diphenylmethane-type intermediates in the intracrystalline void space of a variety of zeolites. The size of the complex required to produce 1,2,4-TMB is smaller than that needed for the 1,3,5- or 1,2,3-TMB isomers[14].

The above three parameters namely, ($p/o$, log(I/D) and 1,3,5/1,2,4-TMB ratios) shown by NCL-1 strongly suggest that NCL-1 is a large pore zeolite.

### 4.3.3 The effect of Si/Al ratio

The influence of the Si/Al ratio of zeolite NCL-1 on $m$-xylene conversion and product distribution is shown in Table 4.2. As the Si/Al ratio increases the conversion of $m$-xylene and the formation of disproportionated products decreases. A similar observation has been reported for zeolite Beta[18]. These are direct consequences of the decreasing concentration or density of the acid sites at higher Si/Al ratios[19].

From Table 4.2 it can be seen that the initial $p/o$ ratio in $m$-xylene isomerization is $ca$. 1.1, independent of the Si/Al ratio and $m$-xylene conversion. The value of the $p/o$ ratio for twelve-membered ring zeolites[9] lies in the range of 1.0-1.2. The ratio of 1,2,3- to 1,3,5-trimethyl benzene for all samples of NCL-1 is around 0.4. A similar value is observed for mordenite[14].

### 4.3.4 Effect of temperature

Table 4.3 shows that the influence of temperature on the $m$-xylene conversion and the product selectivities. The $m$-Xylene conversion and disproportionated products increases with the temperature. The ratio of $p/o$ does not change with the temperature, the values are in the range of 1.09-1.19 for all the temperatures.

Table 4.2     Influence of the Si/Al ratio on *m*-xylene conversion over NCL-1 samples

Conditions:    T = 573 K; $H_2$/*m*-xylene (mole) = 4; WHSV = 3.47; Time-on-stream = 30 min;

Catalyst:      1 g (anhydrous) H-NCL-1.

| Si/Al molar ratio | 23 | 84 | 156 | 257 |
|---|---|---|---|---|
| Conversion (wt.%) | 43.2 | 18.6 | 15.5 | 13.4 |
| Product distribution (wt.%) | | | | |
| Toluene | 16.34 | 10.2 | 10.6 | 10.3 |
| *p*-Xylene | 31.2 | 40.6 | 39.3 | 40.4 |
| *o*-Xylene | 29.4 | 34.1 | 35.4 | 37.0 |
| 1,2,3-TMB[a] | 2.2 | 1.35 | 1.3 | 1.0 |
| 1,2,4-TMB | 13.9 | 9.1 | 8.9 | 7.5 |
| 1,3,5-TMB | 5.2 | 3.4 | 3.3 | 2.8 |
| Others[b] | 1.7 | 1.2 | 1.2 | 1.0 |
| *p/o* ratio | 1.06 | 1.17 | 1.11 | 1.09 |
| log(I/D) | 0.51 | 0.78 | 0.80 | 0.88 |
| I/D ratio | 3.22 | 6.00 | 6.29 | 7.66 |
| 1,2,3-/1,3,5-TMB | 0.43 | 0.39 | 0.39 | 0.37 |

[a] Trimethylbenzene

[b] Mostly Aliphatics, benzene, ethylbenzene and ethyltoluenes.

Table 4.3    Influence of reaction temperature on *m*-xylene conversion over NCL-1

Conditions:    $H_2$/*m*-xylene (mole) = 4; WHSV = 3.47; Time-on-stream = 30 min;

Catalyst:    1 g (anhydrous) (H-NCL-1) (Si/Al = 84)

| Temperature K | 523 | 573 | 598 | 623 |
|---|---|---|---|---|
| Conversion (wt.%) | 5.82 | 18.57 | 31.74 | 42.52 |
| Product distribution (wt.%) | | | | |
| Toluene | 8.4 | 10.2 | 10.3 | 16.8 |
| *p*-Xylene | 41.7 | 40.6 | 39.4 | 31.8 |
| *o*-Xylene | 38.0 | 34.1 | 33.2 | 29.2 |
| 1,2,3-TMB[a] | 0.3 | 1.35 | 1.5 | 2.1 |
| 1,2,4-TMB | 7.7 | 9.1 | 10.4 | 13.9 |
| 1,3,5-TMB | 1.7 | 3.4 | 4.0 | 5.1 |
| Others[b] | 2.2 | 1.2 | 1.2 | 1.1 |
| *p/o* ratio | 1.10 | 1.17 | 1.19 | 1.09 |
| log(I/D) | 0.97 | 0.78 | 0.71 | 0.51 |
| I/D ratio | 9.21 | 6.0 | 5.15 | 3.25 |

[a,b] As given in Table 4.2

### 4.3.5 Effect of space velocity

The influence of space velocity on *m*-xylene conversion and on product selectivities is shown in Table 4.4. It shows that the ratio of *p/o* is almost constant and in the range of 1.12-1.23 with space velocity. The disproportionation of *m*-xylene and the formation of both the, 1,3,5- and 1,2,3-trimethyl benzenes decreases with increasing space velocities.

### 4.3.6 Effect of time-on-stream

The influence of time-on-stream on *m*-xylene conversion and on the product selectivities is shown in Table 4.5. It shows relatively fast deactivation in NCL-1. The formation of both 1,3,5- and 1,2,3-trimethyl benzenes decrease with time-on-stream.

## 4.4 ETHYLBENZENE DISPROPORTIONATION

### 4.4.1 Introduction

Karge et al.[20] and Weitkamp et al.[21] studied the disproportionation of ethylbenzene on various zeolites and developed criteria to discriminate between large pore and medium pore zeolites[21]. The criteria are: (i) the presence or absence of an induction period, (ii) the rate of deactivation (iii) the ratio of yield of diethylbenzenes ($Y_{DE-Bz}$) to benzene ($Y_{Bz}$) and (iv) the distribution of the diethylbenzenes. In large pore zeolites, an induction period and slow deactivation rate were observed. In medium pore zeolites, there was no induction period and deactivation was faster[21].

### 4.4.2 Influence of time-on-stream

Table 4.6 shows the disproportionation of ethylbenzene on H-NCL-1 (Si/Al = 23) zeolite as a function of time-on-stream. The conversion of ethylbenzene increases with time-on-stream initially. Later, after one hour the conversion decreases slowly with time-on-stream. Thus H-NCL-1 shows a short induction period, which is a characteristic feature of large pore zeolites[20,21]. The distribution of diethyl benzenes is shown in Fig. 4.5. The distribution of 1,2-, 1,3- and 1,4-diethylbenzenes remains constant with time-on-stream. However, in medium pore

Table 4.4    Influence of space velocity on *m*-xylene conversion over NCL-1

Conditions:    T = 598 K; H$_2$/*m*-xylene (mole) = 4; Time-on-stream = 30 min.

Catalyst:    1 g (anhydrous) (H-NCL-1) (Si/Al = 84)

| WHSV | 1.74 | 3.47 | 6.94 | 13.02 |
|---|---|---|---|---|
| Conversion (wt.%) | 36.3 | 31.74 | 27.5 | 10.7 |
| Product distribution (wt.%) | | | | |
| Toluene | 14.4 | 10.3 | 9.1 | 11.8 |
| *p*-Xylene | 34.1 | 39.4 | 43.1 | 43.4 |
| *o*-Xylene | 30.3 | 33.2 | 35.9 | 35.2 |
| 1,2,3-TMB[a] | 1.6 | 1.5 | 1.0 | 0.7 |
| 1,2,4-TMB | 13.8 | 10.4 | 8.7 | 6.7 |
| 1,3,5-TMB | 4.4 | 4.0 | 1.7 | 1.9 |
| Others[b] | 1.4 | 1.2 | 0.5 | 0.3 |
| *p/o* ratio | 1.12 | 1.19 | 1.2 | 1.23 |
| log(I/D) | 0.56 | 0.71 | 0.89 | 0.98 |
| I/D ratio | 3.66 | 5.15 | 7.8 | 9.56 |

[a,b] As given in Table 4.2

Table 4.5 Influence of time-on-stream on *m*-xylene conversion over NCl-1

Conditions:     T = 598 K; $H_2$/*m*-xylene (mole) = 4; WHSV = 3.47

Catalyst:      1 g (anhydrous) H-NCL-1 (Si/Al = 84)

| Time-on-stream | 30 min | 1 h | 2 h | 4 h | 7 h | 9 h |
|---|---|---|---|---|---|---|
| Conversion (wt.%) | 31.7 | 20.2 | 13.6 | 9.4 | 6.2 | 5.5 |
| Product distribution (wt.%) | | | | | | |
| Toluene | 10.3 | 9.1 | 7.8 | 5.9 | 6.1 | 2.7 |
| *p*-Xylene | 39.4 | 44.0 | 46.0 | 48.4 | 48.7 | 51.8 |
| *o*-Xylene | 33.2 | 34.1 | 35.3 | 36.9 | 38.1 | 39.8 |
| 1,2,3-TMB[a] | 1.5 | 0.9 | 0.5 | 0.3 | -- | -- |
| 1,2,4-TMB | 10.4 | 9.0 | 8.0 | 6.4 | 6.0 | 4.9 |
| 1,3,5-TMB | 4.0 | 1.8 | 1.2 | 0.7 | 0.3 | -- |
| Others[b] | 1.2 | 1.1 | 1.2 | 1.4 | 0.8 | 0.8 |
| *p/o* ratio | 1.19 | 1.29 | 1.3 | 1.31 | 1.30 | 1.30 |
| log(I/D) | 0.71 | 0.87 | 0.98 | 1.00 | 1.19 | 13.24 |
| I/D ratio | 5.15 | 7.5 | 9.5 | 10.0 | 15.6 | 21.1 |

[a,b] As given in Table 4.2

Table 4.6 Influence of time-on-stream on ethylbenzene disproportionation over NCL-1

Conditions:    T = 523 K; $H_2$/ethylbenzene (mole) = 4; WHSV = 0.26.

Catalyst:    1 g (anhydrous) H-NCL-1 (Si/Al = 23).

| Time-on-stream | 15 min | 30 min | 1 h | 2 h | 4 h | 5 h |
|---|---|---|---|---|---|---|
| Conversion (wt.%) | 11.2 | 11.70 | 12.2 | 10.7 | 7.8 | 6.6 |
| Product distribution (wt.%) | | | | | | |
| Benzene | 71.4 | 53.3 | 50.8 | 50.3 | 50.4 | 51.2 |
| 1,2-DEB[a] | 0.7 | 1.3 | 1.9 | 1.4 | 0.9 | 0.8 |
| 1,3-DEB | 17.0 | 28.6 | 29.7 | 30.2 | 30.4 | 30.0 |
| 1,4-DEB | 9.1 | 15.1 | 15.7 | 16.0 | 16.1 | 15.9 |
| Others[b] | 1.8 | 1.7 | 1.9 | 2.1 | 2.2 | 2.1 |
| DEB/Benzene ratio (wt.%) | 0.38 | 0.84 | 0.93 | 0.95 | 0.94 | 0.91 |

[a] diethylbenzene

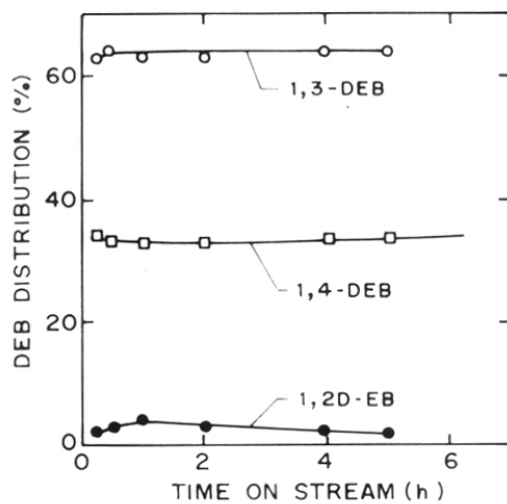[b] Aliphatics, toluene, xylenes and ethyltoluenes.

Fig.4.5    Distribution of diethylbenzenes over NCL-1 as function of time-on-stream in ethylbenzene disproportionation reaction.

zeolites, the 1,3-isomer decreases and the 1,4-diethylbenzene increases with time-on-stream[21]. The ratio of $Y_{DE-Bz}$ to $Y_{Bz}$ after induction period is around 0.9, and is almost constant with time-on-stream. All the above mentioned criteria suggest that NCL-1 is a large pore zeolite.

### 4.4.3 Influence of Si/Al ratio

Influence of Si/Al ratios on conversion and product distribution are given in Table 4.7. As expected, the conversion increases with decreasing Si/Al ratio. The ratio of $Y_{DE-Bz}$ to $Y_{Bz}$ is around 0.9 for all the samples. The distribution of diethylbenzenes are similar for all the samples.

### 4.4.4 Influence of temperature

The influence of temperature on conversion and selectivities over Al-NCL-1 (Si/Al = 83) are listed in Table 4.8. The conversion of ethylbenzene increases with temperature. The distribution of diethylbenzene isomers is almost constant for all the temperatures. The ratio of $Y_{DE-Bz}$ to $Y_{Bz}$ is around 0.9 for all the temperatures.

## 4.5 CONSTRAINT INDEX (CI)

The constraint index of different zeolites were measured under identical conditions. The results are presented in Table 4.9. The constraint index of NCL-1 (1.0) is in the range of large pore zeolites (mordenite (1.2) and Beta (0.6)). On the basis of the values of constraint index obtained under similar reaction conditions, Frilette et al[22]. have distinguished between large pore (CI < 2), medium pore (2 < CI < 12) and small pore (CI > 12) zeolites.

## 4.6 SPACIOUSNESS INDEX (SI)

The spaciousness index is a very useful tool to characterize the void space of large pore zeolites. The SI is independent of temperature and conversion. Coke formation is absent or very slow[2] during the test reaction. The spaciousness index is calculated from the ratio of i-butane and n-butane in the hydrocracked products of butyl cyclohexane[2]. Weitkamp et al.[2] concluded that the medium pore zeolites exhibit the SI values of around 1 or less. Large pore zeolites exhibit a wide range of values (SI = 2-21) of this index. Fig 4.6 shows the spaciousness indices obtained over different medium and large pore zeolites. The results obtained on NCL-1

Table 4.7 Influence of Si/Al on ethylbenzene disproportionation.

Conditions:    T = 583 K; $H_2$/ethylbenzene (mole) = 4; WHSV = 3.47; time-on-stream=20 min

Catalyst:      1 g (anhydrous) H-NCL-1

| Si/Al molar ratio | 23 | 84 | 156 | 257 |
|---|---|---|---|---|
| Conversion (wt.%) | 12.2 | 10.5 | 9.8 | 7.4 |
| Product distribution (wt.%) | | | | |
| Benzene | 51.6 | 51.4 | 50.6 | 52.7 |
| 1,2-DEB[a] | 1.6 | 1.6 | 1.5 | 1.5 |
| 1,3-DEB | 29.1 | 28.9 | 29.4 | 28.5 |
| 1.4-DEB | 15.8 | 15.7 | 16.3 | 15.8 |
| Others[b] | 1.9 | 2.4 | 2.2 | 1.5 |
| DEB/Benzene ratio (wt.%) | 0.90 | 0.9 | 0.93 | 0.87 |

[a,b] As given in Table 4.6

Table 4.8 Influence of temperature on ethylbenzene disproportionation

Conditions:    H$_2$/ethylbenzene (mole) = 4; WHSV = 3.47; time-on-stream = 20 min

Catalyst:    1 g (anhydrous) H-NCL-1 (Si/Al = 84)

| Temperature K | 553 | 583 | 613 | 643 | 673 |
|---|---|---|---|---|---|
| Conversion (wt.%) | 6.12 | 10.5 | 16.61 | 21.6 | 23.7 |
| Product distribution (wt.%) | | | | | |
| Benzene | 51.2 | 51.4 | 50.7 | 51.5 | 49.8 |
| 1,2-DEB[a] | 1.5 | 1.6 | 1.5 | 1.5 | 1.6 |
| 1,3-DEB | 29.6 | 28.9 | 28.9 | 28.8 | 28.9 |
| 1,4-DEB | 16.0 | 15.7 | 16.3 | 15.1 | 15.8 |
| Others[b] | 1.7 | 2.4 | 2.6 | 3.1 | 3.9 |
| DEB/Benzene ratio (wt.%) | 0.92 | 0.90 | 0.92 | 0.88 | 0.93 |

[a,b] As given in Table 4.6

Table 4.9  Mobil's constraint index of different zeolites

Conditions:    Temperature = 523 K; Feed (equimolar ratio of 3-methylpentane and n-hexane)
4 ml/h; time-on-stream = 20 min

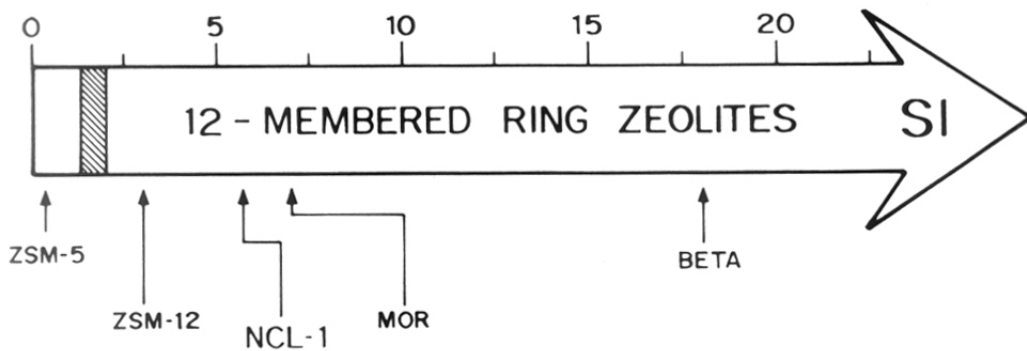| | ZSM-5 | ZSM-12 | MOR | NCL-1 | BETA |
|---|---|---|---|---|---|
| Constraint index | 7.00 | 3.00 | 1.20 | 1.00 | 0.60 |

Fig.4.6    Spaciousness index of different zeolites.

Reaction conditions: Temperature = 523; WHSV = 0.35

Reactant is butylcyclohexane.

are also included in Fig. 4.7. An average value of the spaciousness index of NCL-1 (SI = 6.1) is in the range of large pore zeolites (SI = 2-21), and suggest that the effective void space of NCL-1 is somewhat similar to that of mordenite.

## 4.7 CONCLUSIONS

1. In *m*-xylene conversion, the *p*-xylene/*o*-xylene ratio in the products is 1.1, the ratio of isomerization to disproportionation is given as log(I/D) = 1 and the molar ratio of 1,3,5-trimethylbenzene to 1,2,4-trimethylbenzene in products is 0.1, this suggests that NCL-1 is a large pore (12-membered ring) zeolite.

2. The presence of induction period and the ratio of diethylbenzene to benzene in the ethylbenzene disproportionation shows that NCL-1 probably large pore zeolite.

3. The constraint index shown by NCL-1 (CI = 1) is similar to large pore zeolites.

4. The spaciousness index shown by NCL-1 (6.1) strongly suggests that NCL-1 is a large pore zeolite.

## 4.8 REFERENCES

1.  P.A. Jacobs and J.A. Martens, Stud. Surf. Sci. Catal., **28**, 23 (1986).

2.  J. Weitkamp and S. Ernst, Stud. Surf. Sci. Catal., **38**, 367 (1988).

3.  S. Ernst, R. Kumar, M. Neuber and J. Weitkamp, Proc. IUPAC-Symp. on "characterization of Porous solids", Bad Soden, Federal Republic of Germany, April 26-29, 1987.

4.  S.M. Csicsery, Zeolites, **4**, 202 (1984).

5.  S.M. Csicsery, Pure Appl. Chem., **58**, 841 (1986).

6.  J.Weitkamp, S. Ernst, H. Dauns and E. Gallei, Chem. Ing. Tech., **58**, 623 (1986).

7.  S.B. Kulkarni, V.P. Shiralkar, A.N. Kotasthane, R.B. Borade and P. Ratnasamy, Zeolites, **2**, 313 (1982).

8.  S. Ernst, G.T. Kokatailo and J. Weitkamp, Zeolites, **7**, 180 (1987).

9.  S.G. Hegde, R.N. Bhat, R. Kumar and P. Ratnasamy, Zeolites **9**, 231 (1989).

10. R. Kumar, G.N. Rao and P. Ratnasamy, Stud. Surf. Sci. Catal., **49B**, 1141 (1989).

11. F. Joensen, N. Blom, N.J. Tapp, E.G. Derouane and C. Fernandez, Stud. Surf. Sci. Catal., **49B**, 1133 (1989).

12. P.B. Weisz, Pure Appl. Chem., **52**, 2091 (1980).

13. J. Wei, J. Catal., **76**, 433 (1982).

14. J.A. Martens, J. Perez-Pariente, E. Sastre, A. Corma and P.A. Jacobs, Appl. Catal., **45**, 85 (1988).

15. D.H. Olson and W.O. Haag, in "Catalytic Materials: Relationship between Structure and Reactivity" ACS Symp. Ser., **248**, 275 (1984).

16. V. Mavrodinova, V. Penche, U. Lohse and H. Stach, Zeolites, **9**, 197 (1989).

17. V. Mavrodinova, V. Penche, U. Lohse and T. Gross, Zeolites, **9**, 203 (1989).

18. J. Perez-Pariente, E. Sastre, V. Fornes, J.A. Martens, P.A. Jacobs and A. Corma, Appl. Catal., **69**, 125 (1991).

19. J.A. Martens, M. Tielen, P.A. Jacobs and J. Weitkamp, Zeolites, **4**, 98 (1984).

20. (a) H.G. Karge, J. Ladebeck, Z. Sarbak, K. Hatada, Zeolites, **2**, 94 (1982).
    (b) H.G. Karge, K. Hatada, Y. Zhang and R. Fiedorow, Zeolites, **3**, 13 (1983).

21. J. Weitkamp, S. Ernst, P.A. Jacobs and H.G. Karge, Erdol Kohle-Erdgas-Petrochem., **39**, 13 (1986).

22. V.J. Frilette, W.O. Haag and R.M. Lago, J. Catal., **67**, 218 (1981).

*CHAPTER 5*

## STUDIES ON V-NCL-1

## 5.1 INTRODUCTION

Crystalline microporous vanadium silicates are a new class of materials wherein the oxidative property of vanadium could be combined with the shape selective characteristics imparted by the microporous structure in which the vanadium is located. The synthesis of vanadium containing ZSM-5 has been reported by Marosi et al[1]. It was claimed to be a useful catalyst in cracking and isomerization reactions. Xu Reren et al. showed the possibility of having vanadium ions in three different oxidation states ($V^{3+}$, $V^{4+}$ and $V^{5+}$) in zeolite molecular sieves[2]. The introduction of $V^{4+}$ ions into extra-framework cationic positions by solid state reaction was reported by Kucherov and Slinkin[3]. In 1985, Inui et al. had synthesized V-ZSM-5 by introducing vanadium instead of aluminium in the reaction gel[4]. However, the source of silica (i.e sodium silicate) contained aluminium, and hence, they could not obtain pure vanadium silicates (i.e free from aluminium). They observed that the morphology, acidity and catalytic activity of V-ZSM-5 is significantly different from its aluminium analog[4]. Miyamoto et al. synthesized V-ZSM-5 using different vanadium sources and claimed that vanadium acetyl acetonate is a suitable source to prepare V-ZSM-5 with high crystallinity and high BET surface area[5]. The catalytic activity of V-ZSM-5 was 50 times higher than that of bulk $V_2O_5$ in $H_2$ oxidation, while it was lower in the oxidation of $NH_3$[6]. Vanadium silicates were also found to be active in ammoxidation of xylenes and propane[7,8], oxidation of butadiene to furan[9] and in the oxidative dehydrogenation of propane to propylene[10].

The above mentioned vanadium silicate molecular sieves either contained aluminium or were thermally unstable, being transformed into $\alpha$-crystabolite upon calcination. Recently, Kornatowski et al.[11] and Rigutto et al.[12] have reported the synthesis of vanadium silicate molecular sieves with MFI topology (VS-1). They were thermally stable and free from aluminium. Kornatowski et al. reported that the vanadium species are tetrahedrally coordinated at framework positions[11]. However, Rigutto et al. postulated that the vanadium ions are probably connected to the silicalite framework at defect sites. The $V^{4+}$ ions in the as-synthesized form are penta-coordinated and after calcination, the $V^{5+}$ (on calcination $V^{4+}$ ions are oxidized to $V^{5+}$

ions) ions are in the tetrahedral coordination[12]. Fejes et al. suggested from their ESR studies that the $V^{4+}$ ions in the as-synthesized form are in distorted square pyramidal coordination[13]. Centi et al. have reported that at least two different vanadium species are present in their vanadium silicate molecular sieve (VS-1)[14].

Recently, Rao et al. reported the synthesis of thermally stable vanadium silicate molecular sieves with MEL topology[15] (VS-2). Vanadium incorporated molecular sieves are found to catalyze various oxidation reactions such as oxyfunctionalization of alkanes, hydroxylation of phenol, oxidation of alkyl aromatics, oxidation of aniline and oxidation of sulfides in presence of aqueous hydrogen peroxide under mild conditions[16-19]. These studies have so far been restricted to medium pore structures. Recently, we have synthesized and characterized a new high-silica, large pore zeolite, designated as NCL-1[20]. NCL-1 can be synthesized in a wide range of Si/Al ratio of 23 and above and its Al-free silica polymorph (Si-NCL-1)[20]. The possibility of incorporating vanadium into Si-NCL-1 structure has led to the synthesis, for the first time, of vanadium-containing, large pore molecular sieve (V-NCL-1), which has interesting applications in the oxidation of bulky hydrocarbons[21].

This chapter is divided into two parts. Part A describes the synthesis and characterization of V-NCL-1 through X-ray diffraction (XRD), infra-red (IR), electron spin resonance spectroscopy (ESR), thermal analysis (TG-DTA), adsorption studies and surface area measurements. Evidence for the incorporation of vanadium ions into the zeolite framework has been obtained from XRD, IR and ESR techniques. Additional support is obtained from catalytic activity in various oxidation reactions. Part B describes the studies carried out on the catalytic properties of vanadium silicates in the following reactions.

* Oxyfunctionalization of n-octane and cyclohexane

* Oxidation of toluene

* Oxidation of xylenes

* Oxidation of 1,2,4- and 1,3,5-trimethylbenzenes

* Oxidation of naphthalene

## 5.2 EXPERIMENTAL

### 5.2.1 Hydrothermal synthesis

The syntheses were carried out in stainless steel autoclaves of 80 ml capacity (Figure 2.5 in chapter 2) under autogeneous pressure with agitation (60 rpm). The crystallization was conducted at 443 K. The silica polymorph of NCL-1 (Sample A) and three vanadium silicate samples with Si/V molar ratios of 175 (Sample B), 96 (sample C), and 48 (Sample D) (in the gel) were synthesized hydrothermally. The gel compositions (molar), used in the syntheses were as follows:

Si/V  = 48 to ∞

$OH^-/Si = 0.12$

$R^{2+}/Si = 0.05$

$H_2O/Si = 52$

$Si/Na^+ = 0.16$

The $OH^-$/Si concentration was adjusted to 0.12 by adding appropriate amount of $H_2SO_4$. Raw materials used in the syntheses are given in Table 5.1. In a typical synthesis, a solution containing 0.48 g NaOH in 35 g $H_2O$ was added to 4.5 g fumed silica. This mixture was stirred for 1 h at 298 K. To the above mixture, an appropriate amount of $VOSO_4.5H_2O$ solution (0.11, 0.20 and 0.40 g of vanadyl sulfate in 10 g water for samples having Si/V ratios 175, 96 and 48, respectively) was added. The mixture was stirred for 1 h and then 1.71 g organic additive (hexamethylene bis(triethylammonium bromide)) in 10 g water was added. Finally, $H_2SO_4$ in 10 g $H_2O$ (0.07, 0.11 and 0.15 g $H_2SO_4$ for the samples having Si/V 96, 175 and ∞, respectively) was added. The resultant mixture was stirred for 2 h and charged into the autoclave. The crystallization was carried out under agitation at 443 K. The crystallization time for samples with Si/V molar ratio of 48, 96, 175 and ∞ were 16, 12, 9 and 4 days, respectively. After crystallization, the product was filtered, washed with deionized water, dried at 383 K and calcined at 723 K in air.

Table 5.1. Specification of the reactants used in the syntheses.

| S.No. | Chemical nature | Chemical formula | Purity% |
|---|---|---|---|
| 1. | Fumed silica (Sigama, USA, S-5005) | $SiO_2$ | 99.9 |
| 2. | Vanadyl sulfate (Loba Chemie) | $VOSO_4.5H_2O$ | 100 |
| 3. | Hexamethylene bis(triethyl ammonium bromide) | $C_{18}H_{42}N_2Br_2$ | >95 |
| 4. | Sodium hydroxide (AR grade) | $NaOH$ | 99 |
| 5. | Sulphuricacid (AR grade) | $H_2SO_4$ | 96 |

## 5.2.2 Characterization

The experimental procedures for X-ray diffraction, infrared spectroscopy, adsorption studies, surface area measurements, thermal analysis, scanning electron microscopy and chemical analysis were described in sections 2.3.1, 2.3.2, 2.3.3, 2.3.4, 2.3.6, 2.3.8 and 2.3.9, respectively.

### 5.2.2.1 Electron spin resonance spectroscopy

Electron spin resonance spectra were recorded using Bruker ER-200 D spectrometer at 9.7 GHz (X-band) with a rectangular cavity ST 8424. Modulation at 100 KHz with intensity 1.25 GPP and time constant $10^3$ m sec. was used. The h.f. power was chosen small enough to prevent any signal saturation. The spectra were recorded at 298 K. A constant weight of 21 mg of the sample was taken to record the spectra.

## 5.3 PREPARATION OF OTHER CATALYSTS

VS-2 samples were prepared following the procedure reported in literature by Rao et al[15].

### 5.3.1 Ammonium acetate treatment

The vanadium ions in the non-framework positions can be removed by ammonium acetate treatment. Hence V-NCL-1 samples were treated in the following manner: 1 g of the calcined vanadium silicate was treated with 50 ml of 1M ammonium acetate for 24 h at 298 K, washed with distilled water, dried and calcined in air at 723 K.

### 5.3.2 Reduction experiments

1 g of V-NCL-1 calcined or ammonium acetate treated sample was loaded in a fixed-bed down-flow tubular silica reactor (15 mm). The temperature was raised from 298 K to 703 K with a rate of heating of $1°$ min$^{-1}$, while $H_2$ gas was passed at a rate of 100 ml min$^{-1}$. The sample was held at 703 K for 6 h and then cooled to 298 K in $H_2$.

### 5.3.3 Steaming experiments

The hydrothermal treatment was carried out in a tubular furnace in a flow of 100% steam at 873 K for 4 h. The temperature was raised from 298 to 873 K at a heating rate of $3°$ min$^{-1}$. Then the samples were cooled to room temperature and kept in a desiccator.

### 5.3.4 Impregnation of vanadium

The impregnation procedure was as follows: 1 g of Si-NCL-1 and 100 ml of 0.25% vanadyl sulfate solution (which gives 5 wt.% vanadium in zeolite) were stirred till it became dry. The dried sample was calcined at 723 K. The vanadium content of the final impregnated sample was found to be 4.9 wt.% (from chemical analysis).

## 5.4 CATALYTIC REACTIONS

### 5.4.1 Oxyfunctionalization of alkanes

The oxyfunctionalization of n-octane and cyclohexane was carried out in a stirred autoclave (Parr Instrument, USA) of 300 ml capacity at 373 K under autogeneous pressure. Typically, 100 mg of the V-NCL-1 (Si/V = 250 in product) catalyst, 5 g of alkane and required amount of 26% (by wt.) aqueous $H_2O_2$ were mixed in 20 ml of acetonitrile (solvent). The reaction was carried out for 8 h at 373 K. After the completion of the reaction, 25 ml of acetone was added to the products, which were then separated from the catalyst by filtration and analyzed by GC (HP 5880) using a capillary (50 m; cross linked methylsilicone gum) column and flame ionization detector (FID).

### 5.4.2 Oxidation of alkyl aromatics and naphthalene

The oxidation of alkyl aromatics and naphthalene was carried out in a batch reactor. In a typical reaction, 100 mg of V-NCL-1 (Si/V = 250 in product) catalyst was dispersed in a solution containing 1 g of reactant and 10 g of acetonitrile (solvent). The mixture was vigorously stirred and the required amount of 26% (by wt.) aqueous $H_2O_2$ was then added. After completion of the reaction, the products were separated from the catalyst and analyzed by GC (HP 5880) using a capillary (50 m; crosslinked methylsilicone gum) column and flame ionization detector (FID).

## 5.5 RESULTS AND DISCUSSION

### 5.5.1 Hydrothermal synthesis

#### 5.5.1.1 Influence of Si/V ratio on kinetics of crystallization

Fig. 5.1 depicts the influence of vanadium concentration in the initial gel reaction mixture on the crystallization. The nucleation and crystallization time increase with vanadium content, Curves a to d refer to Si/V (input) = ∞ (sample A), 175 (sample B), 96 (sample C) and 48 (sample D), respectively. The samples with Si/V = 48, 96, 175 and ∞ were fully crystallized after 16, 12, 9 and 4 days, respectively.

Table 5.2 summarizes the physico-chemical properties of all vanadium silicate samples as well as V-free silica polymorph. It is seen that the vanadium uptake from the gel during the crystallization is far from complete. The vanadium uptake from the gel was 32, 38 and 44% for the samples with Si/V ratios of 48, 96 and 175, respectively. The Si/Na ratios of different calcined and ammonium treated samples were included in the Table 5.2.

The samples B, C and D were treated with ammonium acetate and calcined. The resulting samples have Si/V ratio of 432, 319 and 262, respectively, indicating that in these samples, part of the vanadium is extractable and, hence, most probably in non-framework positions. Further treatments of samples B-D with ammonium acetate did not lead to an increase in the Si/V ratio of the sample. The remaining vanadium is apparently firmly bound to the lattice framework and hence, cannot be removed by ammonium acetate treatment.

### 5.5.2 Characterization

#### 5.5.2.1 X-ray diffraction

The powder X-ray diffraction profiles of the three V-NCL-1 samples are shown in Fig. 5.2 (curves b-d refer to samples B-D). They match well with that of the V-free silica polymorph (Si-NCL-1) (curve a). No peaks other than those already present in the silica polymorph of NCL-1 are observed in the V-NCL-1 samples. When the vanadium silicate (Sample D Si/V = 150) sample was treated with ammonium acetate and calcined, this sample shows similar XRD pattern (Fig. 5.2 profile 'e') indicating the absence of any structural collapse due to ammonium
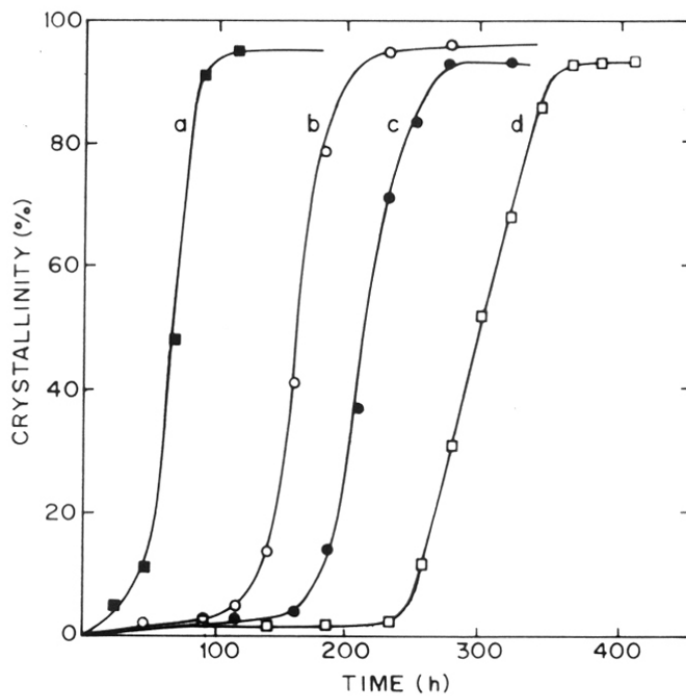
Fig. 5.1. Hydrothermal crystallization of silica polymorph of NCL-1 (sample A) and V-NCL-1 (samples B, C and D) (curves 'a' to 'd', respectively) with time.

acetate treatment. The ammonium acetate treatment is expected to extract out any vanadium present in non-framework positions. XRD data show that the crystalline structure is intact even after removal of such vanadium species.

The unit cell volume increases linearly with the vanadium content in the sample (Table 5.2 and Fig. 5.3) suggesting the incorporation of vanadium probably into the NCL-1 framework. On steaming the samples at 873 K for 4 h, all the vanadium silicates exhibited a reduction in the unit cell parameters to values typical of Si-NCL-1 (Fig. 5.3). The contraction in the unit cell volume on hydrothermal treatment has occurred probably due to the removal of the vanadium ions originally present in the framework positions to non-framework locations. Si-NCL-1 itself did not show any decrease in the unit cell parameters after similar steam treatment. The results of steaming experiments thus suggest that in the calcined V-NCL-1 samples, the vanadium ions are probably located within the silicate structure.

### 5.5.2.2 Infrared spectroscopy

Additional support for the location of vanadium in the NCL-1 structure is suggested from the observation of an IR band at around 960 cm$^{-1}$ for vanadium silicate samples (Fig. 5.4). Vanadium-free sample (Sample A) does not exhibit this band. Similar observations have been made in the case of titanium silicalites (TS-1[22], TS-2[23] and Ti-ZSM-48)[24] and vanadium silicates (V-MFI and V-MEL)[11,15]. This band has been attributed to Si-O-Ti (or V) vibrations, when Ti (or V) is linked to Si-O tetrahedra. The intensity of this IR band increased linearly with vanadium content in the V-NCL-1 samples as shown in Fig. 5.5. This indicates that the vanadium ions are located in the framework of NCL-1 structure.

### 5.5.2.3 Electron spin resonance spectroscopy

The electron spin resonance spectra of as-synthesized samples B-D, recorded at 298 K are shown in Fig. 5.6. They are characteristic of atomically dispersed and immobile, para-magnetic $V^{4+}$ ions with hyperfine structure derived from the interaction of a free electron of $V^{4+}$ ($3d^1$) with the nuclear magnetic moment of $^{51}V$ nuclei (I = 7/2), that gives rise to an 8 fold hyperfine splitting of all anisotropic components. These spectra are similar to those observed on vanadium silicates with MFI and MEL structures[13,15]. The well-resolved ESR spectra of the

Table 5.2. Physico-chemical properties of V-NCL-1 and Si-NCL-1 samples

| Samples | Si/V in gel | Si/V in product sample | Si/V[a] | Total surface area, m²/g[b] | Mesopore area, m²/g | ESR intensity, a.u[c] | Unit cell volume[d], Å³ | Sorption capacity[e], wt.% | |
|---|---|---|---|---|---|---|---|---|---|
| | | | | | | | | n-hexane | mesitylene |
| A | ∞ | >3000 (33)[f] | --- | 339 | 5.4 | --- | 2867 | 6.96 | 4.77 |
| B | 175 | 400 (27) | 432 (144)[f] | 298 | 10.0 | 272 | 2883 | 6.92 | 4.68 |
| C | 96 | 250 (24) | 319 (131) | 310 | 8.3 | 371 | 2896 | 6.85 | 4.63 |
| D | 48 | 150 (20) | 262 (113) | 301 | 5.9 | 462 | 2912 | 6.87 | 4.59 |

[a]  After treating the sample with ammonium acetate.
[b]  From $N_2$ adsorption, $(p/p_o = 0.005 - 0.01)$
[c]  Integrated intensity of the 8 line spectra of as-synthesized sample recorded at 298 K.
[d]  Calculated from the XRD data of calcined samples.
[e]  Gravimetric adsorption at 298 K and at $p/p_o = 0.5$.
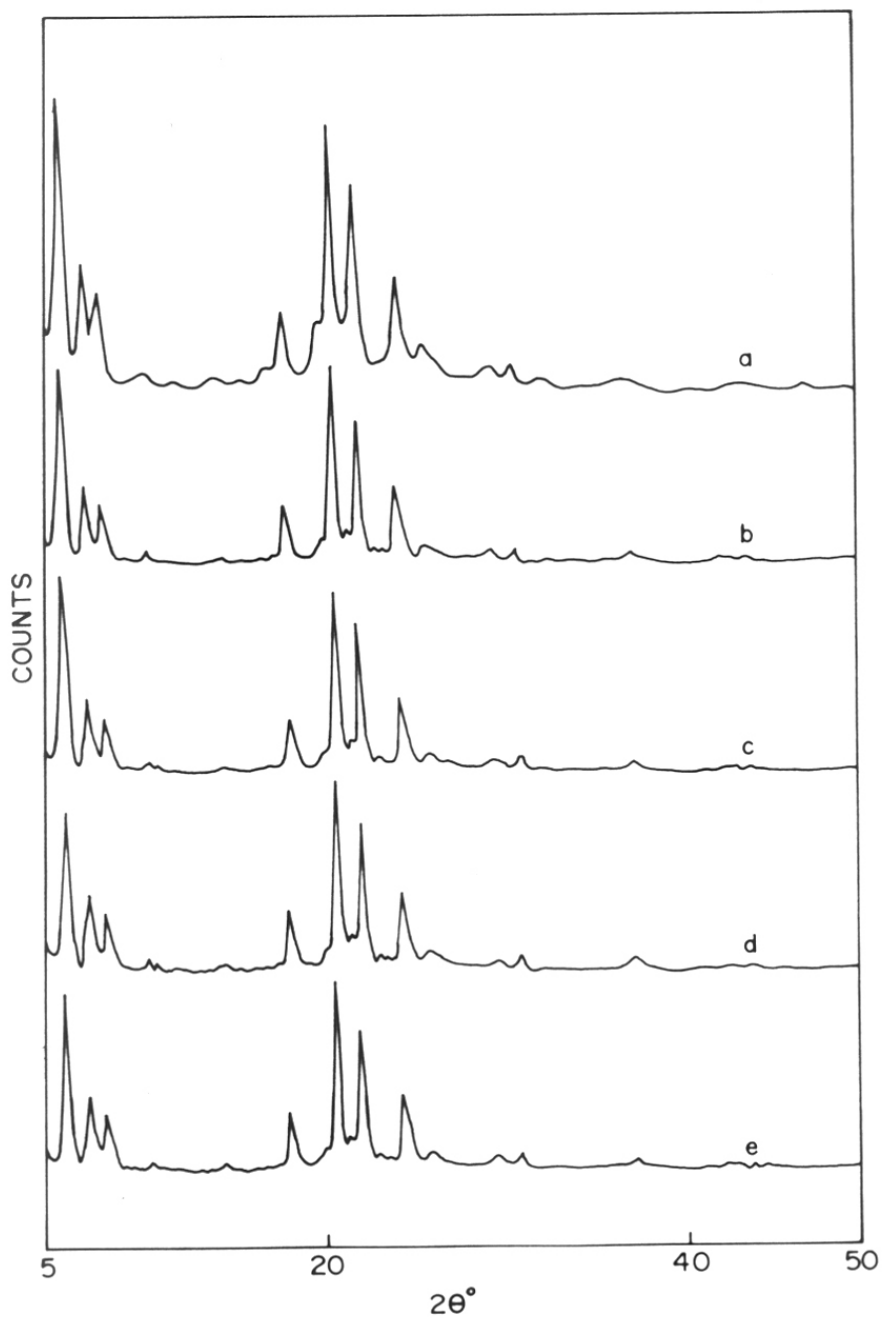[f]  In parentheses are the Si/Na ratio of the corresponding sample.

110

Fig.5.2.     X-ray diffraction profiles of calcined samples A to D, (curves 'a' to 'd', respectively) and of sample D after treatment with ammonium acetate and calcination (curve 'e').
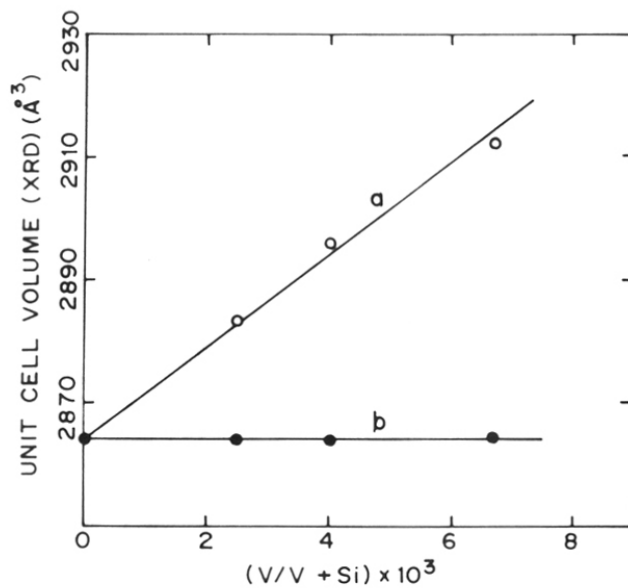
Fig.5.3.    Correlation between the vanadium content in V-NCL-1 (calcined) samples and the unit cell volumes (curve 'a') and after steaming the corresponding samples at 873 K for 4 h in 100% steam (curve 'b').
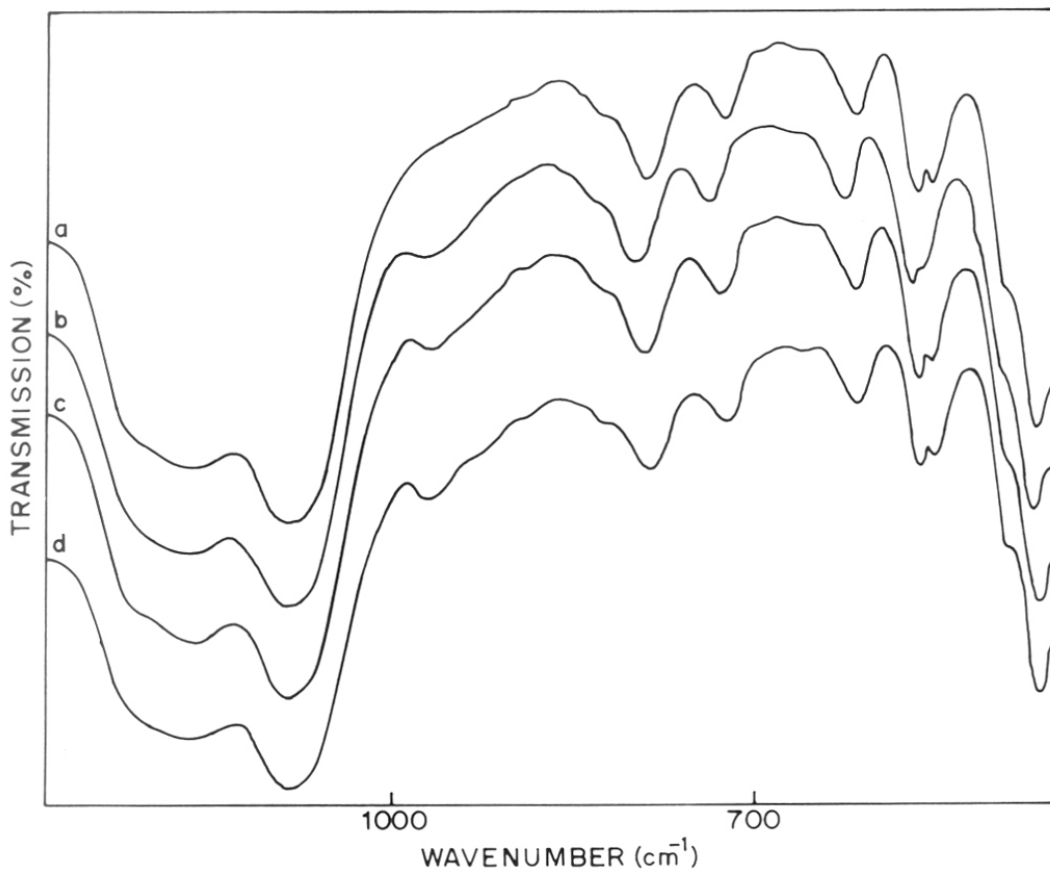
Fig.5.4.    Framework IR spectrum of V-NCL-1 samples (calcined).
Curves 'b' to 'd' refer to samples with Si/V = 400, 250 and 150, respectively, and
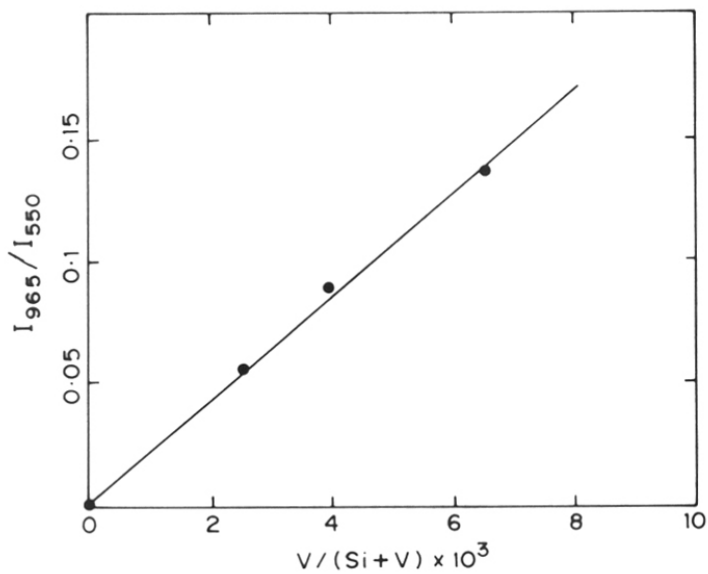Si-NCL-1 (curve 'a').

Fig.5.5.    The ratio of intensities of 965 to 550 cm$^{-1}$ IR bands vs. mole fraction of vanadium in V-NCL-1 (calcined) samples.
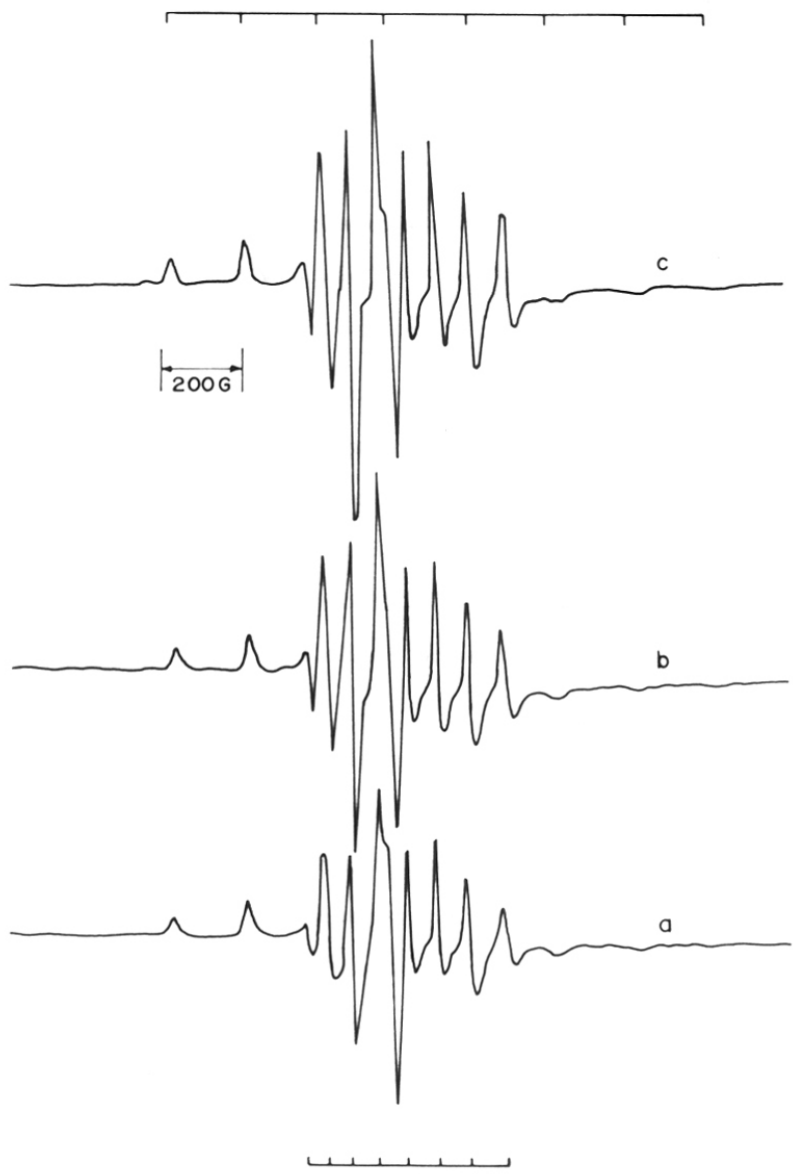
Fig.5.6. ESR spectra of as-synthesized V-NCL-1 samples (curves 'a' to 'c' refer to samples B to D, respectively). Recorded at 298 K.

samples without the superimposition of any large signal due to dimeric or polymeric $VO^{2+}$ species indicate a single type of $V^{4+}$ species in the as-synthesized form. The integrated ESR intensity increased, though not linearly, with vanadium content in the samples as shown in Fig. 5.7 and Table 5.2.

The 'g' values and hyperfine coupling constants (A) calculated from the spectra are given in Table 5.3. The corresponding values for VS-1[13] and VS-2[15] are also included in Table 5.3. The values are assigned to $V^{4+}$ in probable framework positions[13,15].

The vanadium silicate samples, after calcination in air, show no ESR signal indicating the oxidation of most of the $V^{4+}$ ions to diamagnetic $V^{5+}$ species (compare curves 'a' and 'b' in Fig. 5.8). The flat baseline in curve 'a' indicates the absence of $V^{4+}$ clusters in the as-synthesized form. On reduction of the calcined form in $H_2$ at 703 K, the spectrum in curve 'c' is observed. Reduction converts part of $V^{5+}$ species back to $V^{4+}$ ions. In addition to these isolated $V^{4+}$, the presence of a broad signal (in curve 'c') indicates the formation of cluster-like vanadium species on oxidation-reduction of these vanadium silicates. Apparently, these vanadium clusters are formed on oxidation of the as-synthesized sample. To confirm this hypothesis, the calcined form of sample D (Si/V = 48 (input) curve 'b' in Fig.5.8) was treated with ammonium acetate (to extract non-framework vanadium ions), calcined in air at 723 K and further reduced in $H_2$ at 703 K. The ESR spectrum of the resultant sample is included in Fig. 5.8., curve 'd'. Even though both isolated $V^{4+}$ and vanadium clusters are present, the concentration of the vanadium clusters in ammonium acetate treated sample is relatively lower compared to the sample whose ESR spectrum is depicted in curve 'c'. Treatment with ammonium acetate has removed part of the vanadium clusters formed on calcination of the as-synthesized samples.

In summary, in the as-synthesized form most of the vanadium is present as atomically dispersed and isolated $V^{4+}$ located in framework positions though not necessarily with tetrahedral coordination. On calcination in air the vanadium ions are oxidized to the pentavalent state. In addition, part of the vanadium ions leave lattice locations and form non-framework clusters. Ammonium acetate treatment is able to remove at least part of these clusters. When the oxidized
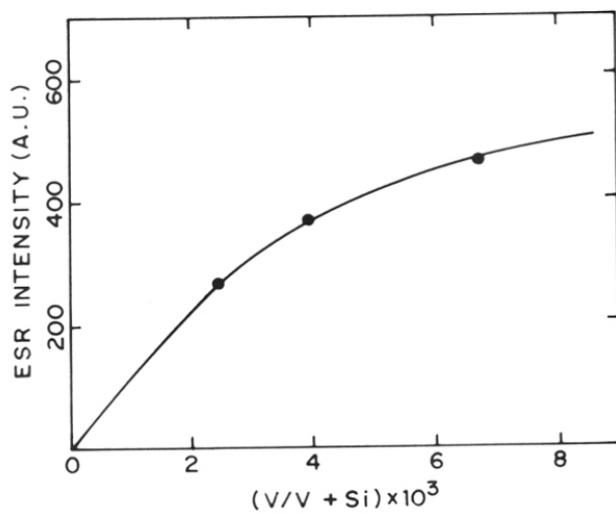
Fig.5.7.    Correlation between the integrated intensity of ESR signals vs. mole fraction of vanadium in as-synthesized V-NCL-1 samples.

Table 5.3. ESR parameters of vanadium silicate molecular sieves[a]

| Samples | Si/V in product | $g_{\parallel}$ | $g_{\perp}$ | $A_{\parallel} \times 10^4$ (cm$^{-1}$) | $A_{\perp} \times 10^4$ (cm$^{-1}$) | References |
|---|---|---|---|---|---|---|
| B (as-synth.) | 400 | 1.935 | 1.972 | 193 | 72.7 | This work |
| C (as-synth.) | 250 | 1.930 | 1.972 | 196 | 71.9 | " |
| D (as-synth.) | 150 | 1.930 | 1.974 | 196 | 72.1 | " |
| D1[b] | 150 | 1.934 | 1.980 | 195 | 73.7 | " |
| D2[c] | 262 | 1.933 | 1.974 | 194 | 73.6 | " |
| VS-1(as-synth.) | 42 | 1.949 | 1.990 | 186 | 72.5 | 13 |
| VS-2(as-synth.) | 78 | 1.932 | 1.981 | 185 | 72.0 | 15 |

[a] Spectra recorded in the X-band at 298 K.

[b] Sample D calcined in air and reduced in H$_2$ at 703 K for 6 h

[c] Sample D calcined in air and treated with ammonium acetate, washed, calcined at 723 K and then reduced in H$_2$ at 703 K for 6 h.
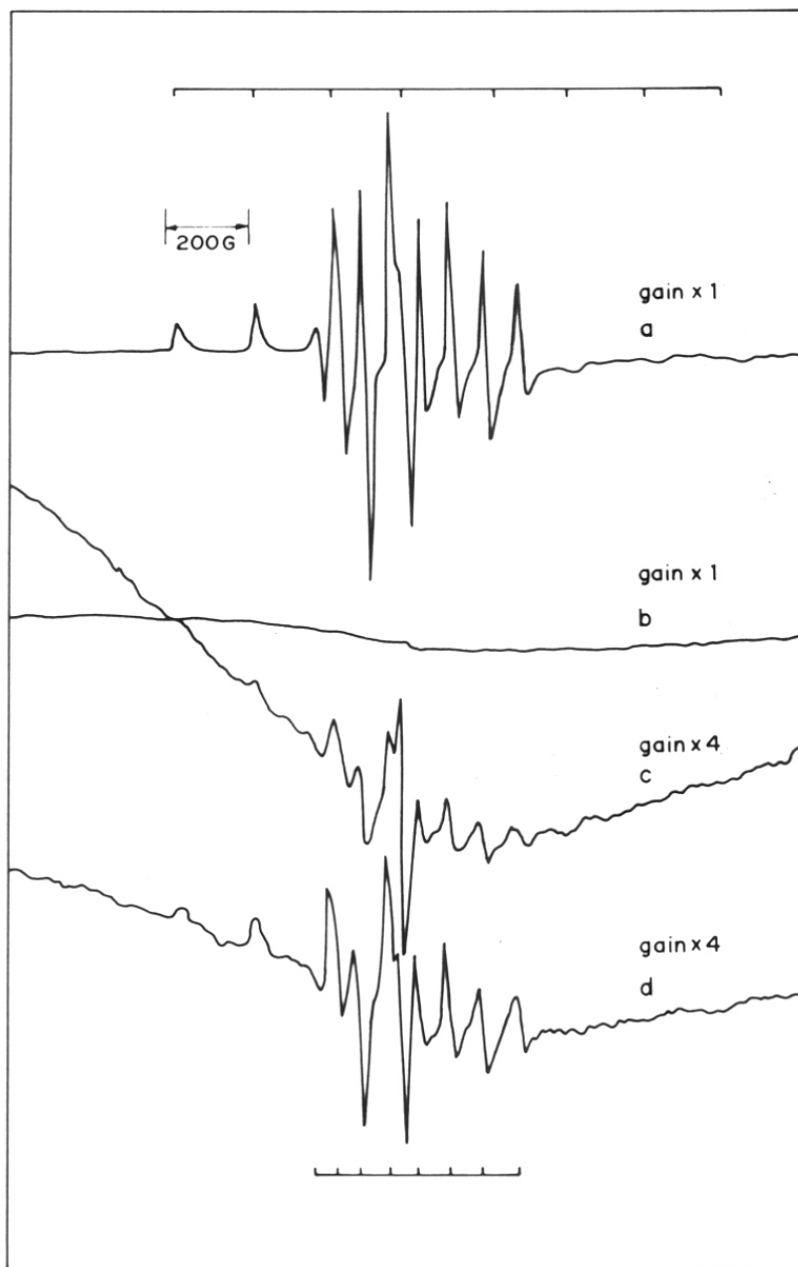
Fig.5.8. ESR spectra of as-synthesized V-NCL-1 sample D (curve 'a'), calcined in air (b), calcined and then reduced in H$_2$ at 703 K for 6 h (c), and calcined in air, treated with ammonium acetate, washed, calcined at 723 K and then reduced in H$_2$ at 703 K for 6 h (d).

sample is reduced, $V^{4+}$ ions are formed again. While part of these $V^{4+}$ ions are isolated, a significant portion are in cluster-like species. The 3-dimensional silicate structure of the molecular sieve is intact during all these treatments.

### 5.5.2.4 Sorption studies

The amount of adsorption (wt.%) of n-hexane and mesitylene on V-NCL-1 samples having different Si/V ratios are listed in Table 5.2. The amount of adsorption of a particular sorbate on various vanadium silicates is similar to that of the V-free silica polymorph indicating that the samples are substantially free from occluded material in the channels. The adsorption of mesitylene on various V-NCL-1 samples show that they are large pore molecular sieves.

### 5.5.2.5 Surface area measurements

The low pressure ($p/p_o = 0.01$) nitrogen adsorption isotherms at liquid nitrogen temperature was typical of a microporous material. The apparent surface area of the vanadium silicates with different Si/V ratios are presented in Table 5.2. In V-NCL-1 samples, the surface area is similar to V-free silica polymorph and the t-area (due to mesoporous impurities) of only 5-10 $m^2/g$, indicating that the content of amorphous phase in the samples is very small.

### 5.5.2.6 Thermal analysis

Simultaneous TG-DTA analyses of V-NCL-1 (sample D) is shown in Fig. 5.9. The calcination of the as-synthesized V-NCL-1 sample in air occurs exothermally. During thermal analysis of V-NCL-1, two distinct weight losses are observed in the range of 350-450 K and 520-690 K, respectively. The former is due to the loss of water and the latter due to the oxidative decomposition of the organic material in the pore system of V-NCL-1. From thermogravimetric analysis, the amount of organic additive decomposed in air between 520 and 690 is calculated to be 6.8 wt.%.

### 5.5.2.7 Scanning electron microscopy

The scanning electron micrographs of V-NCL-1 (Si/V = 250) are shown in Fig. 5.10. For comparison, the scanning electron micrographs of Al-NCL-1 (Si/Al = 84) and Si-NCL-1 are

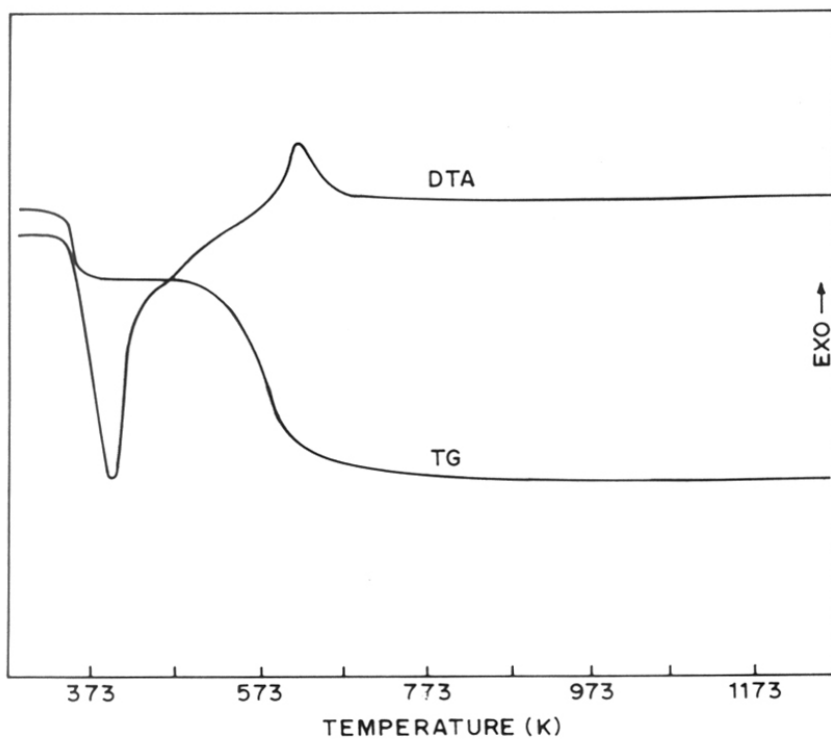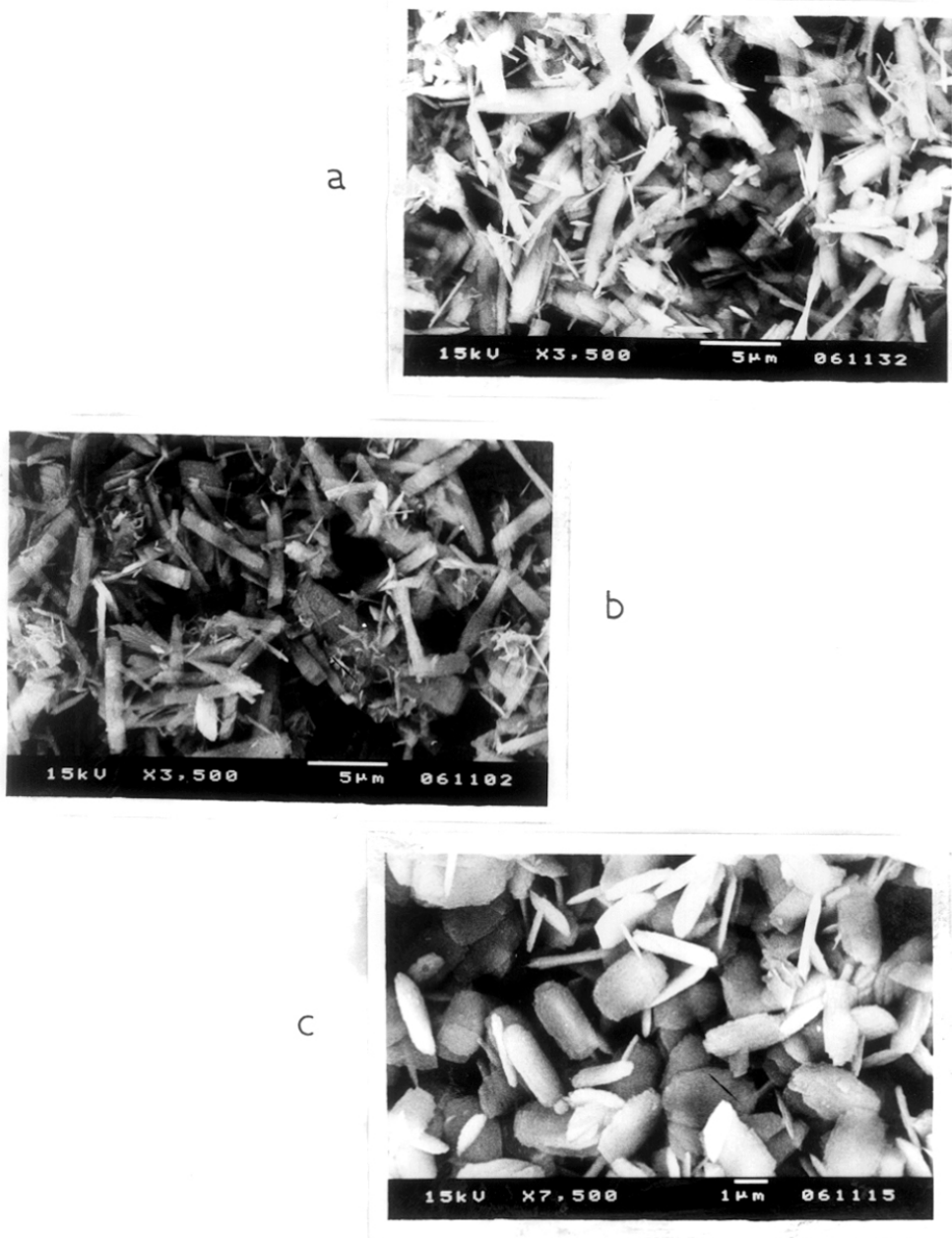Fig.5.9.    Simultaneous TG-DTA of as-synthesized sample D in air.

a

b

c

Fig.5.10.    Scanning electron micrographs of V-NCL-1 (sample C) (a), Al-NCL-1 (Si/Al = 84) (b) and Si-NCL-1 (c).

also shown in Fig. 5.10. These micrographs show the absence of amorphous material. The morphology of the crystals of V-NCL-1 and Al-NCL-1 is similar and in needle shape whereas in Si-NCL-1 many of the crystals are oblong-shaped.

## PART B

## 5.6 CATALYTIC PROPERTIES

### 5.6.1 Oxyfunctionalization of alkanes

The introduction of oxygen containing functional groups in alkanes proceeds with low selectivities over most homogeneous and heterogeneous catalysts with monooxygen donor oxidants, like hydrogen peroxide and iodosobenzene. This reaction has been reported to be catalyzed by Pd-Fe zeolite[25]. Oxyfunctionalization with high selectivities was reported on natural and synthetic metallo porphyrins systems[26] and on vanadium (V) oxo peroxo complexes[27]. The titanium silicate molecular sieves, TS-1[28,29] and TS-2[30], and vanadium silicate molecular sieves[17,19] were reported to catalyze the oxyfunctionalization of alkanes with aqueous hydrogen peroxide under mild conditions and with high selectivities. Unlike titanium silicalites, vanadium silicates are also able to oxidize the primary (terminal) carbon atoms of n-alkanes[17,19]. This appears to be a characteristic feature of vanadium silicates.

The oxidation of n-octane over V-NCL-1 (Si/V = 250) in presence of aqueous $H_2O_2$ (26 wt.%) is shown in Table 5.4. The oxyfunctionalization of n-octane on V-NCL-1 may be illustrated in the following scheme:
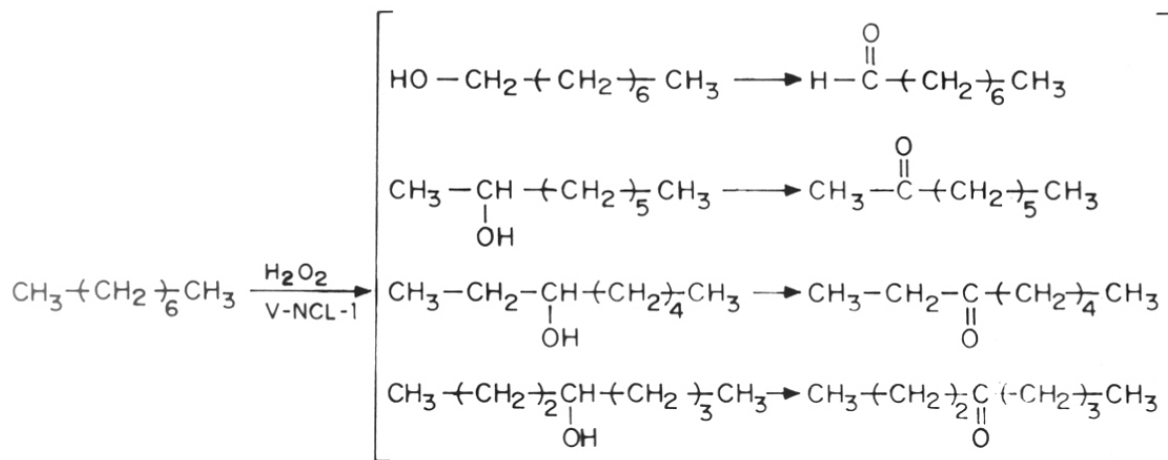
Table 5.4.    Oxyfunctionalization of n-octane over V-NCL-1 (Si/V - 250)[a]

| Catalyst | V-NCL-1 |
|---|---|
| Turnover number[b] | 4.6 |
| $H_2O_2$ selectivity[c], mole % | 39.5 |
| **Product distribution**, wt.% | |
| 1-Octanol | 2.1 |
| 2-Octanol | 8.8 |
| 3-Octanol | 4.8 |
| 4-Octanol | 5.2 |
| 1-Octanal | 3.6 |
| 2-Octanone | 22.5 |
| 3-Octanone | 21.1 |
| 4-Octanone | 15.0 |
| Others[d] | 16.9 |

[a] Reaction conditions: catalyst = 0.1 g; n-octane = 5 g; alkane/$H_2O_2$ (mole ratio) = 3; solvent (acetonitrile) = 20 g; temperature = 373 K; reaction duration = 8 h.

[b] Moles of reactant converted per mole of vanadium $min^{-1}$

[c] $H_2O_2$ utilized for monofunctional product formation

[d] Mostly oxygenates with more than one functional group and lactones

The major products of oxidation of n-octane are the corresponding alcohols and their secondary oxidation products *viz.*, the carbonyl compounds (aldehydes and ketones). An interesting observation is the formation of primary alcohols and aldehydes in addition to the secondary alcohols and ketones. Thus, unlike the titanium silicalites, vanadium silicates are able to activate the primary (terminal) carbon atoms of n-alkanes[17,19]. The product distribution shows that the activation of carbon at the second position (among all the secondary carbon atoms) is preferred to others and follows the order 2C > 3C > 4C > 1C.

Oxidation of n-octane over V-NCL-1, VS-2 and TS-2 in presence of aq. $H_2O_2$ are shown in Table 5.5. The major products of oxidation of n-octane are the corresponding alcohols and their secondary oxidation products (aldehydes and ketones). In the product distribution there is marked difference between vanadium silicates (VS-2 and V-NCL-1) and titanium silicate (TS-2) (Table 5.5). These are: (1) unlike titanium silicates (TS-2 and TS-1), vanadium silicates (VS-2 and V-NCL-1) are able to activate primary carbon atom and (2) in the case of vanadium silicates (VS-2 and V-NCL-1) a higher aldehydes+ketones to alcohol ratio has been observed compared to titanium silicate (Table 5.5). This indicates a greater oxidation ability of the vanadium silicates compared to titanium silicates in the secondary oxidation reaction.

### 5.6.2 Oxyfunctionalization of cyclohexane

The oxidation of cyclohexane was carried out over calcined samples of three different Si/V ratios, *viz.*, 150, 250 and 400. The results are presented in Table 5.6. The oxidation of cyclohexane on V-NCL-1 follows as represented below:
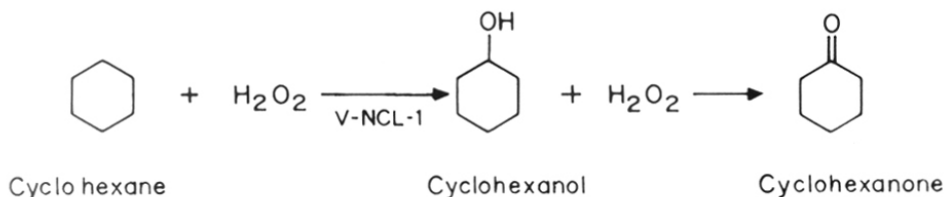


Cyclo hexane                Cyclohexanol            Cyclohexanone

Table 5.5 Oxidation of n-octane over V-NCL-1, VS-2 and TS-2[a].

| Position of activated carbon | Octanone(-al)/octanol ratio, wt.% | | |
|---|---|---|---|
| | V-NCL-1[b] | VS-2[c] | TS-2[d] |
| Conversion, mole% | 8.2 | 12.8 | 14.5 |
| 1-Octanal/1-ol | 1.6 | 1.35 | -- |
| 2-Octanone/2-ol | 2.6 | 3.8 | 1.2 |
| 3-Octanone/3-ol | 4.5 | 3.9 | 1.3 |
| 4-Octanone/4-ol | 3.0 | 3.6 | 1.35 |

[a] Reaction conditions: catalyst = 0.1 g; n-octane = 5 g; alkane/$H_2O_2$ (mole ratio) = 3; solvent (acetonitrile) = 20 g; temperature = 373 K; reaction duration = 8 h.

[b] V-NCL-1: Si/V = 250; [c]VS-2: Si/V = 79; [d]TS-2: Si/Ti = 77.

Table 5.6 Oxidation of cyclohexane on vanadium silicate molecular sieves[a]

| Catalyst | Si/V | Conv., mole% | $H_2O_2$ Sel.[b], mole% | Product distribution, wt.% | | |
|----------|------|--------------|--------------------------|------------|---------------|----------|
| | | | | Cyclohexanol | Cyclohexanone | Others[c] |
| V-NCL-1 | 150 | 11.4 | 48.5 | 33.7 | 60.4 | 5.9 |
| V-NCL-1 | 250 | 9.7 | 40.1 | 33.4 | 61.3 | 5.3 |
| V-NCL-1 | 400 | 7.3 | 29.6 | 34.2 | 59.7 | 6.1 |
| V-NCL-1[d] | 319 | 9.4 | 39.1 | 32.3 | 62.2 | 5.5 |
| Si-NCL-1 | -- | 2.1 | 3.9 | 16.4 | 18.2 | 65.4 |
| Si-NCL-1[e] (V-impreg.) | -- | 2.5 | 4.5 | 15.7 | 17.9 | 66.4 |

[a] Reaction conditions: catalyst = 0.1 g; cyclohexane = 5 g; cyclohexane/$H_2O_2$ (mole ratio) = 3; solvent (acetonitrile) = 20 g; temperature = 373 K; reaction duration=8 h.

[b] $H_2O_2$ utilized for cyclohexanol and cyclohexanone formation.

[c] Mostly oxygenates with more than one functional group and lactones.

[d] The calcined form of V-NCL-1 sample (Si/V = 250) was treated with ammonium acetate and calcined at 723 K.

[e] Vanadium impregnated (4.9%) on Si-NCL-1.

As expected, the conversion and $H_2O_2$ selectivity increased with vanadium content. These three catalysts show high selectivities for mono-functional products (about 94-95%) and the cyclohexanol to cyclohexanone ratio is around 0.55. The catalysts after separation from the products, washing and reactivation were found to have almost similar activity as the fresh calcined samples. The oxidation activity of silica polymorph, vanadium impregnated Si-NCL-1 and ammonium acetate treated V-NCL-1 (Si/V = 250) are also included in Table 5.6 for comparison. The pure silica polymorph and its vanadium impregnated samples show low activity that leads mainly to non-selective oxidation of cyclohexane. This indicates that only isolated vanadium ions are active in the oxidation reactions. Oxidation of cyclohexane over V-NCL-1 (Si/V = 250) and its ammonium acetate treated sample both show similar activities and selectivities (Table 5.6). This again demonstrates that only the isolated vanadium ions are active in this reaction.

### 5.6.3 Oxidation of alkyl aromatics

### 5.6.3.1 Oxidation of toluene

The results of the oxidation of toluene over V-NCL-1 (Si/V = 250) is presented in Table 5.7. For comparison the results obtained on VS-2 are also included in Table 5.7. The oxidation of toluene on V-NCL-1 may be represented as:
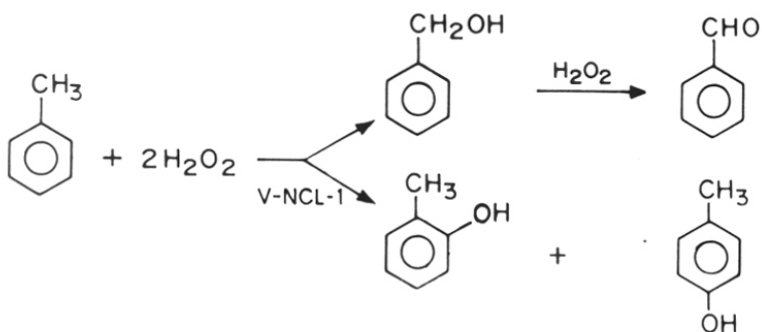
Table 5.7. Oxidation of toluene[a].

| Catalyst | Turnover number[b] | H₂O₂ sel.[c], mole% | Product distribution, wt. % | | | | |
|---|---|---|---|---|---|---|---|
| | | | Benzyl alcohol | Benzal- dehyde | o-Cresol | p-Cresol[d] | Others[e] |
| V-NCL-1[f] | 0.76 | 39.4 | 7.1 | 46.0 | 31.5 | 15.4 | - |
| VS-2[f] | 0.34 | 49.5 | 7.7 | 52.2 | 19.7 | 17.1 | 3.7 |

[a] Reaction conditions: catalyst = 0.1 g; toluene = 1 g; toluene/$H_2O_2$ (mole ratio) = 3; solvent (acetonitrile) = 10 g; temperature = 358 K; reaction duration = 12 h.

[b] Moles of reactant converted per mole of vanadium min$^{-1}$

[c] $H_2O_2$ utilized (mole %) in the formation of benzyl alcohol, benzaldehyde and cresols.

[d] p-cresol includes about 1 wt.% m-cresol also

[e] Mainly oxygenates with more than one functional group.

[f] V-NCL-1: Si/V = 250; VS-2: Si/V = 79

The oxidation of toluene may lead to ring hydroxylation as well as the oxidation of side chain methyl substituents over samples of V-NCL-1. The side chain oxidation is preferred to aromatic ring hydroxylation. This is in marked contrast to titanium-containing molecular sieves[31] which hydroxylate only the aromatic nucleus giving rise to cresols. Thus, in the oxidation of toluene (Table 5.7), the concentration of (benzyl alcohol + benzaldehyde) is more than that of the cresols (53 vs. 46.9 wt.%). Benzaldehyde is formed by the subsequent oxidation of benzyl alcohol. The selectivity to monofunctional products is almost 100%. The ortho hydroxylated product (o-cresol) is formed in twice the quantity than the para hydroxylated one (p-cresol). Being a large pore molecular sieve, there is no steric constraint for the formation of o-cresol in V-NCL-1 and the observed ortho/para ratio of 2.0 is what is expected from purely electronic considerations in the absence of any product shape selectivity. On the other hand, on the medium pore vanadium silicate molecular sieve, VS-2, the formation of o-cresol was only marginally higher than that of p-cresol, indicating the steric constraints in medium pore molecular sieves[19]. The oxidation of benzaldehyde to benzoic acid was not observed in our studies. The pure silica polymorph as well as its vanadium impregnated sample exhibit only negligible activity.

### 5.6.3.2 Oxidation of xylenes

In the oxidation of xylenes over V-NCL-1 (Si/V = 250), conversion and $H_2O_2$ efficiency are similar for the three isomers (Table 5.8). The reaction pathway of oxidation of xylenes represented below:
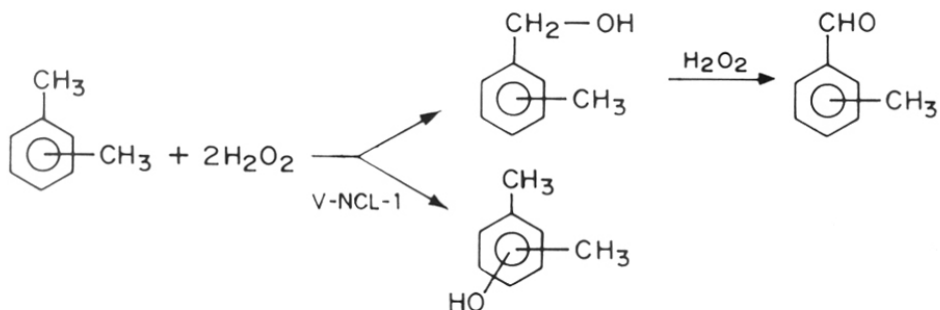
Table 5.8.    Oxidation of xylene isomers over V-NCL-1 (Si/V = 250) molecular sieve[a]

| Substrates | o-Xylene | m-Xylene | p-Xylene |
|---|---|---|---|
| Turnover number[b] | 0.41 | 0.48 | 0.44 |
| $H_2O_2$ sel.[c], mole % | 34.1 | 32.0 | 36.1 |
| **Product distribution, wt.%** | | | |
| 3-Methylbenzyl alcohol | -- | 42.2 | -- |
| 3-Methylbenzaldehyde | -- | 38.9 | -- |
| 2,6-Dimethylphenol | -- | 6.9 | -- |
| 2,4-Dimethylphenol | -- | 4.5 | -- |
| 4-Methylbenzyl alcohol | -- | -- | 43.0 |
| 4-Methylbenzaldehyde | -- | -- | 57.0 |
| 2-Methylbenzyl alcohol | 40.0 | -- | -- |
| 2-Methylbenzaldehyde | 60.0 | -- | -- |
| Others[d] | -- | 7.5 | -- |

[a] Reaction conditions: catalyst = 0.1 g; reactant = 1 g; solvent (acetonitrile) = 10 g; reactant/$H_2O_2$ = 2 moles; temperature = 358 K; reaction duration = 18 h

[b] Moles of reactants converted per mole of vanadium $min^{-1}$.

[c] $H_2O_2$ utilized for formation of methylbenzyl alcohols, corresponding benzaldehydes and dimethylphenols.

[d] Mainly oxygenates with more than one functional group.

The products arising from side chain oxidation are preferred. The pure silica polymorph of NCL-1 as well as its vanadium impregnated samples exhibit only negligible activity. Both o- and p-xylenes do not undergo ring hydroxylation (no dimethylphenols were detected in the products, Table 5.8). Apparently, none of the positions in the aromatic ring is activated for hydroxylation in these substrates. The oxidation of the methyl substituents in o-xylene leads to the formation of 2-methylbenzyl alcohol and 2-methylbenzaldehyde. Similarly, oxidation of p-xylene gives almost exclusively, 4-methylbenzyl alcohol and the corresponding aldehyde. The selectivity to mono-functional products is almost 100 wt.% for both these xylene isomers. On the other hand, oxidation of m-xylene leads also to the formation of dimethylphenols (by ring hydroxylation), in addition to giving predominantly 3-methylbenzyl alcohol and the corresponding aldehyde. These results support the view that the hydroxylation of aromatic ring (with $H_2O_2$ as the oxidant) is probably an electrophilic substitution reaction.

### 5.6.3.3 Oxidation of trimethylbenzenes

The results on the oxidation of 1,2,4- and 1,3,5-trimethylbenzene over V-NCL-1 (Si/V = 250) are presented in Table 5.9. The oxidation of trimethylbenzene follows the following scheme:
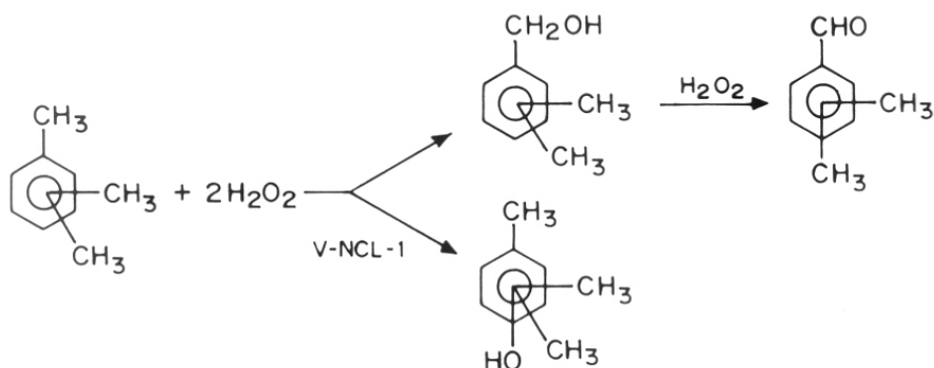
Table 5.9    Oxidation of 1,2,4- and 1,3,5-trimethylbenzenes over V-NCL-1 (Si/V = 250)[a]

| Substrate | 1,2,4-Trimethylbenzene | 1,3,5-Trimethylbenzene |
|---|---|---|
| Turnover number[b] | 0.3 | 0.4 |
| $H_2O_2$ selectivity[c], mole % | 28.9 | 33.0 |
| **Product distribution**, wt. % | | |
| 2,4,6-Trimethylphenol | -- | 12.7 |
| 3,5-Dimethylbenzyl alcohol | -- | 27.2 |
| 3,5-Dimethylbenzaldehyde | -- | 46.2 |
| 2,4-, 2,5-, 3,4-Dimethylbenzaldehydes | 51.1 | -- |
| 2,4-, 2,5-, 3,4-Dimethylbenzyl alcohol | 40.0 | -- |
| Others[d] | 8.9 | 13.9 |

[a] Reaction conditions same as given in Table 5.9.

[b] Moles of reactant converted per mole of vanadium min$^{-1}$.

[c] $H_2O_2$ utilized in the formation of dimethylbenzyl alcohols, corresponding aldehydes and tri-methylphenols.

[d] Mainly oxygenates with more than one functional group.

With 1,3,5-trimethylbenzene, the side chain oxidation of one of the methyl groups leads to the formation of 3,5-dimethylbenzyl alcohol and its aldehyde (27.2 and 46.2 wt.%, respectively). In addition, hydroxylation of aromatic nucleus also occurs, as seen from the formation of considerable amounts of 2,4,6-trimethylphenol in the products (Table 5.9). With 1,2,4-trimethylbenzene, the activation of the three methyl substituents leads to the formation of 2,4-, 2,5- and 3,4-dimethylbenzyl alcohols and the corresponding aldehydes. The hydroxylation of the aromatic ring is not favorable with this substrate because any of three possible positions for hydroxylation is meta position to one of the methyl groups, as no phenolic products were detected. In the oxidation of trimethylbenzenes, VS-2 showed negligible activity and $H_2O_2$ selectivity. This is probably due to the medium size pore openings in VS-2 (V-ZSM-11) which are not accessible for the transportation of the bulkier trimethylbenzenes.

### 5.6.4 Oxidation of naphthalene

The oxidation of naphthalene over V-NCL-1 (Si/V = 250) is illustrated in Fig. 5.11. The probable sequence of the naphthalene oxidation reaction is summarized in the following scheme:
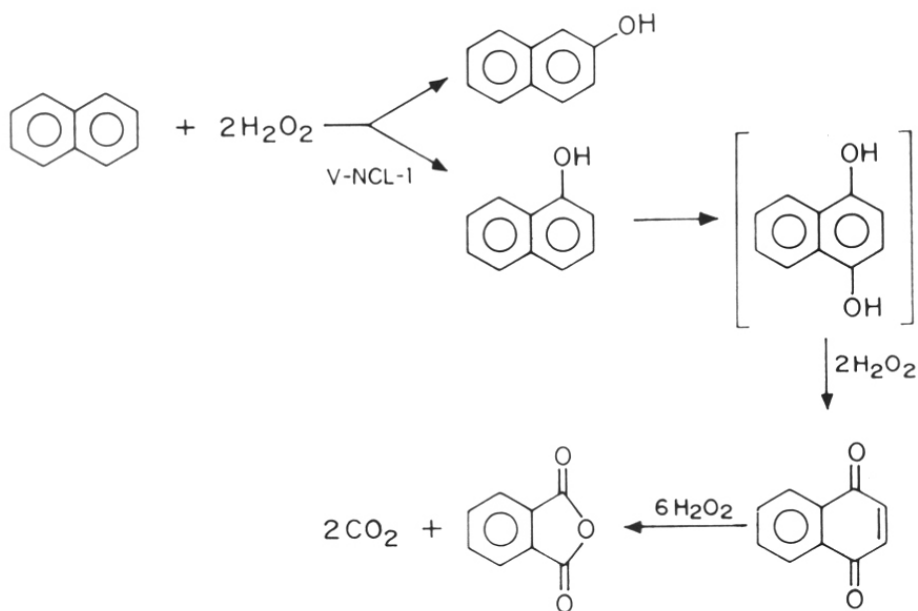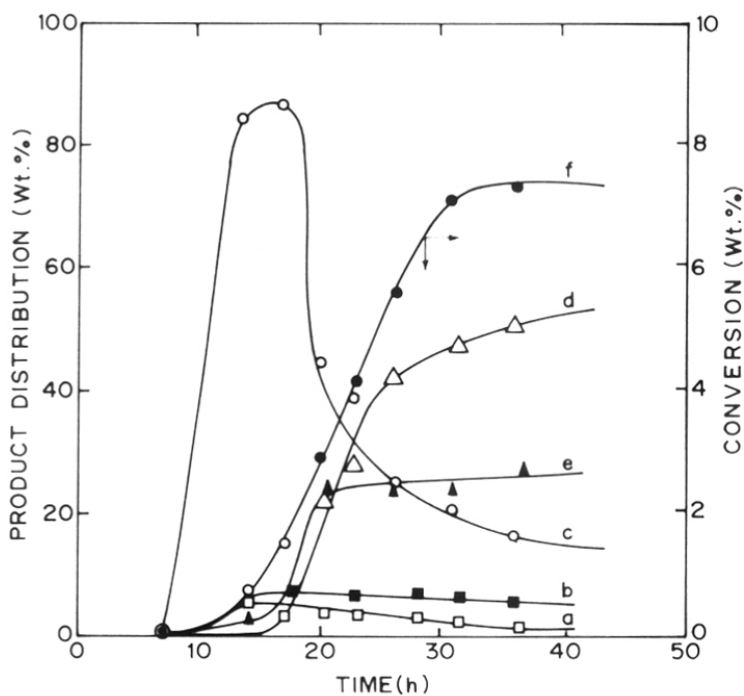
Fig.5.11.    Oxidation of naphthalene on V-NCL-1 (sample C). The formation of 1-naphthol
            (curve a), 2-napthol (b), 1,4-naphthaquinone (c), phthalic anhydride (d) and others
            fragmented products of naphthalene (e) and conversion (f) in wt.% with time.
            Reaction conditions: catalyst = 0.1 g; naphthalene = 1 g; solvent (acetonitrile) =
            10 g; naphthalene/$H_2O_2$ = 2 moles; temperature = 358 K;

It may be mentioned here that VS-2 with medium pore structure does not oxidize naphthalene. The pure silica polymorph of NCL-1 (sample A) and sample A impregnated with vanadium also do not exhibit this activity. The hydroxylation of naphthalene leads to the formation both 1- and 2-naphthols, as the primary hydroxylation products. Hence, both the 1- and 2-carbon atoms in naphthalene are having higher electron density due to its resonance structures. The secondary oxidation of 1-naphthol to 1,4-naphthaquinone (via 1,4-dihyroxy-naphthalene) appears to be very fast as seen from Fig. 5.11. A surprising observation is the presence of significant quantities of phthalic anhydride in the product after 23 h. It is formed by the further oxidation of 1,4-naphthaquinones, which is comparatively a slow reaction. The observed maximum in the concentration of 1,4-naphthaquinone and the subsequent increase in that of phthalic anhydride support the sequential nature of these oxidation reactions. This sequence of reactions is confirmed by using 1-naphthol as the substrate. The oxidation of 1-naphthol (7.5 mole % conversion after 18 h reaction) yields 1,4-naphthaquinone (12.6 wt.%) and phthalic anhydride (81.5 %).

### 5.6.5  Mechanism of oxidation

Vanadium(V) peroxo complexes in non-protic solvents are effective oxidants for olefins (to epoxides), aromatics (to phenols) and alkanes (to alcohols and ketones)[27]. This reactivity was attributed to a peroxo radical $V^{4+}$-O-O$^\bullet$ species generated from peracid-like forms, which adds to double bonds or aromatic nuclei and abstracts hydrogen from alkanes to give a carbon radical intermediate[27]. The peroxo complexes are derived from the reaction of V=O groups with $H_2O_2$ and may be represented as:
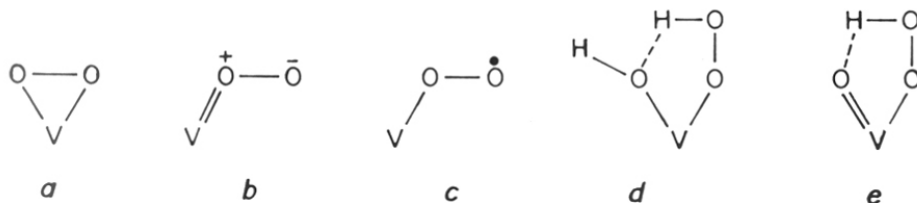
In the homogeneous medium, the oxidation is usually carried out in non-protic solvents such as acetonitrile. The mechanism proposed by Rao et al.[32] on vanadium silicates (VS-1 and VS-2) is shown below:
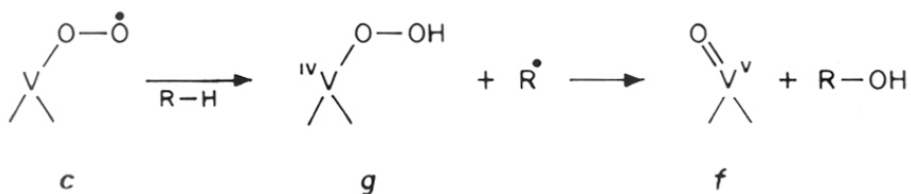


Considering many similarities between VS-2 and V-NCL-1 on the environment of vanadium in the silicalite structure a similar mechanism may operate in the case of V-NCL-1 catalyzed oxidation involving aqueous $H_2O_2$.

## 5.7 CONCLUSIONS

The following conclusions are drawn from this study:

1. Crystalline vanadium silicate analogs of NCL-1 were synthesized using hexamethylene bis(triethylammonium bromide) as the organic template. These vanadium silicates are thermally stable and free from Al impurities.

2. An increase in Si/V molar ratio in the reaction mixture enhances the rate of crystallization.

3. The increase in unit cell volume with the vanadium content suggests the incorporation of vanadium ions in the NCL-1 framework. The contraction of unit cell volumes of V-NCL-1 on hydrothermal treatment also suggest the incorporation of vanadium ions into NCL-1 framework.

5. The ESR spectrum of the as-synthesized samples consist of 8 well resolved lines due to hyperfine splitting. The vanadium ions are atomically dispersed and isolated from each other.

6. Oxidation-reduction experiments suggest that the $V^{4+} <---> V^{5+}$ transition is reversible.

7. The absorption band at around 960 cm$^{-1}$ (due to Si-O-V linkages) and its intensity increases with the vanadium content.

8. Adsorption studies indicate the absence of amorphous material in the V-NCL-1 samples.

9. These vanadium silicate molecular sieves are active in the oxyfunctionalization of alkanes, oxidation of alkylaromatics and naphthalene reactions.

10. Vanadium silicates are able to activate the primary C-H bond of n-octane giving primary alcohols and corresponding aldehydes. They differ from titanium silicate molecular sieves in this respect.

11. V-NCL-1 is also active in the oxidation of bulkier hydrocarbons like trimethylbenzenes and naphthalene.

12. No reactant shape selectivity was observed in the hydroxylation of toluene, xylene and trimethylbenzene reactions. This suggests that V-NCL-1 is a large pore zeolite.

## 5.8 REFERENCES

1. L. Marosi, J. Stabenow and M. Schwarzmann, Ge. Pat. 2831631 (1978).

2. Xu Reren and P. Wenguin, Stud. Surf. Sci. Catal., **24**, 27 (1985).

3. (a) A.V. Kucherov and A.A. Slinkin, Zeolites, **7**, 43 (1987).
   (b) A.V. Kucherov and A.A. Slinkin, Zeolites, **8**, 110 (1988).

4. T. Inui, D. Medhanavyan, P. Praserthdam, K. Fukuda, T. Ukawa, A. Sakamoto and A. Miyamoto, Appl. Catal., **18**, 311 (1985).

5. A. Miyamoto, D. Medhanavyan and T. Inui, Appl. Catal., **28**, 89 (1986).

6. A. Miyamoto, D. Medhanavyan and T. Inui, Proc., 9th Intern. Congr. Catal., (M.J. Philip and M. Terrnan, Eds.) Pub. Chem. Inst. of Canada, Ontario, **1**, 437 (1988).

7. F. Cavani, F. Trifiro, K. Habersberger and Z. Tvaruzkova, Zeolites, **8**, 12 (1988).

8. A. Miyamoto, Y. Iwamoto, H. Matsuda and T. Inui, Stud. Surf. Sci. Catal., **49B**, 1233 (1989).

9. Z. Tvaruzkova, G. Centi, P. Jiru and F. Trifiro, Appl. Catal., **19**, 307 (1985).

10. L.W. Zatorski, G. Centi, J.L. Nieto, F. Trifiro, G. Bellussi and V. Fattore, Stud. Surf. Sci. Catal., **49B**, 1243 (1989).

11. J. Kornatowski, M. Sychev, V. Goncharuk and W.H. Baur, Stud. Surf. Sci. Catal., **65**, 581 (1990).

12. M.S. Rigutto and H. Van Bekkum, Appl. Catal., **68**, L1 (1991).

13. P. Fejes, I. Marsi, I. Kirisci, J. Halasz, I. Hannus, A. Rockenbauer, Gy. Tasi, L. Korecz and Gy. Schobel, Stud. Surf. Sci. Catal., **69**, 173 (1991).

14. G. Centi, S. Perathoner, F. Trifiro, A. Aboukais, C.F. Aissi and M. Guelton, J. Phys. Chem., **96**, 2617 (1992).

15. P.R. Hari Prasad Rao, A.V. Ramaswamy and P. Ratnasamy, J. Catal., 137, 225 (1992).

16. P.R. Hari Prasad Rao and A.V. Ramaswamy, Appl. Catal., **93**, 123 (1993).

17. P.R. Hari Prasad Rao and A.V. Ramaswamy, J. Chem. Soc. Chem. Commun., 1245 (1992).

18. P.R. Hari Prasad Rao, A.V. Ramaswamy and P. Ratnasamy, J. Catal., (communicated).

19. P.R. Hari Prasad Rao, K. Ramesh Reddy, A.V. Ramaswamy and P. Ratnasamy, 3rd Int. Symp. on Heterogeneous Catalysis and Fine Chemicals, Poitiers, France, April (1993), Stud. Surf. Sci. Catal., (in press).

20. (a) R. Kumar, K.R. Reddy, A. Raj and P. Ratnasamy, 9th Intern. Zeolite Conf., Montreal, Canada, 1992, Paper A6.

    (b) R. Kumar, K.R. Reddy and P. Ratnasamy, Ind. Pat. Appl. No. 766/DEL/91 (1991).

    (c) R. Kumar, K.R. Reddy and P. Ratnasamy, EP Appl. No 92300166.3 (1991).

    (d) R. Kumar, K.R. Reddy and P. Ratnasamy, US Pat. Appl. No. 07/816, 211 (1991)

21. (a) K. Ramesh Reddy, A.V. Ramaswamy and P. Ratnasamy, J. Chem. Soc. Chem. Commun., 1613 (1992).

    (b) K. Ramesh Reddy, A.V. Ramaswamy and P. Ratnasamy, J. Catal. (in press) 1993.

22. B. Notari, Stud. Surf. Sci. Catal., **37**, 413 (1987).

23. J.S. Reddy and R. Kumar, J. Catal., **130**, 440 (1991).

24. D.P. Serrano, Hong-Xin Li and M.E. Davis, J. Chem. Soc., Chem. Commun., 745 (1992).

25. B. Meunier, Bull. Soc. Chim. Fr., 578 (1986).

26. N. Herron and C.A. Tolman, J. Amer. Chem. Soc., **109**, 2837 (1987).

27. H. Mimoun, L. Saussine, E. Daire, M. Postel, J. Fischer and R. Weiss, J. Amer. Chem. Soc., **105**, 3101 (1983).

28. T. Tatsumi, M. Nakamura, S. Negishi and H. Tominaga, J. Chem. Soc., Chem. Commun., 476 (1990).

29. D.C. Huybrechts, L.D. Bruyeker and P.A. Jacobs, Nature, **345**, 240 (1990).

30. J.S. Reddy, S. Sivasanker and P. Ratnasamy, J. Mol. Catal., **70**, 335 (1991).

31. J.S. Reddy, and S. Sivasanker, Indian J. Tchnol., **30**, 64 (1992).

32. P. Raja Hari Prasad Rao thesis submitted to the University of Poona p. 103 (1992)

# SUMMARY AND CONCLUSIONS

## SUMMARY

High-silica, large pore zeolites are of special interest in the field of adsorption and catalysis. Till now ZSM-12 is the only large pore 12-membered ring zeolite which can be synthesized in a wide range of Si/Al ratio including the Al-free silica polymorph. Though zeolite Beta can also be obtained in a fairly large range of Si/Al ratio 10-120, its silica polymorph is still unknown. A new high-silica large pore zeolite NCL-1 as well as its Al-free silica polymorph have been synthesized by using hexamethylene bis(triethylammonium bromide) as organic additive. NCL-1 can be synthesized fairly in the wide range of Si/Al ratio (23-∞). This zeolite has been characterized by X-ray diffraction, framework IR, solid state MAS NMR, scanning electron microscopy, thermal analysis, adsorption and catalytic methods. Our preliminary studies indicate that NCL-1 possesses orthorhombic symmetry with a = 1.195±0.003, b = 0.836±0.003 and c = 2.870±0.004 nm. The 'd' values calculated on the basis of the above unit cell dimension compare reasonably well with those observed experimentally. $^{29}$Si MAS NMR spectra of Si-NCL-1 exhibited only one signal at -112 ppm attributed to Si(0Al). In $^{27}$Al MAS NMR spectra, only one signal was observed at 52 ppm, attributed to tetrahedral $Al^{3+}$ ions and no signal was observed due to octahedral $Al^{3+}$ ions. $^{27}$Al NMR spectra of silica polymorph of NCL-1 did not show any signal suggesting absence of aluminium in the sample. From the adsorption of mesitylene (4.8 wt.%), it has been concluded that NCL-1 is large pore zeolite.

The results obtained through acid catalyzed test reactions given below clearly suggest that NCL-1 is a large pore zeolite.

(a)   In $m$-xylene conversion, the $p$-xylene/$o$-xylene ratio in the products is 1.1, the ratio of isomerization to disproportionation is given as log(I/D) = 1 and the ratio of 1,3,5-trimethylbenzene to 1,2,4-trimethylbenzene in products is 0.1.

(b)    The presence of induction period and the ratio of diethylbenzenes to benzene = 0.89 (wt.%) in the ethylbenzene disproportionation reaction.

(c)    Mobil's constraint index = 1

(d)    The spaciousness index (SI) = 6.1

The studies of molecular sieves as oxidation catalysts have been, so far restricted to medium pore molecular sieves. For the first time, vanadium-containing large pore molecular sieve analog of NCL-1 (V-NCL-1) has been synthesized. Most of the vanadium is probably intact within the silicalite structure. Three different Si/V ratios of 150, 250 and 400 were prepared hydrothermally. These are thermally stable and free from aluminium. The unit cell volume increases with the vanadium content. Like vanadium silicate analog of MEL structure (VS-2) reported earlier, V-NCL-1 is also active in the oxidation or hydroxylation of a number of organic substrates in presence of $H_2O_2$. In the selective oxidation of n-octane, V-NCL-1 is able to oxyfunctionalize the primary carbon atom also. However, the activation of the carbon atom at the second position is preferred to others and follows the order, 2C > 3C > 4C > 1C. In toluene oxidation reaction it oxidizes the side chain methyl group leading to the formation of benzyl alcohol and benzaldehyde in addition to ring hydroxylation to yield mainly $o$- and $p$-cresols. The second important observation is that the secondary oxidation to carbonyl compounds is faster in general on vanadium silicates including V-NCL-1. Due to its large pore dimensions, V-NCL-1 is also active in the oxidation of bulkier hydrocarbons. This has been demonstrated in reactions involving trimethylbenzenes and naphthalene.

# LIST OF PUBLICATIONS

## PAPERS

1. K. Ramesh Reddy, A.V. Ramaswamy and P. Ratnasamy,
   "Synthesis and Characterization of a Large Pore Vanadium-containing molecular sieve, V-NCL-1" J. Chem. Soc., Chem. Commun., 1613 (1992).

2. R. Kumar, K. Ramesh Reddy, Anuj Raj and P. Ratnasamy,
   "Synthesis and Characterization of a new high-silica, Large Pore aluminosilicate", NCL-1, 9th Int. Zeolite Conf., Montreal, Canada, Paper A6, (1992).

3. Anuj Raj, K. Ramesh Reddy, J. Sudhakar Reddy and R. Kumar,
   "Catalytic Properties of Ferrisilicate Analogs of some medium pore zeolites in $C_7$ and $C_8$ aromatic hydrocarbon Reactions" 10th Int. Cong. Catal., Poster presentation, Budapast, Hungary (1992).

4. J. Sudhakar Reddy, K. Ramesh Reddy, R. Kumar and P. Ratnasamy,
   "Ferrisilicate analogs of ZSM-11 (MEL)", Zeolites, **11**, 553 (1991).

5. K. Ramesh Reddy
   "Removal of Dialkylphenols from Aqueous Effluents by Selective Adsorption in Novel, Large-pore, Silica Molecular Sieve" J. Chem. Soc., Chem. Commun., (in press) (1993).

   559

6. K. Ramesh Reddy, A.V. Ramaswamy and P. Ratnasamy
   "Studies on crystalline microporous vanadium silicates"
   IV. Synthesis, Characterization and catalytic properties of V-NCL-1 a large pore molecular sieve, J. Catal., (in press) 1993.

7. P.R.H. Prasad Rao, K. Ramesh Reddy, A.V. Ramaswamy and P. Ratnasamy
   "Selective oxidation reactions over vanadium silicate molecular sieves" Proceedings of 3rd Int. Symp. on Heterogeneous Catalysis and Fine Chemicals, Poitiers, France, 5-8 April 1993 Stud. Surf. Sci. Catal., (in press) (1993).

8. K. Ramesh Reddy, Anuj Raj and R. Kumar
   "Toluene alkylation and *m*-xylene isomerization over ferrisilicate analog of Zeolite ZSM-48 ([Fe]-ZSM-48])" Appl. Catal., (accepted).

9. J. Sudhakar Reddy, K. Remesh Reddy and R. Kumar
   "Incorporation of Ga and Fe into framework of ZSM-11" Recent Devolopments in Catalysis" (B. Viswanathan and C.N. Pillai (Eds.)), Published by Narosa publishing house, Delhi, p.275 (1990).

10. K. Ramesh Reddy and R. Kumar
    "A new high-silica large pore zeolite NCL-1: Synthesis and characterization through catalytic test reactions" Presented at 11th National Symposium on Catalysis, IICT, Hyderabad, April 2-4 (1993).

11. A.P. Singh and K. Ramesh Reddy
"Gallosilicate analogs of zeolite ZSM-22" presented at 11th National Symposium on Catalysis, IICT, Hyderabad, April, 2-4 (1993).

12. K. Ramesh Reddy, R. Kumar and A.V. Ramaswamy
"Crystallization kinetics of a new large pore silica molecular sieves, NCL-1" Zeolites (communicated) (1992).

13. A.P. Singh and K. Ramesh Reddy
"Synthesis and Characterization of Ga-ZSM-22"
Zeolites (communicated) (1992).

14. K. Ramesh Reddy, H.S. Soni, V.P. Shiralkar, R. Kumar and A.V. Ramaswamy
"Sorption properties of NCL-1, a large pore high-silica molecular sieve"
J. Phys. Chem., (to be communicated).

15. K. Ramesh Reddy and R. Kumar
"Void volume determination of NCL-1 through catalytic test reactions"
J. Catal., (to be communicated).

## PATENTS (FILED)

1. R. Kumar, K. Ramesh Reddy and P. Ratnasamy
"Process for the preparation of a novel crystalline material"
Ind. Pat. Appl. No. 766/DEL/91;

2. R. Kumar, K. Ramesh Reddy and P. Ratnasamy
"Process for the preparation of a novel crystalline material"
EP Appl. Non 92300166.3. (1991).

3. R. Kumar, K. Ramesh Reddy and P. Ratnasamy
"Process for the preparation of a novel crystalline material"
US Pat. Appl. No. 07/816,211 (1991).

4. R. Kumar, A.P. Singh, K. Ramesh Reddy, P.R.H. Prasad Rao and P. Ratnasamy
"A process for the preparation of crystalline microporous vanadium silicate" Ind. Pat. No. 610/DEL/92.

5. R. Kumar A.P. Singh, K. Ramesh Reddy and P. Ratnasamy
"An improved process for the production of hydroxy naphthalenes"
Ind. Pat. No. 611/DEL/92

6. R. Kumar, A.P. Singh, K. Ramesh Reddy and P. Ratnasamy
"A process for the production of 1,4-naphthoquinone" Ind. Pat. (applied).